ORNL/Sub/81-21099/1&02

26 FEBRUARY 1982 **REPORT EBT-P010**

FUSION ELMO BUMPY TORUS ENERGY

Copy No. 94

Elmo Bumpy Torus Proof Of Principle

PHASE II — TITLE 1 REPORT
Volume II TOROIDAL VESSEL

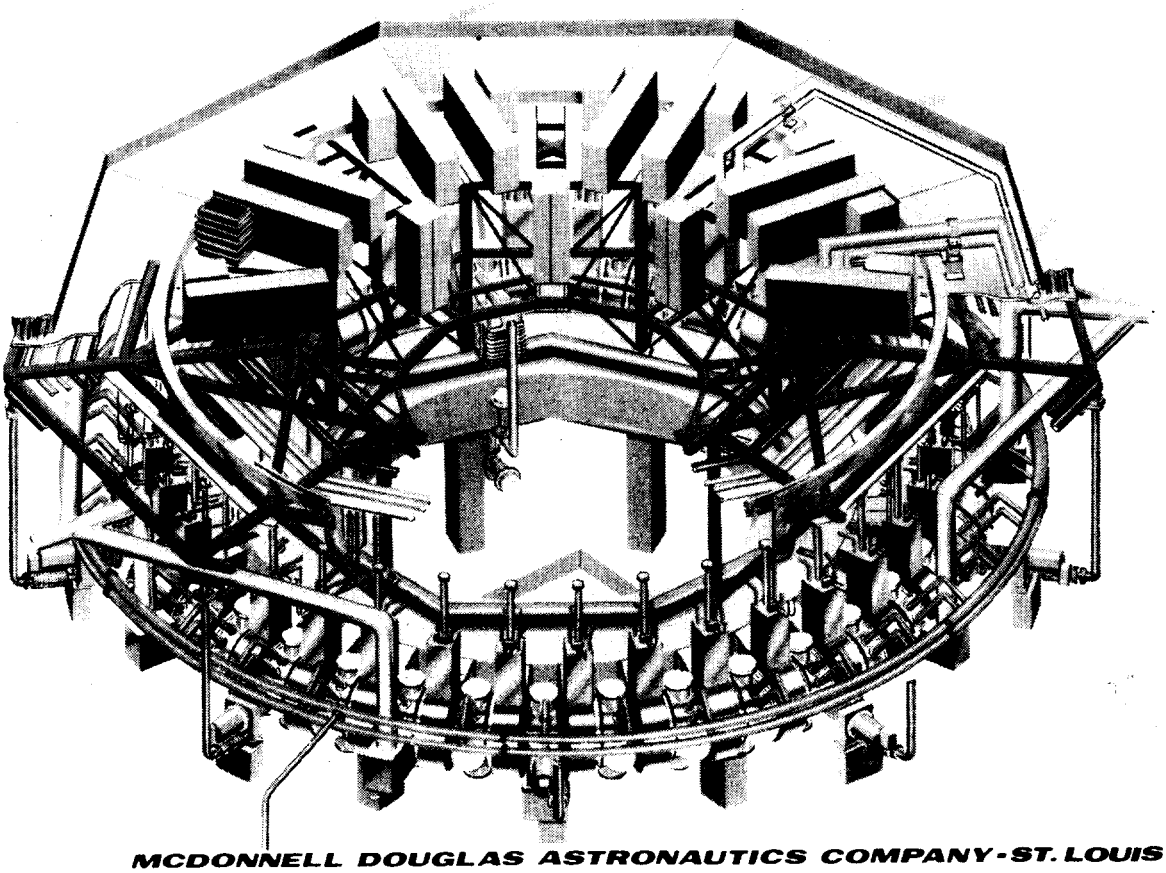

MCDONNELL DOUGLAS ASTRONAUTICS COMPANY-ST. LOUIS DIVISION
Saint Louis, Missouri 63166 (314) 232-0232

MARTIN MARIETTA ENERGY SYSTEMS LIBRARIES
3 4456 0156099 3

MCDONNELL DOUGLAS CORPORATION

PRELIMINARY DESIGN REPORT

EBT-P TOROIDAL VESSEL

VOLUME II

PREPARED BY: Jack L. Conlee
J. L. Conlee, Manager
EBT-P Toroidal Vessel

APPROVED BY: Harry F. Imster
H. F. Imster, Manager
EBT-P Engineering

APPROVED BY: Roy J. DeBellis
R. J. DeBellis, Manager
EBT-P Project - MDAC

APPROVED BY: James D. Stout
J. D. Stout, Manager
EBT-P Engineering - ORNL

APPROVED BY: A. L. Boch
A. L. Boch, Manager
EBT-P Project - ORNL

Reference Index

Volume I — Device Summary

Volume II — Toroidal Vessel

Volume III — Magnet System

Volume IV — Microwave System

Volume V — Vacuum Pumping System

Volume VI — Instrumentation and Control

Volume VII — Cryogenic Systems

Volume VIII — Device Utilities

Volume IX — Support Structure

TABLE OF CONTENTS

SECTION		PAGE
1.0	INTRODUCTION SUMMARY	1
1.1	VACUUM VESSEL SEALS AND WALL MATERIAL TRADE STUDY	1
1.2	TOROIDAL VACUUM VESSEL DESIGN FEATURES	6
1.3	LIMITERS	7
2.0	PURPOSE AND SCOPE	8
3.0	DESIGN CRITERIA	9
3.1	GENERAL CRITERIA	9
3.2	SPECIFIC CRITERIA	10
4.0	TOROIDAL VESSEL DESCRIPTION	13
4.1	MIRROR CAVITY	16
4.2	VACUUM LINER	18
4.3	EBT-P LIMITER DESIGN	18
5.0	SUPPORTING ANALYSES	23
5.1	VACUUM VESSEL SEAL AND MATERIAL TRADE STUDY	23
5.2	TOROIDAL VACUUM VESSEL STRUCTURAL CONSIDERATIONS	62
5.3	EBT-P LIMITER DESIGN AND ANALYSIS	66
6.0	SCHEDULE	84
7.0	REFERENCES	86
APPENDIX A – X-RAY ANALYSIS		A-1
APPENDIX B – TOROIDAL VESSEL DRAWINGS		B-1

LISTS OF PAGES

ii - x
1 - 86
A-1 - A-10
B-1 - B-28

LIST OF FIGURES

FIGURE		PAGE
1.0-1	Toroidal Vessel Assembly	2
1.1-1	Vacuum Vessel Material and Seals Trade Study Chronology	3
4.1-1	Mirror Cavity Port Arrangement	17
4.2-1	Vacuum Liner Configuration	19
4.3-1	Limiters Configuration	21
5.1-1	Vessel Wall Heat Load Definition	26
5.1-2	X-Ray Spectra for an Aluminum Wall	28
5.1-3	X-Ray Dose Accumulation	31
5.1-6	Various Metal Sealing Concepts	38
5.1-7	Stainless Steel Concepts Evaluated	43
5.1-8	Material Trade Study for EBT-P Comparing Stainless Steel with Aluminum for the Vacuum Liner and Mirror Cavity	45/46
5.1-9	Temperatures in Solid Aluminum Vacuum Vessel Walls with Limiters and 7.0 MW Input Power	47
5.1-10	Temperature Gradient is Very Sensitive to Weld Land Width	49
5.1-11	Increasing the Inside Skin Thickness Can Decrease the Peak Temperature	50
5.1-12	Increasing the Outside Skin Thickness Slightly Decreases the Peak Temperature	51
5.1-13	Peak Temperature is Insensitive to Coolant Passage Width	52
5.1-14	Vacuum Liner Temperature and Poloidal Thermal Stress Distributions	53
5.1-15	Corrugated Stainless Steel Concept has High Cooling Capability	54
5.1-16	Vacuum Liner Life is Very Sensitive to Weld Land Width and Surface Heat Flux	57
5.2-1	Toroidal Vessel Support	65
5.3-1	Limiters	68
5.3-2	Resulting Heat Flux Distributions for EBT-P Limiters	72

LIST OF FIGURES (Continued)

FIGURE		PAGE
5.3-3	Limiter Temperature Distributions	75
5.3-4	Temperatures for EBT-P Limiter (Upgrade - 5.0 MW into Torus)	77
5.3-5	Limiter Thermal Stress Distribution-Baseline Power	79
5.3-6	Limiter Thermal Stress Distribution-Upgrade Power	79
5.3-7	EBT-S Test Limiter Installation	81
6-1	Toroidal Vessel Schedule	85
A-1	X-Ray Spectra for an Aluminum Wall	A-5
A-2	Dose Accumulation in Vacuum Seals as a Function of Operating Time for Three Different Sets of Machine Operating Conditions	A-8

LIST OF TABLES

TABLE		PAGE
4.0-1	EBT-P Device Design Summary	14
5.1-1	Parameter Values Utilized in the X-Ray Analysis	29
5.1-2	Plasma Impurity Fraction and Vacuum Seal Dose Rate for Various Input Power Levels	30
5.1-3	A Summary of the Vacuum Seal Chracteristics of Various Elastomers	33
5.1-4	Survey of Fusion Devices	41
5.3-1	Alternate Limiter Material Comparison	69
5.3-2	Limiter Hydraulic Parameters	76
A-1	Parameter Values Utilized in the X-Ray Analysis	A-6
A-2	X-Ray Source Levels as a Function of Energy for the EBT-P Baseline Configuration at Two Different Plasma Impurity Concentrations	A-9
A-3	Dose Calculation for Baseline Configuration with 2% AL Impurity in the Plasma	A-10

LIST OF DRAWINGS

		PAGE
70B372000	Toroidal Vessel Assembly	B-1
70B372004	Mirror Cavity Port Arrangement	B-3
70B372005	Vacuum Liner	B-7
70B372001	Toroidal Vessel Support	B-13
70B375000	Deionized Water Manifold Interface, Torus	B-15
70B375001	Device Coolant Panels	B-19
70B375004	Installation, Device Coolant, Torus	B-21
70B375005	Panel, Device Coolant, Limiter	B-27

ACRONYMS, ABBREVIATIONS AND INITIALISMS

ARE	Aspect Ratio Enhancement
ASME	American Society of Mechanical Engineers
EBT-P	Elmo Bumpy Torus-Proof of Principle
EBT-S	Elmo Bumpy Torus-Scale
EBT-R	Elmo Bumpy Torus-Reactor
ICRH	Ion Cyclotron Resonance Heating
ID	Inside Diameter
MDAC	McDonnell Douglas Astronautics Company-St. Louis Division
OD	Outer Diameter
ORNL	Oak Ridge National Laboratory
OPS	Operational Support
PACE	Plant and Capital Equipment
R&D	Research and Development
RF	Radio Frequency
RFP	Request for Proposal
TF	Toroidal Field
TN	Technical Note
UHV	Ultra High Vacuum
WBS	Work Breakdown Structure
Z	Atomic number

1.0 INTRODUCTION AND SUMMARY

The Toroidal Vessel provides the vacuum enclosure for containing the high temperature steady state plasma. In addition, the Toroidal Vessel must provide several viewing ports for plasma diagnostics, vacuum pumping ports for both high vacuum and roughing vacuum, feed-through ports for ECRH waveguides, limiter feed throughs for cooling and supporting the limiters, and ports for ion gages. The vessel must operate in an intense environment comprised of x-rays, microwaves, magnetic fields and plasma heat loads as well as the atmosphere pressure and gravity loads and the internal thermal stress loads due to heating and cooling of the torus.

A key issue addressed during Title I was the choice of vacuum vessel seal and wall materials. In addition, during the course of the study, ORNL requested that horsecollar diagnostic ports be incorporated in the design. A comprehensive trade study was performed considering the vessel material issues in concert with the impact of the horsecollar port design. A change in baseline from an aluminum vessel with elastomer seals and circular diagnostic ports to austenitic stainless steel vessel with metal seals and horsecollar ports was agreed upon by both MDAC and ORNL towards the end of Title I. The trade study is summarized in this section and the details of the study are presented in Section 5.1.

The Toroidal Vessel system is comprised of 36 sectors with each sector consisting of a vacuum liner and mirror cavity (Figure 1.0-1). The vacuum liner is located through the bore of each mirror coil vacuum dewar and is non-integral with the mirror coil assembly. The mirror cavities contain nearly 500 ports of different sizes and shapes that must be vacuum tight. During Title I, large horsecollar diagnostic ports were requested by ORNL and these were incorporated in the mirror cavity design. Limiters are located adjacent to the vacuum liners to protect the liners against the severe heating and erosion expected near the throat region.

1.1 VACUUM VESSEL SEALS AND WALL MATERIAL TRADE STUDY

The choice of seal and vessel wall material was a key issue addressed during Title I. An extensive study considering both technical and cost factors was performed before reaching a final decision, agreed upon by both MDAC and ORNL. Figure 1.1-1 presents, in

FIGURE 1.0-1 TOROIDAL VESSEL ASSEMBLY

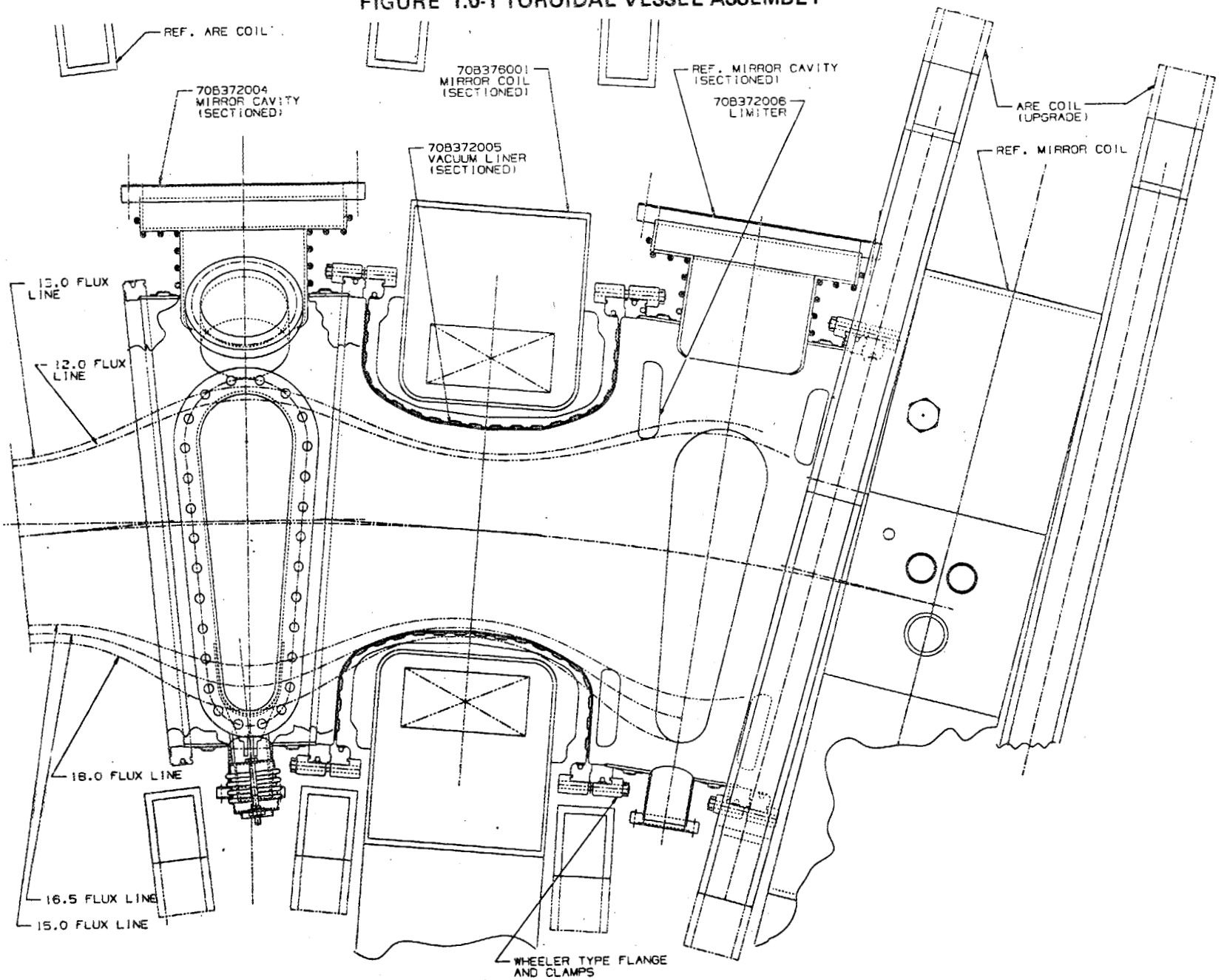

Figure 1.1-1 Vacuum Vessel Material and Seals Trade Study Chronology

Sept. 1980	Began review of elastomer seals; Literature Search and Vendor Survey.
14 Nov. 1980	Report issued (EBT-237) "Use of Non-metallic Vacuum Seals on EBT-P."
Nov. 1980	Initiated investigation of aluminum compatible metal seals.
Jan. 1981	Initiated Aluminum/Stainless Steel trade study
8 April 1981	Initial technical review of trade study results at Quarterly Review meeting in St. Louis.
1 June 1981	Technical results documented in technical note and transmitted to ORNL.
4 June 1981	Full-day presentation of technical results to ORNL.
8 July 1981	Initial cost data comparisons transmitted to ORNL.
16 July 1981	Overview of technical and initial cost data at Quarterly Review meeting in St. Louis.
31 August 1981	Telecon review of refined cost estimates for trade study and impact of horsecollar port shape.
3 Sept. 1981	Telecon review or refined cost estimate for aluminum and metal seal system.
17 Sept. 1981	Transmittal of justification paper on trade study recommendation.

chronological order, the key trade study milestones and illustrates the close coordination between MDAC and ORNL on this study. Documentation of the trade study results is presented in References 1 through 3. A summary of the trade study is presented in this section and the details can be found in Section 5.2 and in the Appendix. The vessel material and seal concepts evaluated included: 1) the initial MDAC baseline of an aluminum vessel with elastomer seals, 2) an aluminum vessel with metal seals and 3) a stainless steel vessel with metal seals. The feasiblity of welded seals were also assessed.

The trade study approach was to first evaluate the adequacy of the baseline aluminum with elastomer seals in the environments predicted for EBT-P. It was concluded that the initial baseline represented too high of risk to the EBT-P project. Alternate seals and vessel materials were evaluated in concert with the horsecollar diagnostic port design. The highlights of the trade study are summarized in subsequent paragraphs:

Detailed calculation of the EBT-P environments established the following conditions for design of the Toroidal Vessel: x-ray dose level of 10^9 rads over the 10-year life of the device, microwave heating of the elastomer seals of about 16 W/cm^2, and wall heat flux of between 5 and 13.5 W/cm^2 with peak values of up to 20 W/cm^2 on the vacuum liner throat.

Microwave seal protection concepts that could protect the seals against microwave heating were identified and appeared feasible. However, protection against x-rays could not be provided by any viable method. Elastomer seal life, according to manufacturers data, is limited to 10^7 rads, although use of up to 10^8 rads has been reported in the literature.. Even using 10^8 rads as the seal life criteria, the elastomer seals would require frequent replacement during the operations phase. The cost and time for such frequent replacement would be prohibitive and is unacceptable for EBT-P operation. The choice then focussed on metal seals for either an aluminum or stainless steel vessel.

A survey of seal vendors and users of vacuum systems was conducted and showed that very little experience exists with aluminum metal sealed vacuum systems. There is limited experience with aluminum Conflats and aluminum flanges with Helicoflex seals but this experience is limited to small diameter (typically 6 to 8 inches) seals under static thermal conditions. The effects of thermal cycling and larger seal size on sealing performance can-

not be assessed because of lack of data. The indium coated C-ring seal was judged the most promising metal seal concept for use with aluminum flanges. An aluminum vacuum vessel design concept with redundant indium coated C-ring metal seals served as the basis for the cost studies. The baseline aluminum flange thickness was increased substantially to provide the high sealing forces required for metal seals. Also, the bolts were replaced by clamps for clearance reasons.

Metal seals with stainless steel vessels are widely used in the high vacuum industry. However, before this concept could be adapted for EBT-P, a concept that provided adequate cooling of the low conductivity stainless steel structure had to be developed. Three stainless steel concepts were evaluated in detail: a skin and tube concept, an integrally-cooled corrugated structure and a stainless steel/copper backed concept with the copper layer providing the high heat transfer path between coolant tubes. The integrally-cooled corrugated structure was considered the best choice because it has adequate cooling and has an established fabrication process. Adequate cooling is achieved by using the corrugations as coolant passages and having a large fraction of the surface in contact with coolant. Stainless steel also has the advantage of a relatively high use temperature and ease of welding. The fabrication process for the stainless steel corrugated structure is well established and structures of this type are commercially available from specialty corrugated panel companies. MDAC has purchased simular corrugated structures for use as shrouds in the large vacuum chambers. These shrouds have performed well without evidence of leakage even after multiple exposures to liquid nitrogen temperatures.

The recommended stainless steel/metal seal design uses Wheeler flanges for the large cavity seal, Conflats for the circular ports and Helicoflex seals for the horsecollar ports. The Wheeler and Conflat seal system (flange, metal gasket and clamps) are off-the-shelf items. The horsecollar vacuum flange and seal system will be developed by MDAC.

The choice of Toroidal Vessel material and seal was difficult to make because of the uniqueness of the EBT-P operating environment, the criticality of the vacuum system on the operation of the device and the prohibitive cost of modifying the device during the installation or operation phases. Retaining the orginal baseline design was viewed as an unjustifiable high risk approach considering the projected x-ray levels for EBT-P which exceed the capabilities of elastomeric seals. The final choice involved a trade of risk verses

cost between aluminum and stainless steel structures with metal seals. Metal seals with stainless steel flanges are proven, widely used in UHV applications, commercially available, and therefore, have substantially less risk than the aluminum/metal seal approach. The corrugated stainless steel structure may be viewed as having an inherently higher risk than the aluminum skin and tube concept, but unlike the vacuum seal issue the stainless steel structure is amenable to analysis, is used in many similar applications where cooling and high structural efficiency are required, and has an established fabrication process with little if any development required.

In assessing the costs between aluminum and stainless steel with metal seals and horsecollar ports the difference in costs was consistently small and was within the accuracy of the cost estimation process. The high costs for fabricating the stainless steel structure is offset by the lower costs of the off-the-shelf metal seal system and the lower development cost of a proven seal concept. Since cost is not a major differentiator, the decision relied heavily on technical factors and risk. The trade study recommendation was for stainless steel vessel with metal seals be adapted for EBT-P because this offers the least risk approach in meeting the project goals. Horsecollar diagnostic ports was considered as an integral part of the revised design. ORNL agreed with the MDAC recommendation. Detail design and analysis of the stainless steel/metal seal concept with horsecollar ports was initiated towards the end of Title I and this activity will continue in the Title II phase.

1.2 TOROIDAL VACUUM VESSEL DESIGN FEATURES

The Toroidal Vessel design that emerged during the Title I effort is shown in Figure 1.0-1. The key features of the design are summarized in subsequent paragraphs:

Vacuum Liner - The vacuum liner segment of the Toroidal Vessel forms a vacuum boundary between each pair of adjacent mirror cavity segments and is internal but not integral to the mirror coil. Attachment to the mirror cavity segments is by a clamp flange arrangement with metal wire seals (Wheeler seal) providing the vacuum seal between the two components. The vacuum liner design is 316L stainless steel and utilizes a double wall shell with die formed coolant passages for cooling. The coolant passage design can be sized to accomodate the anticipated heat flux commensurate with the operating life cycle of the device. The Toroidal Vessel design minimizes thermal growth through flexing of the vacu-

um liner side wall rather than allowing large radial growth which would load up the mirror coil dewars.

The vacuum liner shape, in the magnet coil throat area, is very critical in terms of passing particles and much effort was devoted to shaping and sizing the liner throat corners to maximize the passing particle fraction. Modifications to the baseline design to achieve the greater passing particle fraction included: addition of corner radius on the mirror coil dewars, reducing the mirror coil x-ray shield thickness in the corner area, adding a flat section on the liner corner parallel to the passing particles, and minimizing the wall thickness of the liner.

Mirror Cavity - The mirror cavity segments must accommodate the plasma diagnostic equipment in addition to providing vacuum pumping ports, ECRH waveguide window penetrations, and limiter support and limiter feed-thru penetrations. Also the mirror cavities must allow for ICRH and ARE coil additions during future upgrades. The mirror cavities must also provide adequate structural carry-thru, be adequately cooled and provide a high vacuum seal during operation. Like the vacuum liner, the mirror cavity is a double wall configuration and is fabricated from 316L stainless steel.

1.3 LIMITERS

The limiter configuration and their location within the toroidal vessel are depicted in Figure 1.0-1. Four individually cooled limiters are positioned in the mirror cavity to protect the vacuum liner throat from the high surface heating and erosion. The limiters are placed so that their inner surface is concentric with TF magnet flux lines. The inboard limiters are adjustable and all four limiters can be removed via the horsecollar ports without disassembly of the torus. The limiter configuration consists of an internal copper coolant passage with a thick aluminum overcoat. The copper eliminates possible corrosion problem by eliminating aluminum from the demineralized water. The aluminum provides a high conductivity material for efficient cooling and also a low atomic number material which minimizes the effect of impurities on the plasma and subsequent plasma heat loss.

2.0 PURPOSE AND SCOPE

A key objective of the Toroidal Vessel Title I engineering effort was further development of the Toroidal Vessel design to ensure that all design criteria including interface requirements are met. The choice of vacuum vessel seal and wall material was a critical issue which was resolved during the Tittle I phase. A comprehensive trade study was conducted which involved a detail assessment of the initial baseline design as well as alternate materials and concepts. The trade study approach and results are summarized in Section 1.0 and the details are presented in Section 5.1. During the course of the Title I study, ORNL requested that large horsecollar diagnostic ports be incorporated in the Toroidal Vessel design. Because of the criticallity of the vacuum vessel material decision on the EBT-P project, close coordination with ORNL was maintained during the trade study period through a series of presentations and detail documentation. A final decision for a corrugated stainless steel vessel, with horsecollar ports, and metal seals was agreed upon by both MDAC and ORNL towards the end of the Title I phase. A baseline Toroidal Vessel design based on the stainless steel/metal seals concept was developed and detail thermal/structural analysis was initiated. This activity will continue and be completed in the Title II detail design phase. Work was also initiated to define the test article and test setup for the vacuum seal test program. The information from this test program is desired early in Title II to support the detail design phase. The limiter test program described in section 5.3.5-1 for EBT-S was defined in Title I and testing will commence early in Title II.

3.0 DESIGN CRITERIA

3.1 GENERAL CRITERIA

The Toroidal Vessel forms the first wall of the EBT-P device. It shall be capable of containing a steady-state plasma and shall have a nominal major radius of 4.5 meters and 36 mirror regions. The throat diameter of the vacuum liner at a mirror coil section shall not be less than 34 cm. Maximum flux line for passing partial fraction is 16.0 cm. Ports shall be provided for all diagnostics required to monitor device performance. Additional ports shall be provided for future diagnostic applications and, to the extent practical, all anticipated upgrades. Nominal "horsecollar" ports for diagnostic provide viewing of 17.5 cm flux line inboard and 12 cm flux lines outboard at cavity centerline.

The Toroidal Vessel shall be suitable for operation at a base pressure no greater than 10^{-7} torr. All flanged connections and extensions of the vacuum boundary shall provide vacuum tight joints.

The Toroidal Vessel shall be capable of totally containing the injected microwave energy. Microwave seals shall be provided to ensure microwave containment. The mirror cavity shall be removable without effecting the mirror coil alignment.

The Toroidal Vessel shall maintain its structural integrity when subjected to dead weight, pressure load from vacuum, coolant pressure, thermal load from expansion, contraction of the Toroidal Vessel, and loads due to assembly tolerances. The portion of the vacuum vessel in the coil throat shall be designed for minimum thickness, compatible with structural requirements in order to maximize the coupling between the mirror coils and the plasma. The mirror cavity ports are designed for negligible load for diagnostics and thus diagnostics must provide their own support. Bellows may be required to prevent restraint of the Toroidal Vessel by diagnostics.

The Toroidal Vessel cooling system shall be capable of adequately dissipating 5 MW of input power. The maximum bulk water temperature shall not exceed 93°C (200°F).

Actively cooled limiters of suitable material shall be provided internal to the Toroidal Vessel where required to protect the walls from the heat flux and erosion.

3.2 SPECIFIC CRITERIA

Operating Conditions - The Toroidal Vessel shall be capable of operating for 1000 hours per year of plasma-on time, 7000 hours per year of standby time and 1000 complete thermal cycles per year over the 10-year life of the device. The heating power into the torus will be 2.0 MW the first three years and 5.0 MW thereafter to the tenth year.

Environments - The Toroidal Vessel shall be capable of operation under the following environments.

Pressure - Internal pressure of 10^{-7} torr or less with an external pressure of 14.4 ± 0.5 psia. Coolant supply pressure is 125 psig ± 13 (139 psia ± 14) Toroidal Vessel and limiters. An assumed 150 vacuum cycles per year (1500 total) will be used for life analyses of the vessel walls.

Thermal - Steady-state surface heat flux of 5.0 W/cm^2 on the mirror cavity wall and port surfaces, 13.5 W/cm^2 on the vacuum liner side wall and 20 W/cm^2 on the vacuum liner throat. An assumed 10,000 thermal cycles will be used at these flux values for life analyses of the vessel walls. Each thermal cycle is a full heat up to steady state condition followed by a complete cool down.

X-Ray - Accumulated x-ray dose of 10^9 Rads over the 10-year lifespan.

Vibrations - The Toroidal Vessel shall be designed to minimize the effects of vibration to the maximum extent practicable. Where this is not possible, the effects of vibration shall be considered in Toroidal Vessel design.

Seismic - For preliminary design, estimated incremental acceleration values due to a seismic event shall be determined using the Uniform Building Code specified methods and seismic zone 2.

For detailed design, a dynamic response analysis shall be performed to verify the adequacy of the preliminary design acceleration values.

Structural Criteria - The Toroidal Vessel shall satisfy the strength requirements, using as a guide the ASME Boiler and Pressure Vessel Code, Section VIII, Division 2. The following specific data must be adhered to. The maximum shearing stress theory of failure will be used.

Design Stress Intensity Values (S_m) for Materials (Least of Following)

Vessel Walls

- 1/3 of minimum ultimate tensile strength at room temperature
- 1/3 of minimum ultimate tensile strength at temperature
- 2/3 of minimum tensile yield strength at room temperature
- 2/3 of minimum tensile yield strength at temperature

Bolts

- 1/3 of minimum tensile yield strength at room temperature
- 1/3 of minimum tensile yield strength at temperature

Allowable Stress Intensity Limits

- General primary membrane stress $\sim$ K S_m
- Local primary membrane stress $\sim$ 1.5 K S_m
- Primary membrane plus bending stress $\sim$ 1.5 K S_m
- Primary plus secondary stress $\sim$ 3.0 S_m
- Normal operation, K = 1.0
- Fault or earthquake conditions, K = 1.2

Factors of safety for shell buckling:

- Theoretical linear analysis including linear Eigenvalue solutions from finite element and finite difference computer codes. - 5.0
- Theoretical analyses methods that take into account at least one nonlinearity. - 3.0
- Empirical analysis or theoretical analyses utilizing a correlation factor based on test results. - 1.5

Fatigue

- ASME code methods and allowables will be used.

Deflections

- No detrimental deflections will be allowed.

4.0 TOROIDAL VESSEL DESCRIPTION

The Toroidal Vessel has a major radius of 4.5 m and is comprised of 36 sections. Each sector is made up of a vacuum liner and mirror cavity. The vacuum liner is located in the bore of each mirror coil vacuum dewar with a radial clearance that results in the vacuum liner being non-integral with the mirror coil assembly. The sidewall of each vacuum liner acts as a flex joint to accommodate thermal expansion and misalignment of the torus. Access ports are provided in each mirror cavity, which is located between each vacuum liner. Each mirror cavity contains actively cooled limiters which protect the toroidal vessel walls from excessive heating and erosion. (See Figure 1.0-1).

The toroidal vessel is non-integral with the mirror coils. A nominal clearance of .25 inch between the mirror coil x-ray shield bore and the vacuum liner allow external magnet alignment without loading up the dewar side walls. The mirror cavities and vacuum liners are assembled by clamping flanges together with a copper wire gasket providing the vacuum seal. The vessel is designed for suitable operation at a base pressure no greater than 10^{-7} torr. The vessel maintains its structural integrity at steady-state proof-of-principle plasma requirements.

During Title I, much effort was devoted towards selecting the vessel materials, port size and shape and selection of the vessel and port seal/flange combination. The mirror cavities are designed for removal from the torus without affecting the mirror coil alignment. The limiters can be removed and replaced without removal of the mirror cavities.

Much additional effort was devoted to the design of the vacuum liner shape to maximize passing particles. Nominal flux lines are shown in Figure 1.0-1. The following items were modified to maximize passing particles: 1) the mirror coil dewar corners in the throat were rounded, 2) an extensive x-ray analysis was performed to allow trimming the corners of the x-ray shield, 3) the vacuum liner surface was designed such that it was contoured to match the flux lines; and 4) the wall thickness of the vacuum liner was minimized.

Table 4.0-1 summarizes the design characteristics of the Toroidal Vessel.

Table 4.0-1 EBT-P Device Design Summary

System Element	Design Characteristics
• Toroidal Vessel	• Major radius of 4.5 meters • Non-integral with mirror coils which allows individual adjustment of mirror coils • Provides 36 mirror regions • Cooling system for 5 MW input power - Maximum bulk cooling water temperature 93°C (200°F) • Provides ARE coil upgrade accommodation • Clamped joints for easy disassembly • Operation base pressure 10^{-7} torr
• Vacuum Seals	• Proven flange/seal technology • Metal seals for x-ray and microwave environments
• Microwave Seals	• Metal-to-metal seal
• Mirror Cavity	• 316L stainless steel • Actively cooled construction • Ports provided for: - Large ports 13.7 in. (34.8 cm) for primary high vacuum pumping and diagnostic viewing - Other Ports For: - Toroidal Vessel vacuum roughing - Diagnostics and anticipated diagnostic upgrades - ECRH feed-throughs - ICRH upgrade feed-throughs - Ion gauges - Fuel injection - Limiter Feed-Throughs (Four Per Cavity) • Future anticipated upgrades such as direct ion heating, partical control, and alternate fueling methods
• Vacuum Liner	• Material: 316L stainless steel - Integrally cooled double wall construction - Minimize wall thickness throughout part - Maintain minimum distance between mirror coil and plasma to maximize plasma coupling • Sized to maximize passing particles

Table 4.0-1 EBT-P Device Design Summary (Continued)

System Element	Design Characteristics
• Limiters	• Actively water cooled for 5 MW total upgrade power • Material is aluminum casting with a copper alloy liner for coolant system corrosion protection • Adjustable to provide uniform heating and can reduce plasma radius • Provides protection to the Toroidal Vessel
• Toroidal Vessel Support	• Nonintegral with mirror coils - Allows individual alignment of mirror coils • Compatible with ARE coil upgrade accomodations • Adjustable struts • Cantilever support for lateral constraint

present fabrication plan is to attach the port extensions to the basic shell by intermittent welds around external side of the shell followed by a continuous full penetration weld on internal side of the shell. After all extensions have been welded the extension would be straightened and sized if necessary prior to installing, aligning, and welding the port flanges.

4.2 VACUUM LINER

The vacuum liner is also designed for fabrication of a double wall heat exchanger type construction as shown in Figure 4.2-1. Section View shows the cross section of the coolant passages. The inner sheet thickness is 0.10 inch with the outer embossed sheet 0.062 inch thick. The vacuum liner is fabricated in two halves then assembled onto the mirror coil dewar and butt welded at the internal diameter of the two halves. Each vacuum liner half will be preassembled with the "wheeler" vacuum flange prior to installing them onto the coil dewar. The vacuum liner assembly is designed slightly undersize on the sector width to allow clearances when being installed on the torus and attached to the mirror cavity sections. During removal of the adjacent mirror cavity, removing the clamping forces between the mirror cavity and the vacuum liner will allow the liner to return to the original undersize configuration. Undersizing the liner width also reduces the thermal stresses in the side wall during operation. The proper undersizing and springrate of the vacuum liner will be determined during Title II design and from the machine R&D Seal Development Test Unit.

4.3 EBT-P LIMITER DESIGN

The limiter segments are semi-circular in shape, basically rectangular in cross-section with round edges. A pair of segments forms a limiter ring and in operating position slightly overlap at the vertical extremities, each segment being out-of-plane with its corresponding segment by its own thickness plus clearance.

The limiter consists of an inner copper casting which provides the coolant channels and structure, and an outer coating of aluminum. The aluminum cast around the inner copper core provides a good thermal interface between the two materials. An aluminum/copper allow casting will be checked for vacuum outgassing properties and dissimilar metal compatibility in machine R&D during Title II.

FIGURE 4.2-1 VACUUM LINER CONFIGURATION

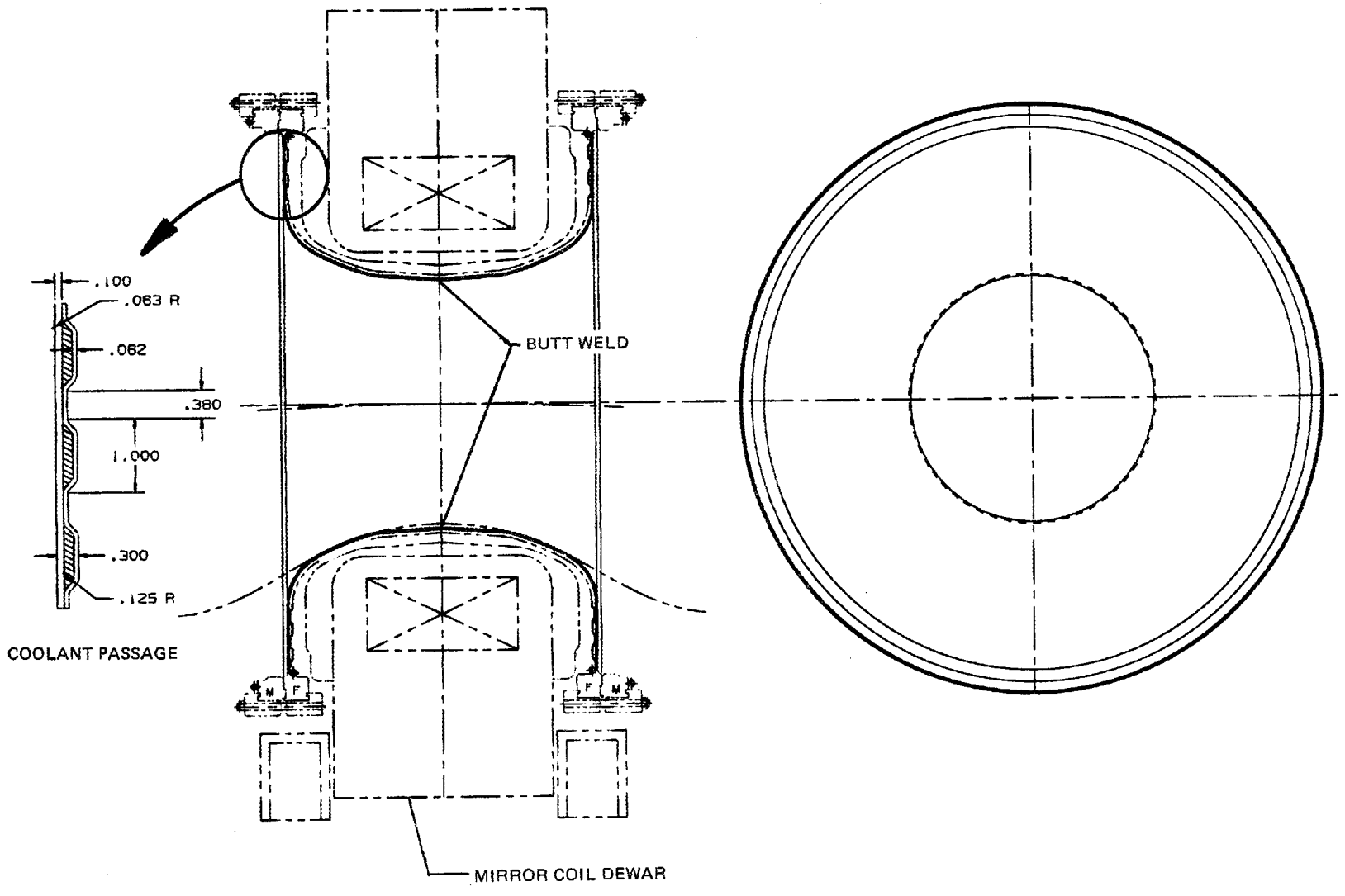

The use of aluminum in the EBT-P demineralized water system was originally prohibited. This restriction was self imposed by MDAC, primarily based on MDAC experience on spacecraft water systems. The restriction on the use of aluminum was causing the design of the limiters to include a bimetal design in order to provide an external aluminum limiter surface for plasma purity and also provide an internal copper alloy cooling channel surface for corrosion reasons. The baseline design concept was to cast a copper alloy intercasting to serve as the coolant passage and cast an aluminum outer surface around the copper alloy casting to provide a low Z material which is exposed to the plasma.

A thorough investigation was initiated to determine if the self imposed restriction is viable for the EBT-P experimental device.

The results of the investigation is documented in EBT-P-TN-011 and concludes that the use of stainless steel, aluminum, and copper in the EBT-P demineralized water system is not expected to cause any major problems. With the approval of EBT-P-TN-011 the limiter will be redesigned during Title II to use an all aluminum limiter design.

The following description pertains to the baseline limiter design.

As previously stated, the copper was thought to be necessary to avoid corrosion problems between aluminum and the dimeneralized water supply. Copper also provides sensing by the spectrometer if the aluminum erodes sufficiently to expose the copper thus indicating need for limiter replacement. Figure 4.3-1 shows an adjustable limiter elevation and section.

The inboard limiter segments are all adjustable; one pair of limiters in one cavity is remotely adjustable from the control room, the remainder are manually adjustable. Adjustments of $\pm .50$ inches from nominal is provided.

The inner bearing area of the stainless steel feed-thru tube welded to the cavity, supports the limiter on the feed-thru arm which is machined to obtain a close clearance fit.

FIGURE 4.3–1 LIMITERS CONFIGURATION

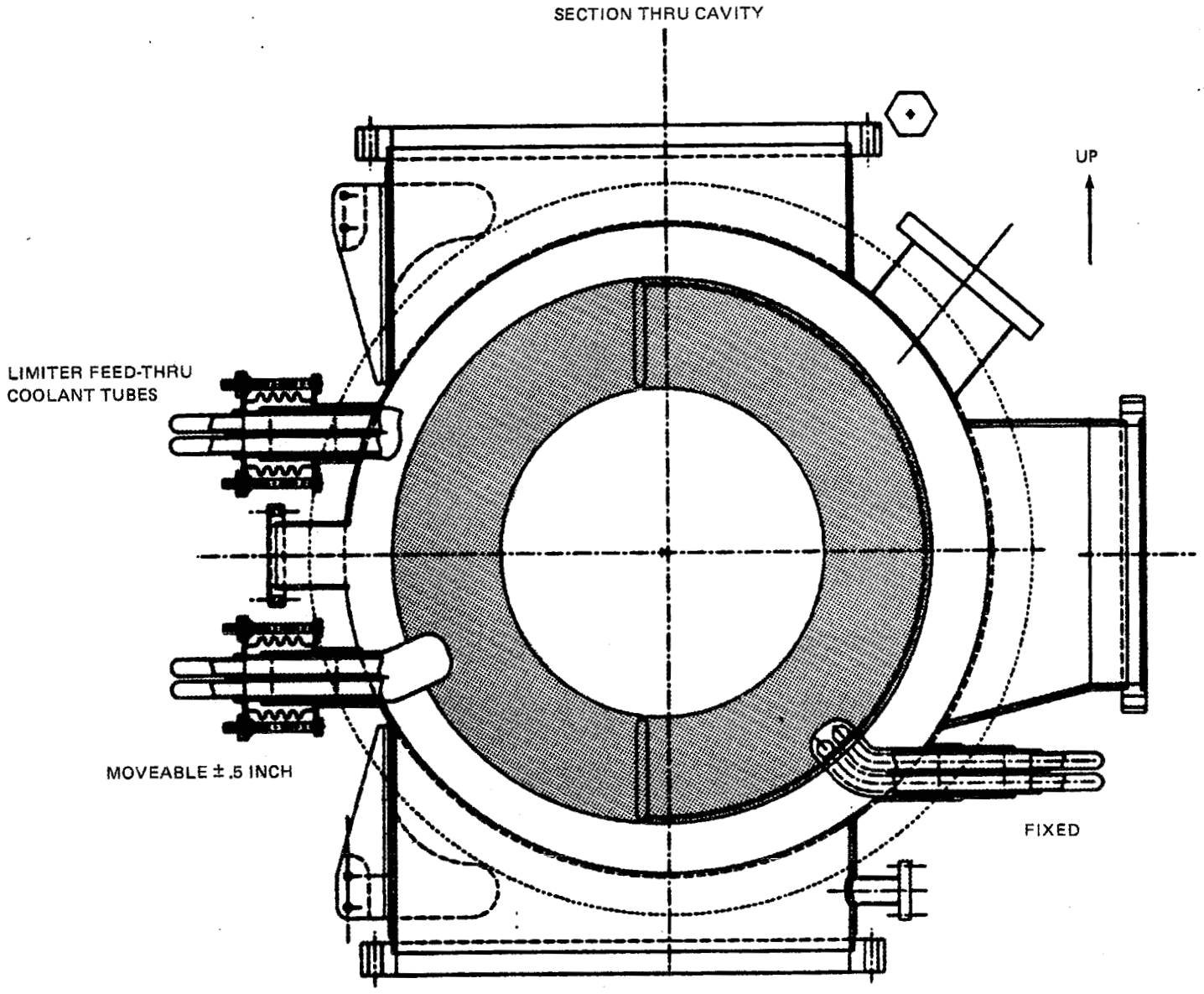

The inner circular copper core extends radially outwards, and provides an outer support reacting against the steel feed-thru. A formed bellows, is welded to the feed-thru at the inner end and to a stainless steel flanged fitting at the outer end. This fitting is brazed to the copper core completing the vacuum seal.

Two studs located either side of the feed-thru in the vertical plane are attached to the feed-thru at the inboard end, and pass through holes in the flanged fitting at the outboard end. Adjustment of the limiter is effected by turning the retaining nut on each stud in the direction required.

Absolute location is determined by an adjustable pointer fastened to the flanged fitting and indicating location on a series of grooves machined into the upper stud. Initial setting of the pointer is made upon installation of the limiter using a basic reference determined by the position established by the remotely adjustable limiters. The limiter adjustment system will be designed to prevent the limiter from being retracted to the point where the vacuum liner is limiting the plasma size.

Title II will establish the actuation arrangement for the remotely controlled limiters (one cavity-two limiters). Displacement capability will be 1.0 inch total, with location sensed by a linear potentiometer. Water temperature sensing and thermocouples in the limiter will also be provided. Limiter configuration, feed-thru's, support, and connections are similar to the manually adjustable limiter arrangement.

The outer limiter segments, which are less critical, are fixed in place and hermetically sealed by brazing the copper outlet arm to the stainless steel feed thru. A close tolerance fit on the inner support gives accurate poloidal positioning and precludes microwave losses. Radial adjustment of $\pm .25$ inches, prior to final brazing is provided.

5.0 SUPPORTING ANALYSES

The Title I analysis supporting the Toroidal Vessel design are presented in this section. Three major topics are discussed: The Vacuum Vessel Seal and Material Trade Study (Section 5.1); the Structural Features of the Recommended Design (Section 5.2); and the EBT-P Limiter Analysis (Section 5.3).

5.1 VACUUM VESSEL SEAL AND MATERIAL TRADE STUDY

An extensive trade study on the choice of vacuum vessel seal and wall material was conducted during the Title I engineering phase. The study was prompted by the concern over the baseline elastomer seals being able to survive the intense x-ray, thermal and microwave environments projected for EBT-P.

The trade study approach was to first assess the adequacy of the baseline aluminum vessel/elastomer seal design. This required detail computation of the environments imposed on the vessel wall and seals. The results of the analysis indicated that the seals would be subjected to x-ray levels of 10^9 rads and substantial microwave heating. The microwave heating of elastomer seals could be minimized by a microwave seal protection scheme but protection against x-ray was not feasible. The only recourse would be frequent replacement of the elastomer seals which would be prohibitively expensive and unacceptable for EBT-P.

Since elastomer seals were considered unacceptable for EBT-P other candidate seals, e.g. polyimide or soft-metal seals, that are compatible with an aluminum vessel were evaluated. Polyimide materials, although having a higher threshold to x-ray or thermal damage than elastomers, have not been used for large O-ring applications and are a relatively hard material. Soft metal seals have been used with aluminum flanges, but this experience has been limited to small diameter seals in applications with static conditions. Since alternate seals that could be used with an aluminum vessel did not appear promising, a concentrated effort was initiated to evaluate various stainless steel wall concepts with metal seals. Stainless steel vessels with metal seals are extensively used in the vacuum industry and metal seal systems are available as off-the-shelf items.

After completing the technical assessment of the aluminum and stainless steel options, detail cost data were developed for the best concept within each option. An integrally-cooled corrugated stainless steel structure with metal seals was recommended as the best approach for meeting the project objectives.

A summary of the trade study is presented in this section. The items summarized include the definition of the vacuum vessel environments, assessment of elastomer seals, evaluation of metal seals for aluminum and stainless steel concepts, analysis of various stainless steel concepts and comparison of costs for the aluminum and stainless steel options. Detail information on the trade study is presented in References 1 through 3.

5.1.1 Thermal and X-Ray Environments - Detailed calculations of the x-ray, microwave heating of seals, and vessel wall heat loads were performed to provide the basis for material selection. The level of these environments depend on the RF power into the torus and the accumulated time of operation over the 10-year life of the facility.

The following table presents the RF power levels proposed for EBT-P and, as-a-point-of-comparison, the operating power for EBT-S.

EBT Power Profile

Facility	Type	Baseline	Upgrade
EBT-P	Bulk ECRH	1.2 @ 60 GHz	3.0 @ 90 GHz
	Annulus ECRH	.4 @ 28 GHz	1.4 @ 45 GHz
	ICRH	1.0	2.6
	TOTAL	2.6 x η[1]	7.0[2]
EBT-S	ECRH	.20 @ 28 GHz	
	ICRH	.10 @ 10-30 MHz	
	TOTAL	.30 x η[1]	

NOTES: 1 η = RF transmission efficiency from RF generators to torus
$0.70 \leqslant \eta \leqslant 1.00$
(Per RFP Design
Criteria)

2 Power into torus (Per RFP Design Criteria) Reduced to 5.0 MW to account for 70% RF Transmission Efficiency

In the computing the accumulated x-ray dose, it was assumed that the facility would operate, on the average, for 1000 hrs/yr over the 10-year life span of the facility.

5.1.1.1 Wall Heating Analysis - Heating of the vessel wall is from two sources: absorption of microwave energy and from plasma particles interacting with the wall surface. These processes are depicted in Figure 5.1-1. Microwave power is reflected numerous times before it is completely absorbed. Most of the microwave energy is attenuated within the plasma (coupled power) but a small portion is absorbed at the wall (uncoupled power). Since the reflectivity of aluminum is .9996 and for stainless steel it is .9979, the absorption of microwave energy for either material is very small. Gaps and imperfections have a much higher absorption. Estimating the energy absorbed by the plasma microwave or the heating of the wall due to particle interaction is extremely difficult. Thus, in establishing the wall heat loads an empirical but conservative approach based on prior EBT-S experience was used. It is a known fact that all of the RF energy reaching the torus must be removed as heat by the vessel coolant system. It was conservatively assumed that 50% of the microwave power input is absorbed at the wall. Assuming uniform absorption over the entire vessel surface, results in a wall heat flux of 5.0 W/cm^2. The other 50% of the microwave power is assumed to be absorbed by the plasma as coupled power. The plasma absorbed energy is then assumed to be transferred uniformly just to the vacuum liner with none to the mirror cavity. This adds another 8.5 W/cm^2 of heat flux to the vacuum liner resulting in a total flux of 13.5 W/cm^2. In reality, the majority of the plasma energy will be absorbed by the limiters. To account for hot spot heating, it was stipulated that the throat region of the liner be capable of withstanding a local heat flux of up to 20 W/cm^2.

FIGURE 5.1–1 VESSEL WALL HEAT LOAD DEFINITION

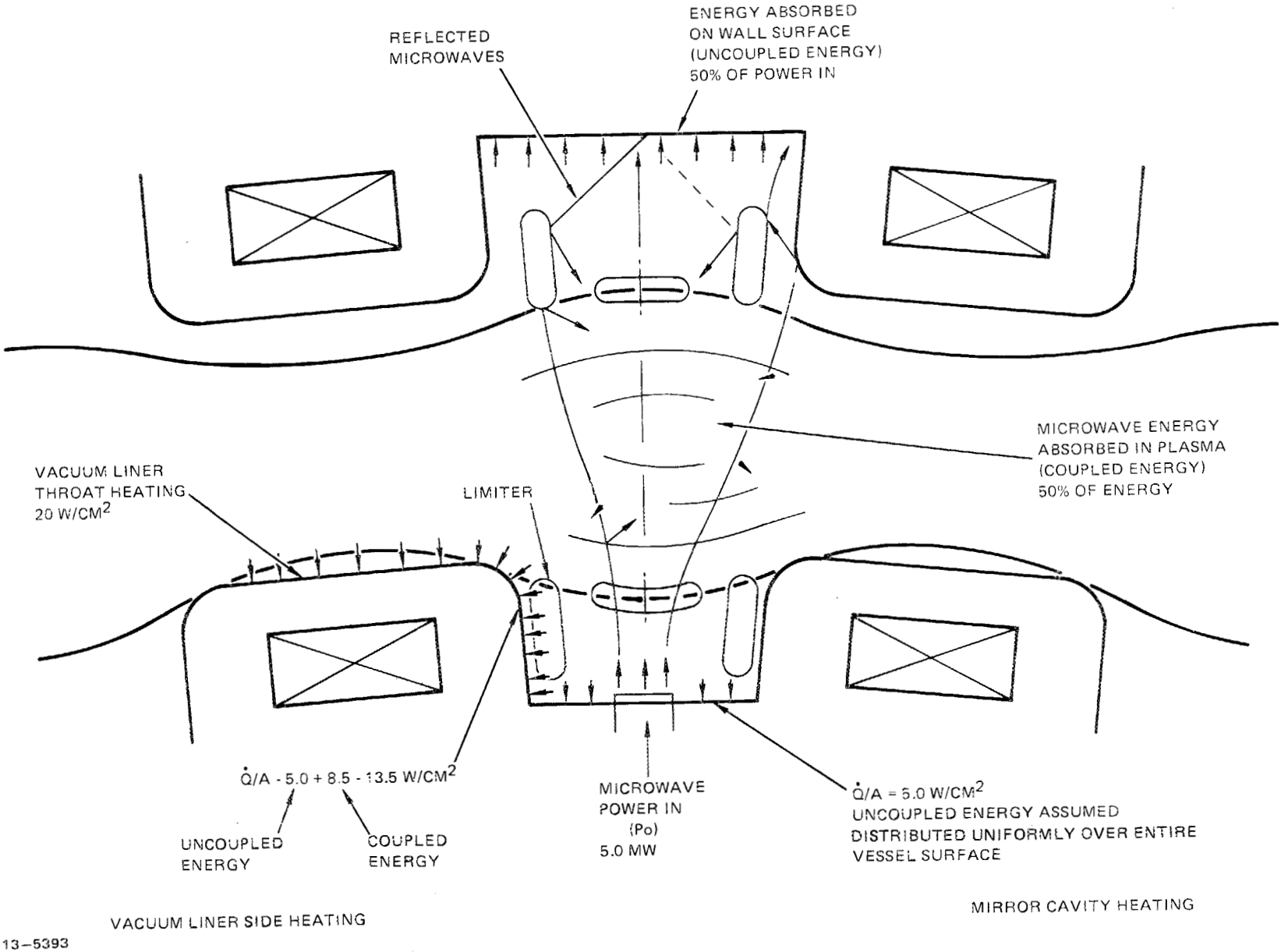

13–5393

5.1.1.2 X-Ray Analysis - Two sources of x-rays are imposed on the vessel wall: direct x-rays, i.e., x-rays emitted directly from the ring, and scattered x-rays, i.e., x-rays emitted by electrons which are scattered out of the ring, as they slow down in the wall or limiters. The seals are essentially unshielded; consequently they will see the full spectrum of x-ray energies, attenuated only by geometric effects. The dose rate in the vacuum seals depends primarily upon the intensity and distribution of the source. X-ray predictions have been made using the model discussed in Appendix A. The methodology and results are summarized in this section.

The direct and scattered x-ray source components are calculated using the following equations developed in Appendix A:

$$P_D\,(E) = 7.12\,(10)^{-5}\,V_R\,f_c\,\beta_R\,B_R^4\,\left[\frac{1 + f_z\,(Z_i^2 - 1)}{1 + f_z\,(Z_{ef} - 1)}\right]\,F_D(E) \tag{5.1-1}$$

$$P_S\,(E) = 7.12\,(10)^{-5}\,V_R\,f_c\,\beta_R\,B_R^4\,\left[\frac{1 + f_z\,(Z_i^2 - 1)}{1 + f_z\,(Z_{ef} - 1)}\right]\,F_S(E) \tag{5.1-2}$$

In these equations P_D (E) and P_S (E) are the direct and scattered x-ray powers per unit of emitted x-ray energy in watts, V_R is the ring volume in cm^3, f_c is the ratio of the background electron density to the microwave cutoff density, β_R is the electron ring beta, B_R is the magnetic field at the ring in Tesla, f_z is the fractional plasma impurity concentration Z; and Z_{ef} are the total and effective charge, respectively, of the sputtered impurity ions in the plasma, and F_D (E) and F_S (E) are given by the curves shown in Fig. 5.1-2. The x-ray dose thus scales as B_R^4 in going from the baseline to the upgrade configuration and increases as $(1 + f_z Z_i^2)$ with the plasma impurity level, since the ring volume, beta and position (which affects f_c) are expected to show little deviation from their nominal values given in Table 5.1-1. It should be noted that these equations are not directly dependent on the microwave input power level. This is because the experiment is expected to operate in a mode where the rings only receive enough of the input power to establish the nominal operating parameters of Table 5.1-1. The remainder of the microwave power is absorbed by the background plasma and does not contribute to the high-energy x-ray component that causes problems for the vacuum seals.

FIGURE 5.1–2 X–RAY SPECTRA FOR AN ALUMINUM WALL

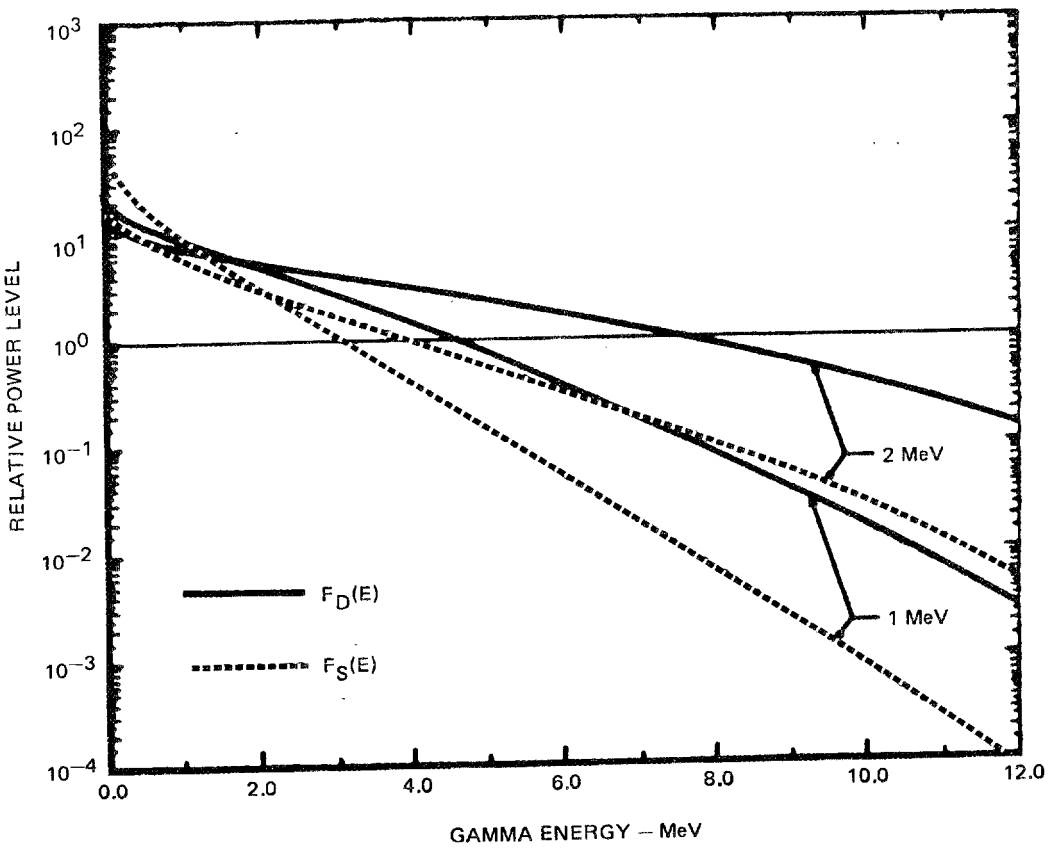

Table 5.1-1 Parameter Values Utilized in the X-Ray Analysis

Parameter	Baseline	Upgrade
V_R (cm^3 per cavity	8333	8333
B_R	0.3	0.3
$\underline{B}_R$ (T)	1.07	1.6
T_R (MeV)	1 – 2	1 – 2
f_c	0.5	0.5
f_z	0 – 0.02	0 – 0.02
Z_i, Z_{ef} (Al ions at 100 eV)	13, 8	13, 8

For the nominal ring operating parameters given in Table 5.1-1, the following assumptions have been made. The ring volume, which is ~ 10% of the total plasma volume, and the cutoff density fraction, which is 0.5, are based on observations from EBT-I and -S. The ring beta of 0.3 represents a physics goal for the EBT-P program, and it corresponds to an upper bound for the present analysis, since effort will focus on raising the background beta once a ring beta of 0.3 is obtained. Various ring temperatures between 1 and 2 MeV have been considered since there is a broad minimum in the ring power requirement over this energy range; however, while different ring temperatures alter the high-energy portion of the x-ray spectra as is indicated in Figure 5.1-1, they have little effect on the dose rate because the lower energy groups, which contribute most of the total dose, are unchanged. Accumulated doses are, therefore only presented for a ring temperature of 1 MeV. The least-well-defined parameter is the plasma impurity fraction, f_z. It is presently thought to be ~ 0.005 for EBT-S conditions, but it will likely be larger in EBT-P where higher ion energies should lead to increased sputtering from exposed surfaces. For this reason f_z is typically set equal to 0.01 for lower input power levels and 0.02 for higher power levels in the present dose calculations, because these impurity fractions are thought to be the maximum allowable before plasma performance is seriously degraded.

The expressions describing the x-ray source (Eqs. 5.1-1 and 2), and the information given in Table 5.1-1 are used to evaluate the dose rate at the vacuum seals, as discussed in Appendix A. For the present vacuum seal radius of 38 cm, the dose rate in the vacuum seals

with no plasma impurities is found to vary from a minimum of 3 Rad/s, for the baseline configuration, to a maximum of 16 Rad/s, for the upgrade configuration. Simlarly for a 2% Al impurity level, the dose rate varies from 8.4 Rad/s in the baseline configuration to 42 Rad/s in the upgrade. Dose rates corresponding to various input levels and plasma impurity fractions are summarized in Table 5.1-2. This information is combined with the projected RF power buildup history to construct the dose accumulation curves shown in Figure 5.1-3. This figure illustrates that even without impurities, the vacuum seals will receive their maximum dose limit of 10^8 Rads in a typical year of upgrade operation and suffer serious performance degradations during the baseline phase.

Table 5.1-2 Plasma Impurity Fraction and Vacuum Seal Dose Rate For Various Input Power Levels

Configuration	Power Level (MW)	Impurity Fraction (%)	Dose Rate (Rads/sec)
Baseline	1.2	1	6.5
Baseline	2.6	2	8.4
Upgrade	2.6	1	32.3
Upgrade	4.0	2	42.0
Upgrade	5.0	2	42.0
Upgrade	6.0	2	42.0
Upgrade	7.0	2	42.0
Baseline	(all)	0	3.1
Upgrade	(all)	0	15.5

5.1.2 Vacuum Seals - A thorough discussion of the shortcoming of the baseline elastomer seals and the key features of alternate seal materials is presented in this section.

FIGURE 5.1–3 X-RAY DOSE ACCUMULATION

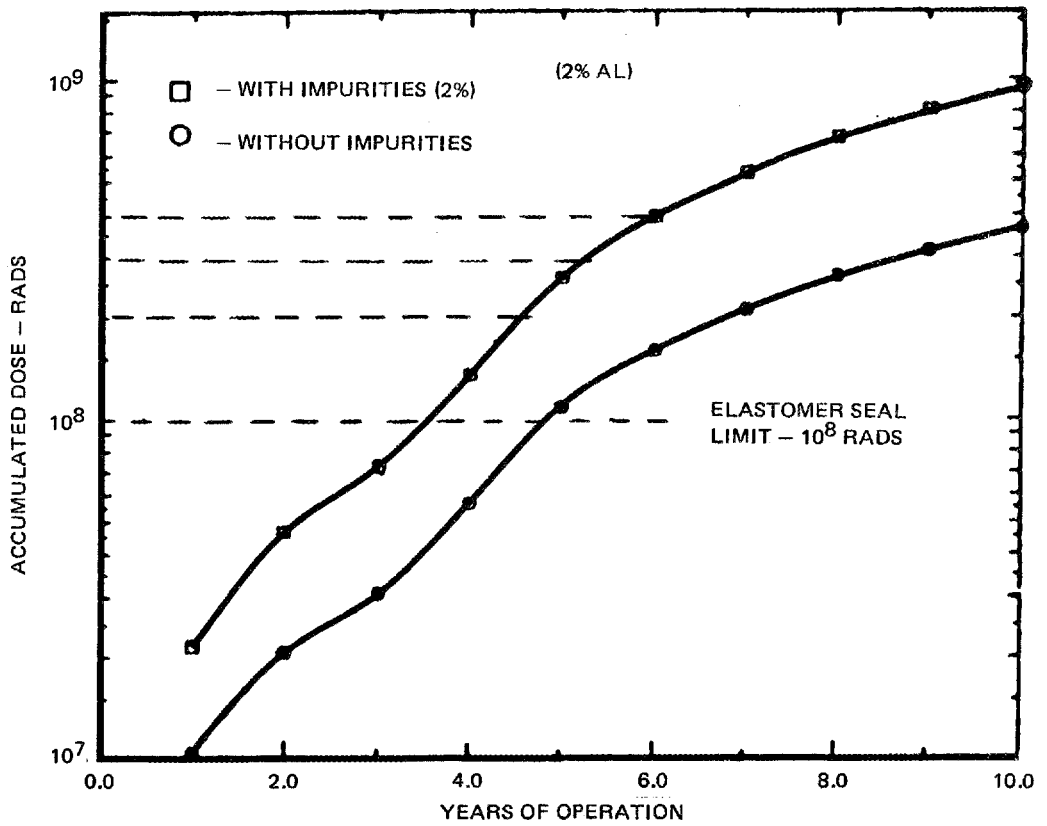

5.1.2.1 Elastomeric Seals - Elastomer o-rings are the most commonly used vacuum seals. A great deal of data and experience in their use exists and shows them to be reliable and easy to use even in very large sizes. However, they are quite sensitive to the thermal and radiation environment. The elastomers most commonly used as o-rings are Buna-N and Viton.

A thorough survey[3] of elastomer materials was performed during Title I. During this survey 10 vendors and 5 engineers familiar with high vacuum seals were contacted. Several technical papers were obtained. The most thorough review of elastomer seals is provided by R. N. Peacock[5]. His review is a compilation of data obtained from 52 technical papers and reports.

The primary considerations in evaluating elastomer materials for use as EBT-P vacuum seals were:

- High vacuum sealing capability
- Low gas permeation
- Low outgassing
- High temperature capability of approximately 250°C
- Radiation capability of approximately x 10^9 rads

A summary of potential elastomers and their capabilities is provided in Table 5.1-3. This information was obtained from the data provided by Peacock[5].

Only three of these elastomers were noted to have good vacuum sealing capabilities, the two Viton compounds and Buna-N. The remainder of the materials are judged not suitable[5] (general concensus of vendors and engineers) due to high outgassing, high permeation or poor vacuum sealing capability. It is recognized that the maximum radiation doses quoted above are conservative and it was assumed that doses one decade higher could be tolerated. Viton and Buna-N are seen to have neither the temperature capability nor radiation resistance required for the EBT-P environment.

Table 5.1-3 A Summary of the Vacuum Seal Characteristics of Various Elastomers

	Maximum Recommended X-Ray Dose Rads	Maximum Recommended Operating Temperature °C	Outgassing Unbaked $\frac{\text{torr liter}}{\text{sec cm}^2}$	Gas Permeation	Prime Seal Application
Fluoroelastomer Viton E-60C*	1×10^7	150	4×10^{-7} to 2×10^{-5}	moderate	generally used vacuum seal
Viton A	1×10^7	150		moderate	generally used vacuum seal
Buna-N	1.5×10^7	85	2×10^{-7} to 3×10^{-6}	moderate	best all-around, low cost vacuum seal
Buna-S	1.5×10^7	75		high	little vacuum application
Neoprene	1.5×10^7	90	5×10^{-5} to 3×10^{-4}	moderate	oil resistance, low cost
Butyl	1×10^6	unknown	2×10^{-6} to 1×10^{-5}	moderate	for specific chemical application
Polyurethene	8×10^7	90	5×10^{-7}	moderate	radiation, mechanical properties
Propyl	8×10^7	175	unknown	high	good mechanical properties
Silicone	1×10^7	230	4×10^{-6} to 2×10^{-5}	very high	electrical applications
Perfluoroelastomer	unknown	275	3×10^{-9}		general checmical resistance
Teflon	3×10^4	280	2×10^{-8} to 4×10^{-6}	moderate	general chemical resistance
KEL-F	4×10^6	200	4×10^{-8}	low	general chemical resistance
Polyimide	1×10^8	275	8×10^{-7}	moderate	high temeprature, general chemical resistance

* Baseline Vacuum Seal

The elastomer o-rings will be heated both indirectly, by plasma heating of the vessel wall, and directly, by the attenuation of microwave power in the seal material. As discussed in the previous section, the microwave heating represents the more severe type of heating and seal temperatures subsequently higher than 150°C will be attained depending on gap size. Microwave heating is a problem, as evidenced by the seal degradation noticed in EBT-S at substantially lower microwave power than EBT-P, but this problem can be minimized by incorporating a microwave seal protection scheme. Two microwave seal protection concepts were evaluated; the baseline lip configuration and a metal o-ring gasket between the plasma heated surface and the elastomer ring. A vacuum passageway for pump down of the virtual leak volume between the metal and elastomer gasket was also provided. Verification testing of the microwave seal protection concept would not be possible until after the Title II design is completed because of schedule problems with the ORNL microwave test facility.

Even if adequate microwave heating protection of the seals is provided, the intense x-ray environments predicted for EBT-P preclude the use of elastomer seals. Detailed calculations by MDAC have established the accumulated x-ray dose level at 10^9 rads. (This value has been corroborated by independent calculations made by ORNL). The 10^9 rads prediction should be viewed as realistic since it is based on nominal modeling procedures, the specified baseline and upgraded physics parameter and an average run time of ~1000 hrs/yr for the 10-year life of the facility. Design safety factors to account for uncertainties in the analysis or for spacial or temporal non-uniformities have not been added. The seal life for elastomer seals is limited to 10^7 rads, according to the manufacturer's data, although successful utilization up to 10^8 rads has been reported in the literature. Even using 10^8 rads as the seal life criteria, the elastomer seals would require replacement at the end of three years, while operating in the baseline power condition, and every nine-months thereafter while operating in the upgrade power mode. The cost and time for such frequent replacement would be prohibitive and is unacceptable for EBT-P operation.

X-ray radiation affects o-rings by causing hardening, embrittlement, and compression set. When the material loses its resistance to the compressive forces of the flanges, its ability to conform to the minute surface imperfections is impaired and vacuum leaks result.

Polyimide is a very attractive seal material candidate in all respects except for the general concensus that, due to its hardness, it would not be a suitable ultra high vacuum o-ring seal. To substantiate this, five persons who have designed and operated at least six major fusion devices were contacted Ref. 6-10. They were:

Contact	Affiliation	Fusion Devices
D. H. Mullaney	Princeton Plasma Physics Laboratory PPPL	PLT, PDX, TFTR
R. B. Fleming	Princeton Plasma Physics Laboratory PPPL	PLT, PDX, TFTR
Don Polk	United Technologies	Univ. of Texas Tokamak
Jim Doggett	Lawrence Livermore Laboratory LLL	MFTF
John Miller	General Atomic GA	Doublet III

Each of these persons has considered polyimide for use as a high vacuum seal, but none use polyimide seals in O-ring configuration. Jim Doggett did report that some success has been achieved with polyimide gaskets (flat sheets) between Conflat type knife edge flanges used in special applications at LLL. No other successful applications were reported.

Several reasons were noted for not using polyimide including: 1) material hardness, 2) potential high temperature creep, 3) lack of seal availability and cost, and 4) high outgassing rate measured at G.A. The material hardness prevents plastic flow into minor surface irregularities[10]. This plastic flow is necessary for elastomer seals to function properly. Perhaps the most significant finding was reported by Bob Fleming. He said that the TFTR polyimide sealed gate valves, which have been the subject of extensive development by VAT Valve, still do not seal properly. VAT has determined that the seal is extremely sensitive to minute particulate contaminants such as dust, lint or sputtered materials. Such contaminants are very difficult to control. Based on these findings, MDAC feels that it is inappropriate to propose using polyimide seals in the EBT-P vacuum vessel.

The review and evaluation of elastomers yielded no promising approach which would allow retention of the baseline O-ring sealed system. Elastomers have lower radiation resistance and temperature capabilities than required for EBT-P. Polyimide has not been found to be a suitable material for use as an O-ring type seal.

5.1.2.2 Metal Seals - Recognizing the shortcomings of elastomer seals, MDAC investigated the potential for using metal vacuum seals on EBT-P. The criteria for a successful metal seal were:

- compatibility with an aluminum vacuum vessel
- proven ultra high vacuum (UHV) seal
- capability to seal during EBT-P thermal cycling
- Availability; preferrably off the shelf

Four metal vacuum seals were investigated:

- Conflat
- Wheeler
- Helicoflex
- C-ring

Numerous technical publications were reviewed and several persons involved in UHV technology were contacted. It is noted that only two metal seal "systems" are commercially available, the Conflat and Wheeler; both are fabricated of stainless steel. The term "systems" is used because a complete vacuum seal consists of a pair of flanges, a seal, and clamping device. Each element is equally important in design and development of the flanges and clamping mechanisms are left to the user. A detailed discussion of each candidate vacuum seal and its potential for use in aluminum or stainless steel vacuum vessels was provided in the MDAC Design Note[1]. A summary is presented below.

Very little experience exists in aluminum, metal sealed vacuum vessels. No experience with the Wheeler or C-ring seal on an aluminum system was discovered. There is limited experience with aluminum Conflats[11] and aluminum flanged Helicoflex seals[12]. However, this experience has been limited to small diameter (typically 6 to 8 inch) seals, and the thermal cycling characteristics are not known. The effects of thermal cycling and increased vacuum seal size cannot be minimized, since changes in size and temperature are known to impact sealing performance[13,14].

There is extensive experience with Conflat and Wheeler vacuum seals in stainless steel vacuum vessels. They are routinely heated to above 450°C, far higher than required for EBT-P, and are off-the-shelf vacuum hardware in the sizes required for EBT-P. Conflats and Wheelers are, however restricted to round configurations. Helicoflex seals have been developed for the large rectangular ports on TFTR. They have been subjected to simulated thermal cycling to verify their performance in the TFTR environment.

Though the Helicoflex seal is not commercially available as a seal "system", extensive engineering data was available describing its performance, especially in the thermal environments. As discussed below, this data serves to lower the risk of such a seal and it is presently one of our candidate seals. The Helicoflex, Conflat and Wheeler concepts, our primary metal vacuum seal candidates are shown in Figure 5.1-6 and are discussed below.

The first concept shown is the Conflat vacuum seal. A copper gasket seal is squeezed between two knife-edged flanges. It employs stainless steel flanges and is the most widely used seal in the high vacuum industry. Its reliability and high temperature capability (450°C) are excellent. However, as the size is increased beyond 0.3 meter diameter, dimensional accuracy and dimensional stability during thermal cycling present difficulties in maintaining good high vacuum seals (Reference 13), though the EBT-P thermal environment will not affect the vacuum integrity of Conflat flanges. Conflat flanges have been made of aluminum for special purpose applications, (Reference 14) though the thermal performance is totally different than for stainless steel. Aluminum alloy (2219) flanges with a CrN coating for hardening, are used with high purity 1050 aluminum gaskets. Other problems with such flanges include their reusability and problems associated with welding large numbers of aluminum flanges into the Toroidal Vessel. Reusability is a concern because the aluminum knife-edge flange, which is much softer than the proven stainless steel flange, may suffer degradation for high temperature use or from numerous seal replacements.

A second type of metal vacuum seal is the Wheeler seal. A copper wire seal is captured in a triangular flange groove. Its advantages are identical to those just described for the Conflat flange except that it is available in sizes up to one meter diameter. Aluminim versions of this flange were not found. Its primary advantage is the capability to be used in

Figure 5.1-6 VARIOUS METAL SEALING CONCEPTS

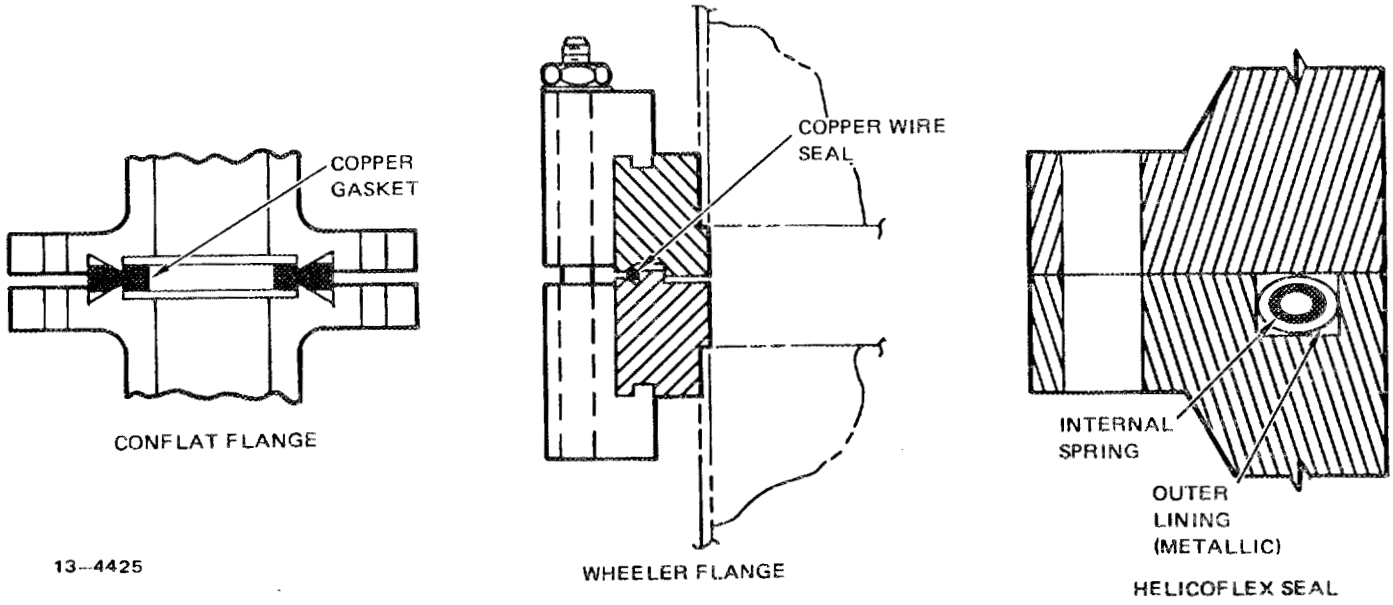

DETAIL OF THE HELICOFLEX SEAL

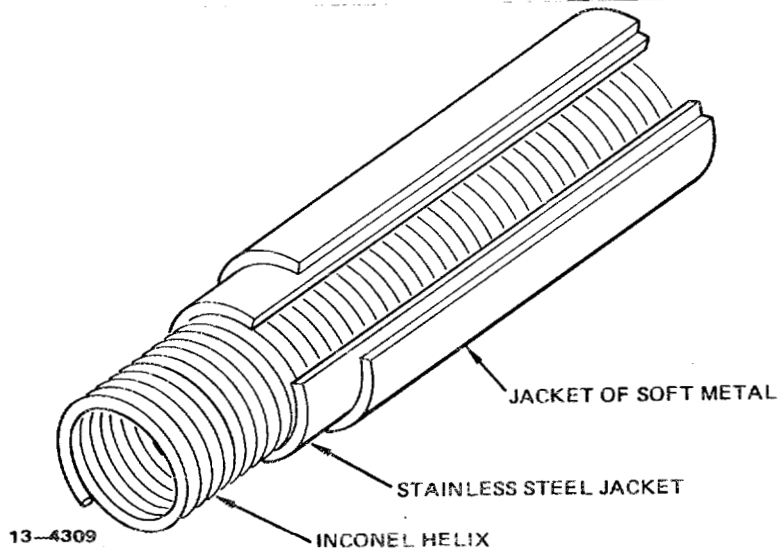

large sizes, making it a candidate for use on the 76 cm diameter seal connecting the mirror cavity to the vacuum liner.

A third metal sealing concept is the Helicoflex seal. The seal, squeezed between two flanges, has a circular cross-section and is all-metal construction. Details of the seal are shown in Figure 5.1-6. A stiff coiled spring is surrounded with a stainless steel jacket and provides resistance to the compressive sealing loads. The jacket is coated with a softer material which, under load, is deformed into the flange surface imperfections to make a high vacuum seal. Such seals are used in high vacuum applications, mostly in Europe. Their use in fusion devices includes the large (74 cm x 89 cm) rectangular port on TFTR (Reference 15). A primary advantage of this seal is its capability to be used in large, noncircular applications, making it a candidate for the 76 cm diameter seal in EBT-P. Two disadvantages are its sensitivity to thermal cycling which could result in vacuum leaks, and that a seal "system" is not available. This seal also requires approximately 1700 pounds per inch sealing forces which increases the design complexities. In discussions with the seal manufacturer, it was determined that use with aluminum was possible and some experience exists (Reference 12). A disadvantage is the thickness of the aluminum flanges required to apply the high sealing forces. Mirror cavity access in EBT-P is already quite limited and very thick flanges will only aggrevate the problem.

Dag Pfieffer of Advanced Products (9-9-80 and 3-2-81), Barry Corona of Production Products (10-10-80 and 4-8-81), and Mike Rothkopf of UAP (early 81) visited MDAC to discuss metal coated C-rings. They did not feel such seals were well suited for use on EBT-P, because of the cyclic thermal environment and the requirement to reach an ultimate pressure of at least 1×10^{-7} torr.

ORNL found that some experience existed at BNL with indium coated C-rings on a stainless steel vessel. A visit was arranged and the findings were reported. We found that the seals have been made to work, though with difficulty. The impact of thermal cycling has not been determined, since their seals remain at room temperature. BNL personnel recommend that, for a new design, Conflat seals be used wherever possible.

A further investigation of the use of indium coated C-rings in the fusion community was performed. We found that these seals are not used in any of the 7 fusion devices discussed.

Bob Fleming (PPPL) reported success with this seal at cryogenic temperatures, but felt that high temperature (150C) use would present numerous problems. Dave Mullaney (PPPL) and John Miller (G.A.) have tried indium coated C-rings, both without success. John Miller also expressed the belief that a large size C-ring, such as the 76 cm seal on EBT-P, would be very difficult to seal reliably because of required flange flatness.

MDAC has some recent experience in the use of C-rings. MDAC and Hughes received contracts from LBL to build prototype TFTR neutral beam ion sources. Because of the TFTR radiation environment, metal seals rather than elastomers were desired by LBL/PPPL. Knife-edge type seals and metal C-rings were candidate seals. After extensive development testing, a rectangular shaped, lead coated C-seal was selected, both my MDAC and Hughes. MDAC awarded a subcontract to Advanced Products and Hughes selected Pressure Science Inc. to fabricate seals. Both subcontractors had extreme difficulty in fabricating acceptable seals. Problems were also encountered in using the seals. Ultimately the C-seals were replaced with O-rings to meet scheduled delivery dates. The radiation hardness requirement was deleted.

C-ring seals have been exhaustively studied. BNL has been successful in replacing O-rings with C-rings, but notes that a new facility design should incorporate a more reliable, easier to use seal. C-rings are not used in the fusion devices surveyed; prospective users including MDAC have found difficulty in achieving UHV seals. Our discussions with vendors and literature reviews have not disclosed any favorable information on C-rings. For these reasons we feel it is inappropriate to propose that EBT-P be designed to use C-ring seals.

Survey of Fusion Devices - During the week of 20 July 1981 a survey was performed in which engineers responsible for 7 major fusion devices were contacted. A summary of our findings is presented in Table 5.1-4. Six of the devices are constructed of stainless steel and one of Inconel. None successfully use polyimide O-rings, though polyimide gaskets between knife-edge flanges are used on MFTF; the TFTR VAT valve polyimide seals experience problems related to particular contamination. None of the devices use indium coated C-rings. All devices, except PLT, use Conflats wherever possible; we find it to be the universally used metal vacuum seal for round ports up to 12 inch diameter. G.A. uses 24 inch diameter Conflats on Doublet III and routinely heats them to 250°C. ISX uses

Table 5.1-4 Survey of Fusion Devices

Device	Contact	Material	Vessel Polyimide	C-Rings	Vacuum Seals	Comments
PLT	Mullaney Fleming	Stainless Steel	not used	not used	Gold wire	Gold wire seals too expensive.
PDX	Mullaney Fleming	Stainless Steel	not used	not used	Conflats Indium coated Copper wire	Conflats used wherever possible Indium coated copper wire used on special ports.
TFTR	Mullaney Fleming	Stainless Steel	VAT valves not working properly	not used	Helicoflex Conflats	Helicoflex used for rectangular ports Conflats used for round ports.
Doublet III	Hager Miller	Inconel	not used	not used	Conflats	Conflats used everywhere up to 24 inch diameter
ISX	Johnson	Stainless Steel	not used	not used	Conflats Wheelers	Wheeler type seal used in non-round applications.
MFTF	Doggett	Stainless Steel	Special gaskets used	not used	Elastomers Conflats	Radiation dose very low. Conflats used where hard seals are required.
Univ. of Texas Tokamak	Polk	Stainless Steel	not used	not used	Indium coated Copper wires Conflats	Indium coated copper wire used for rectangular ports. Conflats used wherever possible.

more than 200 Conflats and Wheeler flanges. TFTR uses Helicoflex seals on large rectangular ports; Univ. of Texas tokamak uses indium coated copper wire for racetrack ports.

Vessel Seal Recommendations - Three major seal options were evaluated; 1) the baseline concept of an aluminum vessel and elastomer seals; 2) an aluminum vessel with indium-coated C-ring metal seals for the large flanges and aluminum Conflats for the port seals; and 3) metal seals with a stainless steel vessel. The use of elastomer seals for the postulated EBT-P X-ray environment was considered too high of risk and eliminated from any further consideration. In order to choose between an aluminum or stainless steel vessel with metal seals, required further assessment of candidate stainless steel options that have adequate cooling for dissipating the vessel wall heat loads. The stainless steel concept evaluation is discussed in the next section.

5.1.3 Vacuum Vessel Wall Material Comparisons - The objective of the vessel wall material study was to first identify candidate stainless steel concepts that could provide adequate cooling and second perform detail thermal/structural analysis and fabrication assessment to ensure selection of a viable concept of near optimum geometry . The drawback of stainless steel as a vessel material is due to its inherently low thermal conductivity. To overcome this deficiency, the distance between the heated surface and coolant must be minimized. After some initial screening, three basic stainless steel concepts emerged as viable candidates. These are depicted in Figure 5.1-7 and consists of: 1) a skin and tube concept that is similar to the initial aluminum baseline but differs in material; 2) an integrally-cooled corrugated structure with the corrugations forming the integral passages for coolant flow; and 3) a copper-backed stainless steel composite with the copper layer providing a high heat transfer media. Within each of the three concepts, a number of variations, principally introduced by the fabrication process, were studied.

In order to assure that all facets influencing the choice of materials have been considered, all MDAC EBT-P project disciplines were asked to assess the impact of the material choice from their point of view. A summary of the responses is presented in Figure 5.1-8. No major obstacle was identified as precluding the use of either stainless steel or aluminum, although there were definite preferences noted for each material on selected issues. A definite overall preference towards the use of stainless steel became apparent. The key is-

Figure 5.1–7 STAINLESS STEEL CONCEPTS EVALUATED

SKIN AND TUBES	COPPER-BACKED CONCEPT	CORRUGATED STRUCTURE √
		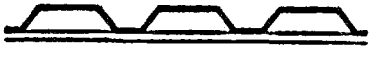
FRABRICATION • SPINFORMING WITH GRAZED ON TUBES	• EXPLOSIVE BONDING • ROLL BONDING • ELECTROFORMED • FLAME SPRAYED • PLASMA SPRAYED	• DIE FORMED (LINER) • HYDROSTATIC FORMED (CAVITY) • HYDROSTATIC FORMED (CAVITY) • CHEM MILLED
COMMENTS • EXCESSIVE TERPERATURE GRADIENTS AND THERMAL STRESSED	• FABRICATION DEVELOPMENT REQUIRED	• LARGE COOLING CONTACT AREA

sues driving the selection were vacuum sealing, particularly resealing and in-situ welding and repairing. All other issues indicated either material was acceptable.

5.1.3.1 Thermal Analysis - Thermal analysis of the various stainless steel design concepts was performed to establish the thermal feasibility of this material as a vacuum vessel structural material. While stainless steel offers many advantages for vacuum sealing and welding, its inherently low value of thermal conductivity makes the thermal designs more challenging.

The thermal analysis was performed with a steady state finite difference heat transfer code called STEDROM. Inputs to the analysis included the design heat flux environments of 5 W/cm^2 on the mirror cavity, 13.5 W/cm^2 on the vacuum liner or 20 W/cm^2 on the liner throat for hot spot heating evaluation. Coolant flow conditions were selected which represent realistic estimates of the demineralized water flow conditions. A convective film coefficient of 1.85 $W/cm^2 °C$ was assumed in coolant flow passages, which corresponds to a reasonable flow velocity of $\sim$ 4 m/s. A mean coolant temperature of 46°C (115°F) was used. Thermal conductivities for stainless steel and aluminum were 18 W/m °K and 151 W/m °K, respectively.

Skin and tube concept. To provide a basis for comparison, Figure 5.1-9 presents the peak temperatures for the initial baseline aluminum design at three vessel locations. The spacing between tubes in the aluminum design was optimized as required by thermal stress considerations. A similar skin and tube concept for stainless steel was examined but it was quickly concluded that a stainless steel skin and tube concept is not practical since it would require exceedingly small tube spacing to limit the temperature gradients and thermal stresses. These conclusions were based on initial estimates of maximum flux on the vacuum liner of 13.5 W/cm^2. The use of later estimates of peak heat flux of 20 W/cm^2 would make the skin and tube concept even less practicle for the vacuum liner.

Integrally - Cooled Concepts - This concept is very attractive from a thermal point-of-view because of the proximity of coolant to the heated surface and the large surface area in direct contact with coolant. The corrugated structure can be fabricated by either die forming the corrugations and seam welding or by spot welding two metal sheets and forming the coolant passages with hydrostatic pressure.

FIGURE 5.1–8 MATERIAL TRADE STUDY FOR EBT-P COMPARING STAINLESS STEEL WITH ALUMINUM FOR THE VACUUM LINER AND MIRROR CAVITY

MATERIAL 216L STAINLESS ← | PREFERENCE 2219-T87 ALUMINUM →

ITEM OF CONSIDERATION	ALUMINUM UNACCEPTABLE	STAINLESS STEEL NEEDED	STAINLESS STEEL PREFERRED	NO PREFERENCE	ALUMINUM PREFERRED	ALUMINUM NEEDED	STAINLESS UNACCEPTABLE	COMMENTS
INITIAL VACUUM SEALING		X						STAINLESS STEEL VACUUM SEAL SYSTEM AVAILABLE CAN WELD SEAL S.S.
VACUUM RESEALING (MATERIAL HARDNESS)		X						ALUMINUM FLANGES MAY BE COINED AND EASIER TO MAR
SEAL FLANGE SIZING			X					STAINLESS STEEL FLANGES ARE THINNER. STANDARD FLANGES AVAILABLE WITH S.S.
STAYING WITHIN ENVELOPES			X					STAINLESS STEEL ALLOWS THINNER FLANGES AND REQUIRES LESS WALL DEPTH
LEAK DETECTION					X			MORE DIFFICULTY IN DETECTING FLAWS IN THE STAINLESS STEEL DOUBLE WALL
OUTGASSING				X				NO DIFFERENCE
MICROWAVE RESISTANCE				X				S.S. HIGH DC RESISTANCE, LOW AC RESISTANCE; ALUM. LOW DC RESISTANCE, HIGH AC RESISTANCE
MICROWAVE ABSORPTION				X				ALUMINUM ABSORPTION LESS THAN S.S., BUT AT 28 AND 60 GHZ, THE DIFFERENCE IS SMALL
MICROWAVE SHIELDING TO SEALS			X					MICROWAVE SHIELDING OF SEALS BETTER WITH S.S. DUE TO LOW ELECTRICAL CONDUCTIVITY
X-RAY INTENSITY AND SHIELDING				X				BREMSSTRAHLUNG APPROXIMATELY TWICE AS HIGH WITH S.S., BUT ALUM. LIMITERS CONTROL IMPURITIES
MAGNETISM OF METAL WALL					X			STAINLESS STEEL MAY HAVE MINUTE RESIDUAL MAGNETISM AT WELDS, BUT NOT AT ROOM TEMP.
ELECTROMAGNETIC FORCES AND FIELD ERRORS					X			STAINLESS STEEL MAY HAVE MINUTE RESIDUAL MAGNETISM AT WELDS PRODUCING SLIGHT ERRORS
EMBRITTLEMENT OF METAL WALL					X			ALUMINUM LESS LIKELY TO EMBRITTLE BUT EMBRITTLEMENT OF STAINLESS IS NOT LIKELY IN EBT-P
CORROSION (COOLANT SYSTEM)			X					STAINLESS STEEL IS PREFERRED. ALUMINUM DESIGN REQUIRES COPPER COOLANT PASSAGES
SPUTTERING EROSION			X					ALUMINUM SPUTTERS TWICE AS FAST AS S.S. EITHER ACCEPTABLE WITH LIMITERS IN PLACE
SPUTTERING AWAY FROM LIMITERS			X					MINIMAL SPUTTERING AWAY FROM LIMITERS
SPUTTERED METAL EFFECTS (RECOATING)				X				IRON SPUTTERS LESS BUT ALUMINUM MAY BE EASIER TO CLEAN FOR DIAGNOSTIC WINDOWS
MATERIAL AVAILABILITY				X				BOTH READILY AVAILABLE EXCEPT IN FORGINGS OR CASTINGS
FABRICATION TO CONFIGURATION (FORMING, MACHINING, PORTS)				X				ALUMINUM IS EASIER TO FORM AND MACHINE BUT CORRUGATED STAINLESS SYSTEMS EXIST
WELDING (SHOP FABRICATION)			X					EITHER SHOP WELDABLE, ALTHOUGH STAINLESS IS EASIER. ALUMINUM MAY BE MORE POROUS
WELDING IN-SITU REPAIR		X						STAINLESS STEEL IS EASY TO FIELD WELD, ALUMINUM IS NOT DUE TO EXTREME CLEANLINESS
MANIFOLDING COOLANT					X			INTEGRAL MANIFOLDING IN STAINLESS STEEL CORRUGATED VACUUM LINER MAY BE SLIGHTLY STIFFER
COOLANT PASSAGE DESIGN AND ROUTING					X			ROUTING OF COOLANT MUCH LESS SENSITIVE WITH ALUMINUM DUE TO HIGHER THERMAL CONDUCTIVITY
COOLANT FLOW RATE, PRESSURE AND Δ					X			PRESSURE DROPS MAY BE LOWER IN THE COOLANT TUBES OF THE ALUMINUM BASELINE
MAXIMUM TEMPERATURE OF WALL			X					STAINLESS HAS A HIGHER TEMPERATURE CAPABILITY, ALTHOUGH THERMAL STRESS LIMITS ITS USE
THERMAL EXPANSION			X					THERMAL EXPANSION RATE OF ALUMINUM IS HIGHER, ALTHOUGH TEMPERATURES ARE HIGHER WITH S.S
STIFFNESS OF VACUUM LINER					X			ALUMINUM HAS A LOWER MODULUS OF ELASTICITY, BUT STIFFNESS IS ALSO DESIGN DEPENDENT
EVACUATION STRESS			X					THE HIGHER MODULUS OF ELASTICITY OF STAINLESS STEEL REQUIRES LESS CROSS SECTION
THERMAL STRESSES					X			LOWER WITH ALUMINUM DUE TO HIGHER THERMAL CONDUCTIVITY
FATIGUE LIFE					X			ALUMINUM HAS LONGER FATIGUE LIFE DUE TO LOWER THERMAL STRESSES
WEIGHT					X			ALUMINUM WOULD BE LIGHTER
COST				X				NO SIGNIFICANT COST DIFFERENCE IDENTIFIED
RISK		X						OVERALL RISK IS LOWER WITH STAINLESS STEEL DUE TO VACUUM SEALING AND WELD REPAIR

FIGURE 5.1–9 TEMPERATURES IN SOLID ALUMINUM VACUUM VESSEL WALLS WITH LIMITERS AND 7.0 MW INPUT POWER

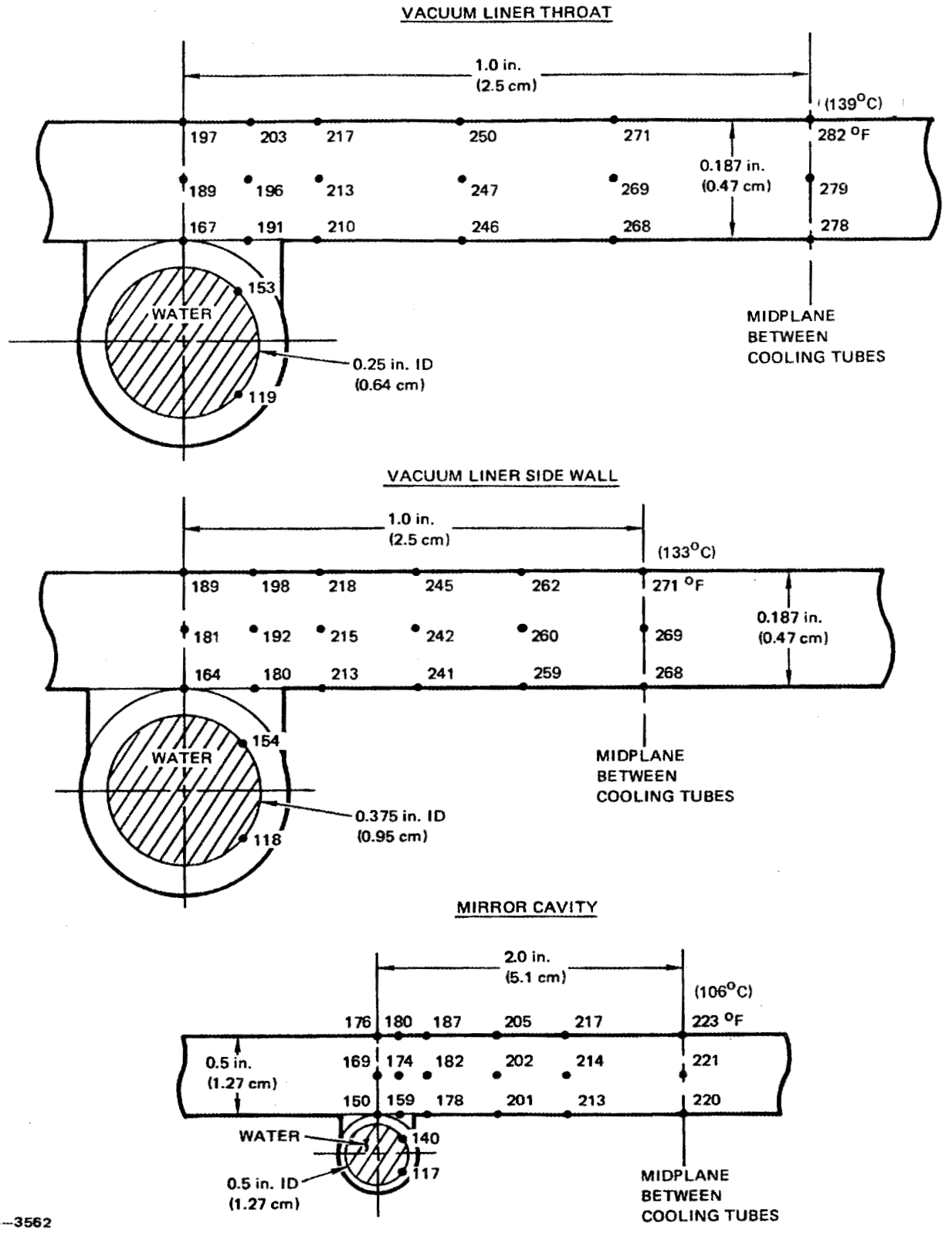

13–3562

Parametric thermal analysis were conducted to evaluate the sensitivity of temperatures with wall thickness and distance between coolant passages or channels.
The parametric results are presented in Figures 5.1-10 to 5.1-15. It should be noted that the parametric analyses were initially based on 13.5 W/cm^2. The same trends in sensitivity are expected for the increased heat flux of 20 W/cm^2 and slight variations in the wall geometry. Determination of the final geometry is an iterative process using the results of the sensitivities shown in Figures 5.1-10 to 5.1-15. Figures 5.1-10 to 5.1-14 show the sensitivity of peak temperature to variation in wall thickness, channel dimensions, and heat flux. These parametric data were used to optimize the corrugated structure configuration. Figures 5.1-10 shows that to minimize the thermal gradients and thermal stresses the weld land width between corrugations should be limited to that required for welding. Initially a minimum weld land width of .32 inches was used. For the die formed concept, the vendors report that the weld land width is be limited to .375 inch minimum. Figure 5.1-15 compares the peak temperatures for a near optimum corruaged steel design with the initial alumimum baseline. The stainless steel design can tolerate heating rates of up to approximately 30 W/cm^2, which is even higher than the design requirement of 20 W/cm^2. The capability of the aluminum concept, which was originally designed for 13.5 W/cm^2, can be extended to higher heating levels by reducing the distance between tubes.

Copper Backed Concept - This concept utilizes a copper layer in back of the stainless steel skin to enhance heat flow to the coolant tubes. Only small temperature gradients will develop within the copper clad steel structure. This concept is very attractive from thermal considerations, however fabrication costs and development expenses are high. Fabrication considerations of the copper backed concept are presented in Section 5.1.3.3.

5.1.3.2. Strength and Life Analyses - Structural analysis was performed for several of the vacuum liner design concepts. Analysis considered mechanical stresses, thermal stresses, and thermal fatigue life. Mechanical stresses result from coolant pressure (approximately 150 psi) and the vacuum loading. Thermal stresses result from constraining the vacuum vessel from thermal expansion, temperature gradients through the wall, and internal constraint resulting from the vacuum liner being colder at the coolant passages.

Thermal fatigue of the vacuum liner was considered to estimate design life. Life predictions were made using the design curves in the ASME Boiler and Pressure Vessel Code for

FIGURE 5.1–10 TEMPERATURE GRADIENT IS VERY SENSITIVE TO WELD LAND WIDTH

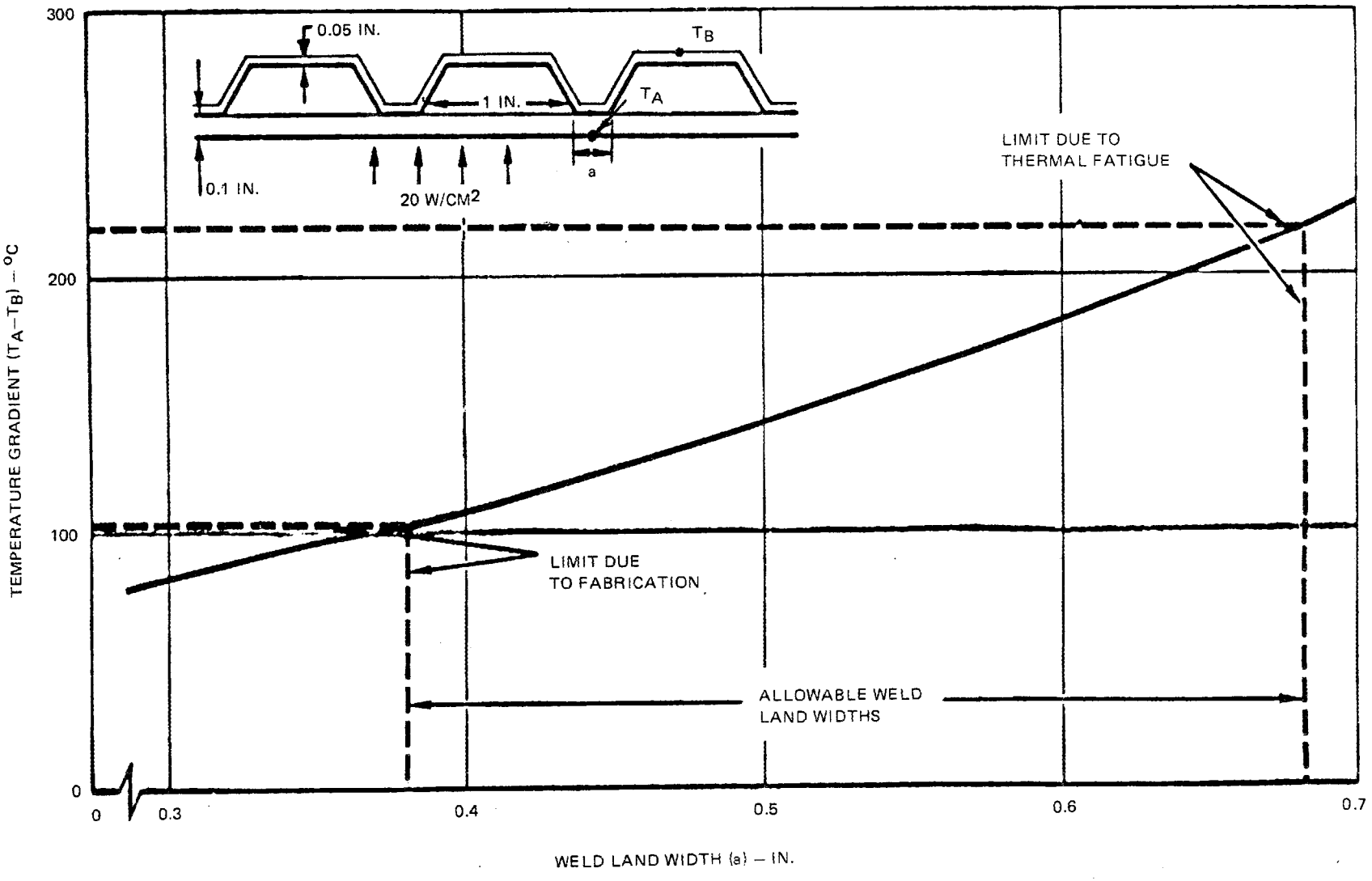

FIGURE 5.1–11 INCREASING THE INSIDE SKIN THICKNESS CAN DECREASE THE PEAK TEMPERATURE

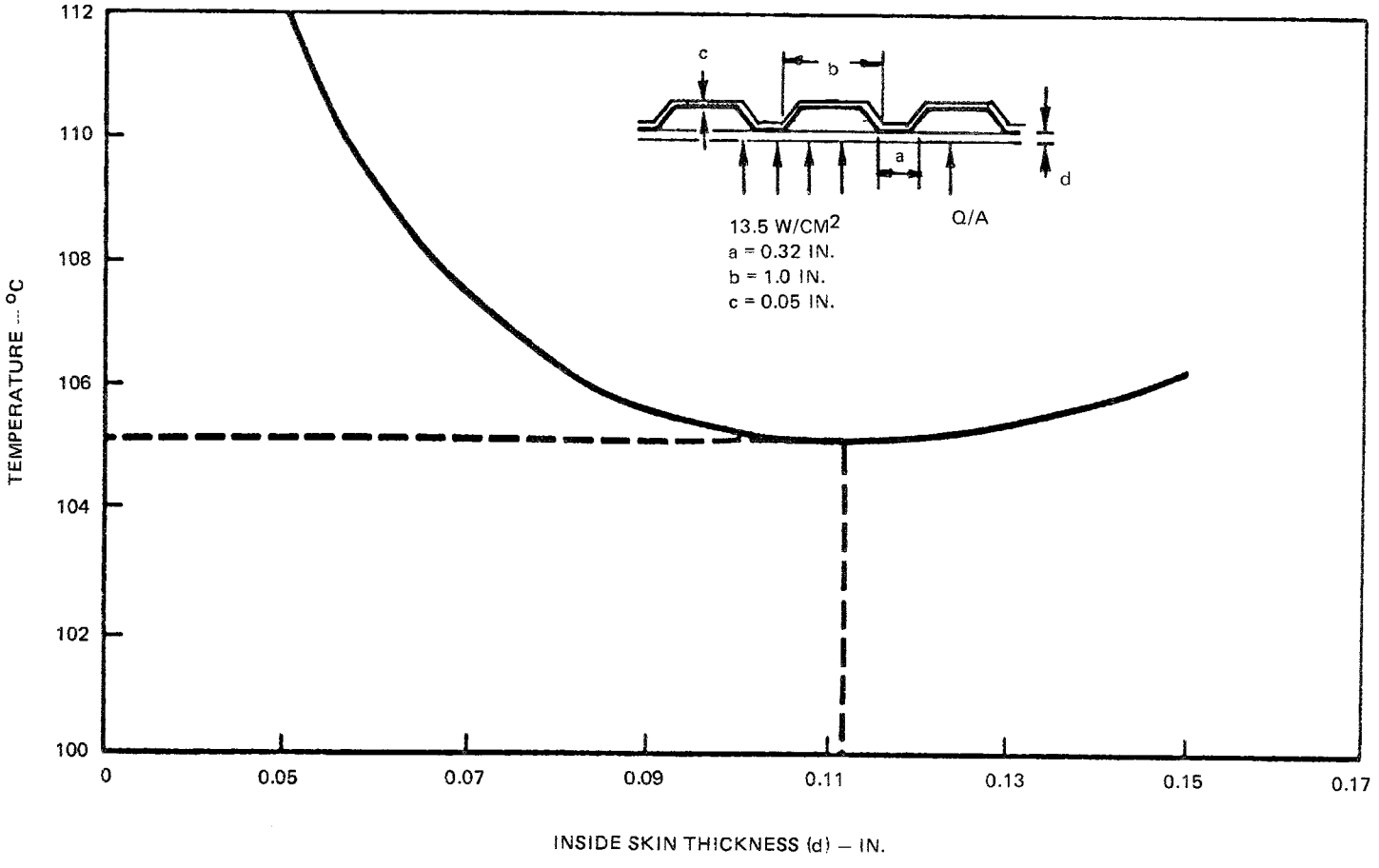

FIGURE 5.1–12 INCREASING THE OUTSIDE SKIN THICKNESS SLIGHTLY DECREASES THE PEAK TEMPERATURE

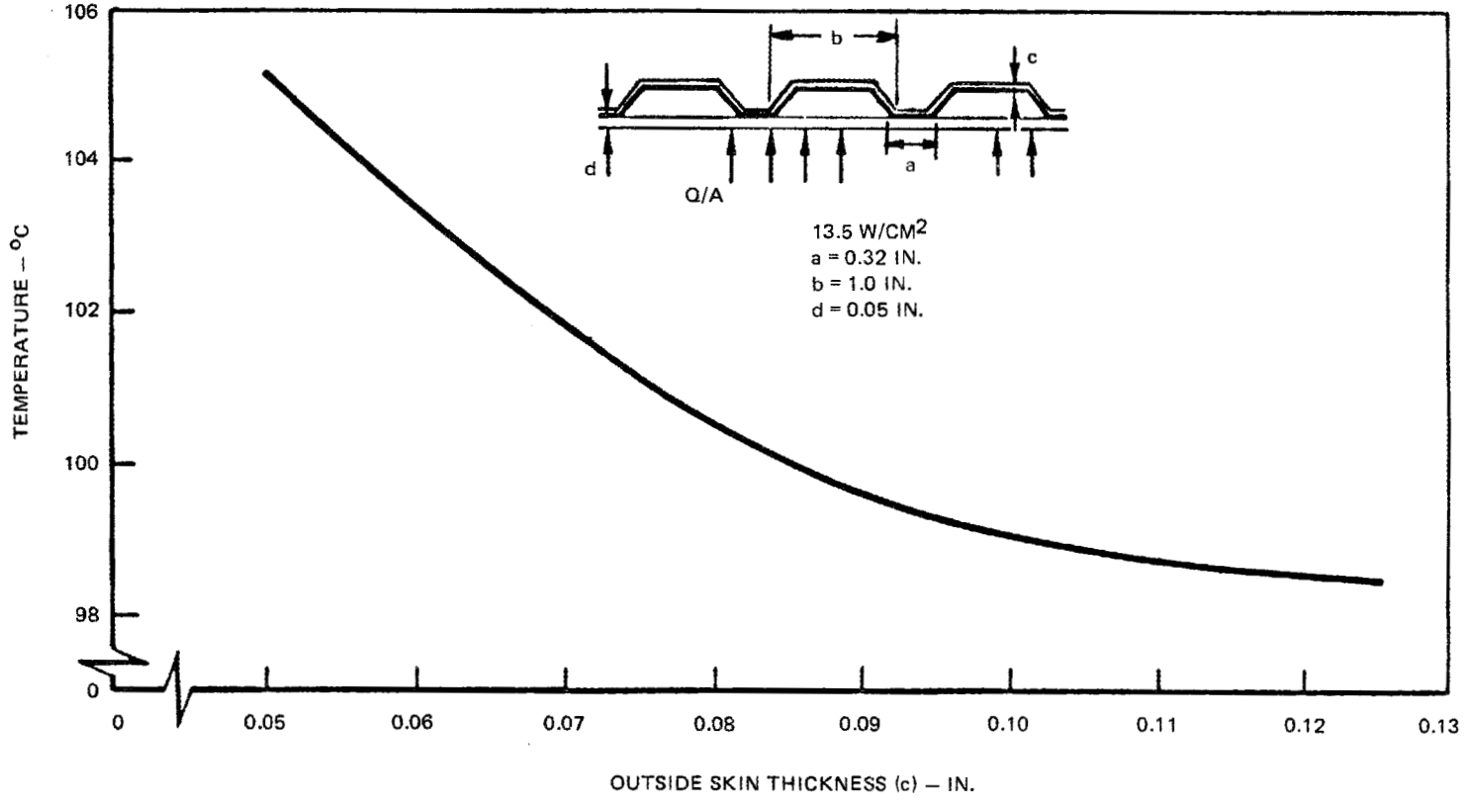

FIGURE 5.1–13 PEAK TEMPERATURE IS INSENSITIVE TO COOLANT PASSAGE WIDTH

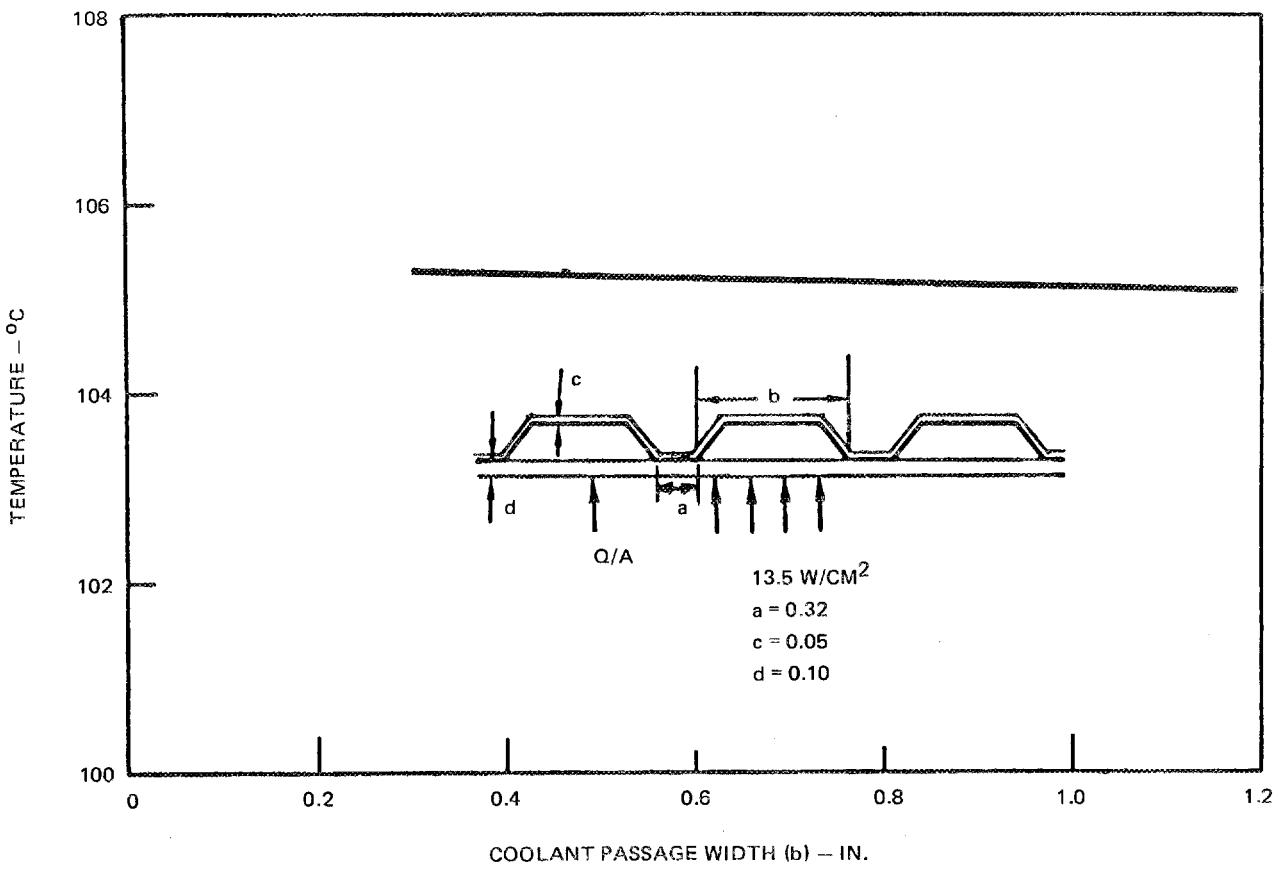

FIGURE 5.1–14 VACUUM LINER TEMPERATURE AND POLOIDAL THERMAL STRESS DISTRIBUTIONS

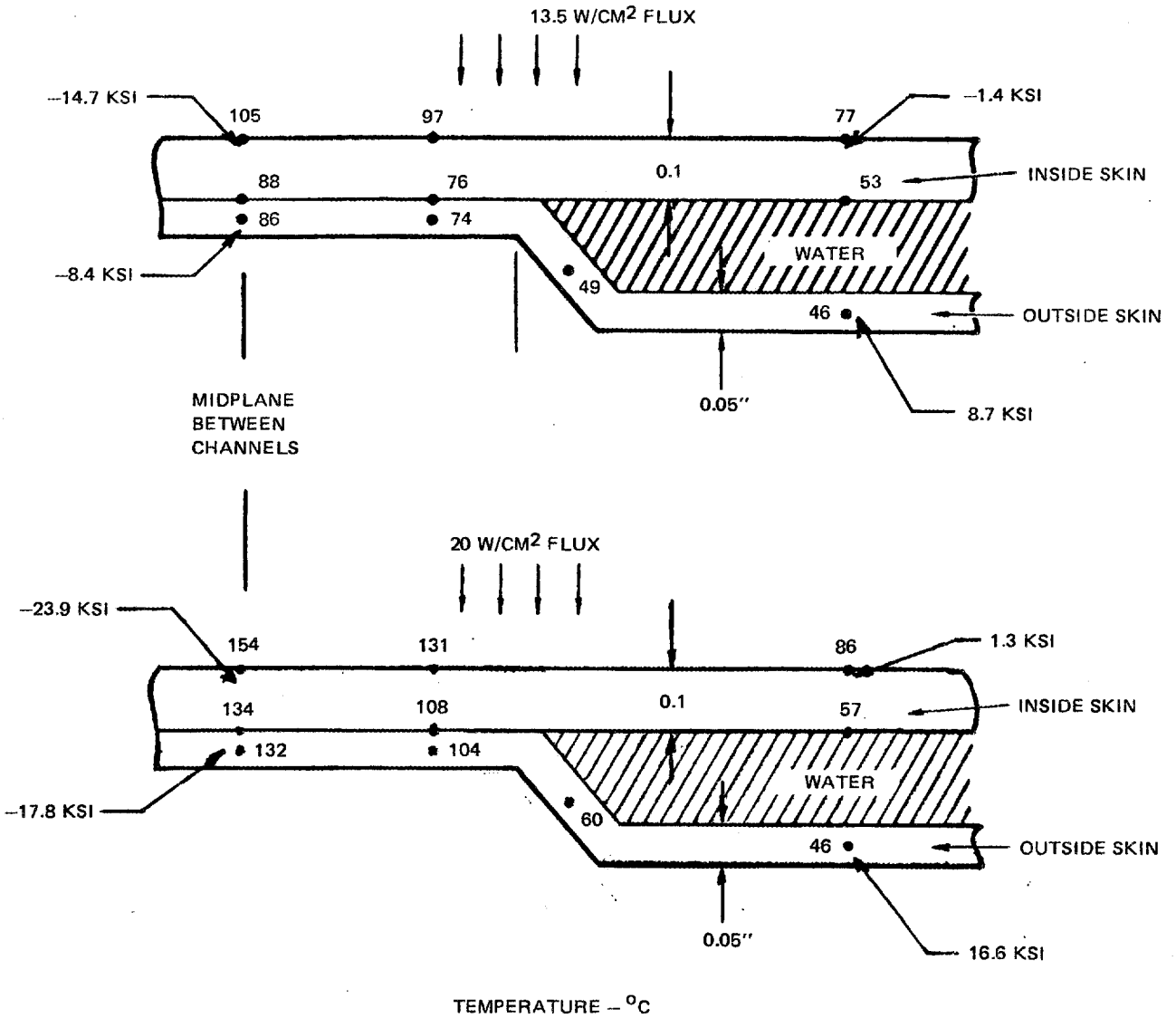

FIGURE 5.1-15 CORRUGATED STAINLESS STEEL CONCEPT HAS HIGH COOLING CAPABILITY

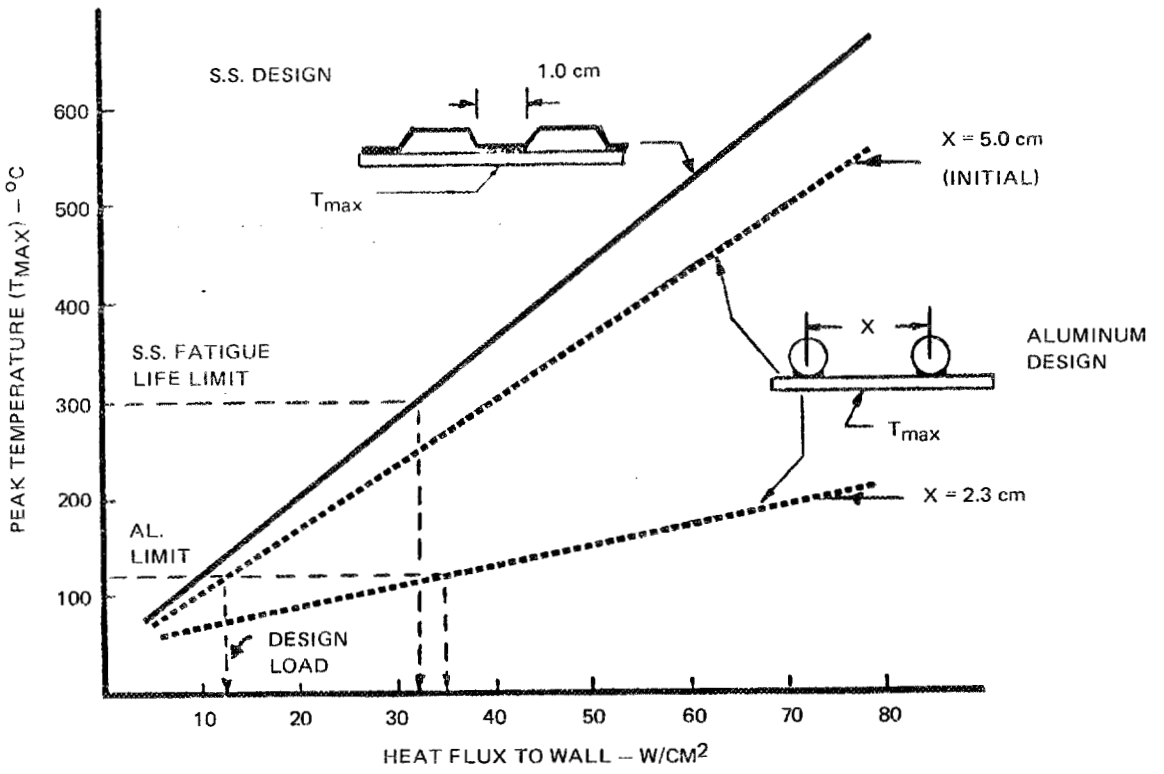

316 stainless steel annealed and Miner's rule of cummulative damage. The ASME Boiler Code fatigue curves are based on mechanical fatigue. Thermal fatigue is similar to mechanical fatigue, but the continuous change in temperature can affect life, especially if the temperature is high enough to cause metallurigcal effects to take place in the metal. To take into account these effects, the mechanical fatigue curve corresponding to the peak temperature of the vacuum liner was used to predict thermal fatigue life.

Initial Aluminum Baseline Compared to Stainless Steel with Brazed on Tubes - An analytic comparison was made between aluminum and stainless steel vacuum liner concepts using coolant tubes prior to MDAC's proposal preparation. The results showed that a stainless steel skin and tubes vacuum liner was approaching impracticality for the high heat flux ($\geqslant$13.5 W/cm^2). Thus, the initial baseline design was 2219-T87 aluminum with brazed on copper tubes. Vacuum liner thickness was 0.1875 in., with a 2.0 inch spacing of coolant tubes. Coolant would be provided by 0.25 in. inside diameter copper tubes on the vacuum liner throat and 0.375 inch inside diameter copper tubes on the side walls. This design was compared with a 316L stainless steel design with brazed on stainless steel coolant tubes. For the stainless steel design, vacuum liner thickness was 0.1875 inch with a 1.0 inch spacing of 0.25 inch inside diameter stainless steel tubes on the vacuum liner throat and 1.0 inch spacing of 0.375 inside inch diameter stainless steel tubes on the side walls. The 0.1875 inch wall thickness is adequate to resist buckling of the vacuum liner under the vacuum loading with a factor of safety of 5.0.

Maximum thermal stresses in the vacuum liner result from combining thermal stresses from the temperature gradient through the wall and the temperature gradient between coolant tubes. For a surface heat flux of 13.5 W/cm^2 the thermal stresses in the vacuum vessel are 7.7 ksi for aluminum and 42.6 ksi for 316L stainless steel. Thermal stresses in the 316L stainless steel structure are higher due to the larger thermal gradients and the higher modulus of elasticity for 316L stainless steel, which is approximately a factor of three higher than aluminum. The stainless steel design exceeds the design allowable being used at that time of 1.6 times the yield strength of annealed 316L stainless steel. This allowable was based on the Nuclear Energy (NE) Standards. The thermal gradients between tubes for stainless steel can be reduced by closer spacing of the tubes, but this does not appear to be practical, especially since other concepts are available that provide more uniform surface cooling.

Integrally-Cooled Stainless Steel Design - The die formed design concept was analyzed parametrically to determine thermal stress and fatigue life sensitivity to wall dimensions. Thermal stress analysis was performed using the PLATSA thermal stress code. This is a two-dimensional finite element code, developed at MDAC-St. Louis, that allows the actual nonlinear temperature dependent stress-strain behavior to be input to improve computational accuracy. PLATSA handles the nonlinear response through an iterative procedure. The strain on all elements are iterated until all strain compatibilities and force balances are satisfied. With a 0.375 inch uncooled weld land width between coolant passages and a surface heat flux of 20.0 W/cm^2 plastic stress levels are reached. The major component of thermal stresses results from the temperature gradient between coolant passages.

Life of the vacuum liner was predicted using the ASME Boiler Code fatigue curves for annealed 316 stainless steel. These curves are for a stress ratio (minimum stress/maximum stress) of $R = -1$ and have a life scatter factor of 20 on cycles. Life is extremely sensitive to peak temperature which in turn depends on heat flux and spacing between coolant passages. Structural analyses show that the stainless steel integrally cooled design meets the 10 year life requirement of EBT-P. Life is extremely sensitive to peak heat flux and to the spacing between coolant passages (weld land width), as shown in Figure 5.1-16. Decreasing applied heat flux from 20 W/cm^2 to 13.5 W/cm^2 would increase the allowable number of thermal cycles from 50,000 cycles to 1,000,000 cycles. This indicates that most of the fatigue damage will occur during operation of EBT-P at the higher power levels. For the die formed design concept, the minimum weld land width is 0.375 inch. Increasing front sheet thickness from 0.05 inch to 0.10 inch improves the life slightly, because the thermal gradient between coolant passages is reduced without significantly increasing the thermal gradient through the thickness.

Mechanical stresses in the integrally cooled stainless steel design resulting from coolant pressure can be limited by proper sizing of the coolant passages. Buckling of the vacuum liner or mirror cavity is not critical.

Copper Backed Concept - A PLATSA thermal stress model was constructed of the copper backed design concept to determine thermal stresses and fatigue life. The concept analyzed was a 0.05 inch stainless steel sheet with 0.375 inch OD stainless steel coolant tubes on 1.5 inch centers brazed to the back of it. A 0.125 inch layer of copper is then

FIGURE 5.1–16 VACUUM LINER LIFE IS VERY SENSITIVE TO WELD LAND WIDTH AND SURFACE HEAT FLUX

- ANNEALED 316L STAINLESS STEEL
- ASME BOILER CODE FATIGUE DESIGN CURVES
- TEMPERATURES (°C) SHOWN ARE FOR 0.6 IN. WELD LAND WIDTH AT 20 W/CM^2

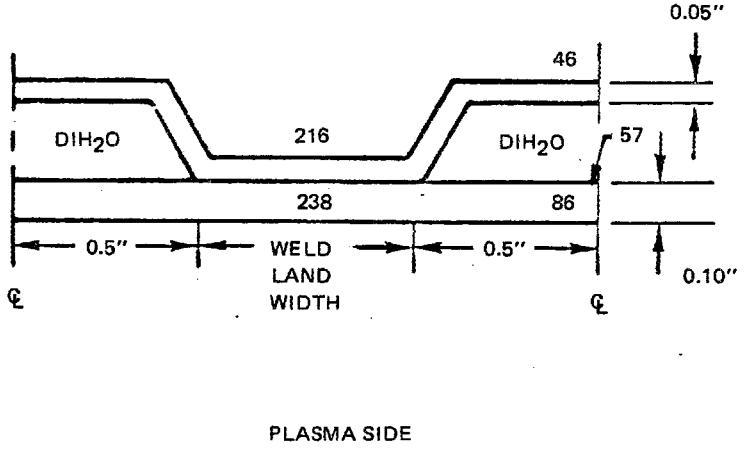

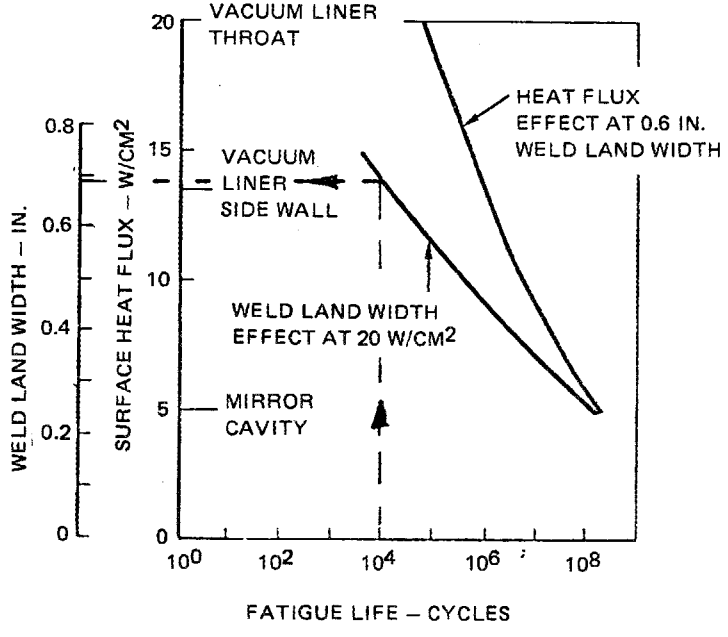

plasma sprayed to the back of the stainless steel assembly. At 7 MW plasma power, small plastic strains occur in the cool regions of the stainless steel coolant tubes. The maximum stress level in the copper is 3870 psi (compression). This design concept has a predicted life greater than 1 x 10^6 thermal cycles at a plasma power of 7.0 MW. Therefore, adding the copper to the back of the stainless steel greatly increases fatigue life and lowers the sensitivity to heat flux and design details.

5.1.3.3 Fabrication Considerations - The fabrication approaches, advantages, disadvantages and risks for each vacuum liner concept configuration discussed previously will be addressed in this section. A discussion of fabrication techniques for the baseline aluminum vacuum vessel is included for comparison with the various stainless steel concepts.

Initial Baseline Aluminum Vacuum Liner with Soldered on Copper Coolant Tubes - The fabrication sequence for this concept involves spinning a 3/16 inch thick aluminum sheet to form one half the vacuum liner. An aluminum vacuum seal flange would then be welded to the vacuum liner. The next step would be to solder copper tubes to the vacuum liner using a Cd-Zn solder with a melting point of 500°F. This soldered joint involves the risk of failure due to differences in thermal expansion if the parts aren't cooled uniformly and slowly from the soldering temperature. Also the fumes evolved from the solder and flux are toxic and must be vented adequately during soldering. The fabrication risk with this approach is relatively low since the process is considered state-of-the-art.

Stainless Steel Vacuum Liner with Brazed on Stainless Steel Coolant Tubes - The fabrication sequence involves spinning steel sheet to form the disc portion (side walls) of a vacuum liner half and rolling and welding another sheet to form the cylindrical (throat) portion of the vacuum liner. These two sections would then be welded together to form one-half of a vacuum liner. Stainless steel coolant lines would then be brazed to the vacuum liner in either a vacuum or inert atmosphere. Stainless steel seal flanges would then be welded to the vacuum liner. The fabrication risk involved in this concept is minimal since all of the procedures are relatively conventional. With this configuration of separate tubes there is essentially no risk of leaking coolant to the inside.

Integrally Cooled Stainless Steel Vacuum Liner - This concept utilizes a double walled structure in which the inner plasma-exposed skin would be smooth, and the at-

tached outer skin being corrugated to provide water coolant passages. The corrugations are made by a die forming or hydrostatic forming process. The two sheets are attached by resistance seam welding. There are several commercially available manufacturers that can fabricate this concept; Panelcoil, Platecoil, and Temp-Plate are the three leaders in this field. It is proposed that the flange portion and cylindrical portion of the vacuum liner would be made separately and then welded together. The advantage to this concept is the large fraction of surface area in contact with coolant. The industry currently manufactures components to tolerances of ± 1/8", which is too large for our needs. We are evaluating several alternate approaches to this technique to improve the tolerances to acceptable levels. A potential problem with this concept is its thermal stress sensitivity to design configuration. To reduce this sensitivity the weld seam should be limited to less than 0.60 inch in order to limit the thermal stresses. This appears feasible with current fabrication procedures.

The fabrication risks with this concept are maintaining the proper manufacturing tolerances and minimizing distortion due to welding; it is believes that both of these can be minimized by utilizing proper tooling.

MDAC is procuring a seal development test unit that consists of one full size mirror cavity and two vacuum liners. These components will closely simulate the operational components so they will furnish fabrication techniques for controlling welding distortions and manufacturing tolerances. Sizing of the two vacuum liner halves in the throat area is required to ensure proper fit-up prior to welding.

Copper Backed Stainless Steel Vacuum Liner - This concept utilizes the higher thermal conductivity of copper to distribute the heat to the coolant tubes. Ways of adding the cooper backing are by plasma spraying, flame spraying, electroforming, roll bonding, or explosive bonding. Each method will be explained.

Plasma or Flame Sprayed Copper - These methods would utilize the stainless steel vacuum liner with stainless steel coolant tubes as a base, followed by spraying copper between and over the tubes. The risks involved in these concepts are ramifications of the distortion resulting from spraying and the unknown material characteristics of thermal conductivity of sprayed copper, and the mechanical/thermal integrity of the bond line

between copper and stainless steel. Flame spraying is preferred to plasma spraying due to less distortion of the parts during spraying.

Electroformed Copper - This method could plate 1/8 inch copper onto a formed stainless steel vacuum liner. Copper coolant tubes would then be soldered to the copper. A possible variation of this design would be to integrally electroform the coolant passages into the copper. The advantages of electroformed copper appear to be minimum distortion and the possibility of incorporating cooling passages within the copper. The risks involved in this process are the ramifications of the unknown material characteristics of thermal conductivity and the mechanical/thermal integrity of the bond line between the copper and stainless steel. Another area requiring development is the weld joint design to prevent copper dissolution into the stainless steel weld.

Explosive Bonded Copper on Stainless Steel - A 1/8 inch thick copper sheet would be explosively bonded to a thin (.050 to .070 inch thick) stainless steel sheet. This material then would be spun or drawn to form the disc portion of the vacuum liner and rolled and welded to form the cylindrical portion of the liner. These two segments would then be welded together to form a vacuum liner half. Copper coolant tubes would then be soldered to the copper cladding. The risks involved in this process are the same as those for the electroformed copper discussed above, plus the unknown formability of the copper clad stainless steel sheet.

Roll Bonded Copper on Stainless Steel - The combination of material thicknesses desired for this concepts are not available by roll bonding, therefore this concept was dropped.

5.1.4 Cost Comparisons - Detail cost estimates were made for various aluminum and stainless steel options and these costs were presented to ORNL by WBS element.

The initial baseline design represents the simplest fabrication concept. The mirror cavity and circular ports are machined from an aluminum forging with very little welding required. The seals are inexpensive Viton O-rings. The drawback of this concept is the high risk of surviving the x-ray and microwave heating environments.

The other three concepts include the cost increase for incorporating the horsecollar ports on the mirror cavity. The addition of horsecollar ports changes the fabrication of the aluminum cavity from simple machining of a forging to a complex machining of a forging, or roll forming of aluminum plate and welding. The large horsecollar ports may also necessitate welding port extensions for the other ports and penetrations to avoid interference problems. Increased cost in the aluminum cavity is attributed to the addition of horsecollar ports for the aluminum/elastomer seal system. The horsecollar cost increase for stainless steel is about half of aluminum cost increment because of lower welding costs and the smaller impact on the fabrication of the stainless vessel. A preliminary design was also made for machining the cavities from a large forged ring billet to determine feasibility of a one piece machining.

Higher costs for the aluminum design with metal seals (indium coated C-ring) relative to the baseline is attributed to the following: Higher PACE costs reflect the greater cost of the horsecollar ports, the thicker flanges, and the machining of the thick flanges needed to provide the higher sealing force ($\approx$1700 lbs/in.). Higher OPS costs reflects the greater cost for developing the metal seal system.

Stainless steel cost data were obtained for the corrugated vessel structure and metal seals discussed previously. Detail engineering drawings of this concept were developed in Title I and these formed the basis for vendor cost quotes. Quotes from three vendors are included in the stainless cost estimate: 1) for fabrication of the vacuum liner, 2), for fabrication of the mirror cavity, and 3) for supplying the Wheeler and Conflat flanges, welding the flanges to the vessel and leak checking the vacuum welds. Vendors were chosen because they are generally competitive in cost and MDAC's satisfaction with prior work. Higher PACE cost were reflected because of the larger expenditure for fabricating the stainless steel structure whereas lower OPS cost reflects the higher confidence and proven reliability of the stainless steel/metal seal concept.

5.1.5 Conclusions/Recommendation - The choice of toroidal vessel material and seal has been difficult to make because of the uniqueness of the EBT-P operating environment, the criticality of the vacuum system on the operation of the device and the prohibitive cost of modifying the device during the installation or operation phases. Retaining the elastomer seal is viewed as an unjustifiable high risk approach considering the present

knowledge of EBT-P x-ray levels which exceed the capabilities of elastomeric seals. The choice then revolves about the risk and cost factors between aluminum and stainless steel structures with metal seals. Metal seals with stainless steel flanges are proven, widely used in UHV applications, commerically available and therefore have substantially less risk and cost than the aluminum/metal seal approach. The corrugated stainless steel structure may be viewed as having an inherently higher risk than the aluminum skin and tube concept, but unlike the vacuum seal issue, the stainless steel structure is amenable to analysis, is used in many similar applications where cooling and high structural efficiency are required, and has an established fabrication process with little if any development required.

In assessing the costs between aluminum and stainless steel the difference in costs has been consistently small and is within the accuracy of the cost estimation process. The higher costs for fabricating the stainless steel structure is offset by the lower costs of the off-the-shelf metal seal system and the lower development cost of a proven seal concept. Since cost is not a major differentiator, the decision should be based on technical factors and risk. It is MDAC's recommendation that a stainless steel vessel with metal seals be adapted for EBT-P because this offers the least risk approach in meeting the project goals. Horsecollar diagnostic ports should be included in the revised design. ORNL has accepted MDAC's recommendation and all future work will focus on a stainless steel vessel with metal seals.

5.2 TOROIDAL VACUUM VESSEL STRUCTURAL CONSIDERATIONS

The stainless steel toroidal vacuum vessel design has several advantages over the aluminum vessel with elastomeric seals that was baselined in the EBT-P proposal. Principal structural advantages stems from the increased stiffness of the vessel structure due to the stainless steels higher modulus of elasticity. The additional stiffness allows less deflection in the seal flange area, which improves seal performance and also permits the use of elongated "horsecollar" diagnostic ports by providing adequate load paths to carry loads around the port penetrations. The lower thermal conductivity of stainless steel is alleviated by the integral coolant channel configuration.

Primary structural issues that are discussed herein and will be further evaluated during Title II are: 1) stresses and deflections due to evacuation loading, 2) assuring adequate

vacuum liner side wall flexibility to accomodate thermal expansion and installation deformations, 3) stresses due to thermal loading, 4) adequate load paths around penetrations of the mirror cavity to minimize load peaking in seal flanges, 5) stresses and deflections due to localized loads introduced by the vacuum vessel support struts, and 6) preload assembly stresses.

The vacuum liner design (see Fig. 4.2-1) was analyzed as part of the seals and wall material trade study as discussed in Section 5.1 and Reference 1. The poloidal layout of the integral coolant passages ensures that the vacuum liner will have adequate buckling strength while retaining flexibility of side walls. The skin gages were sized to ensure low enough stresses from thermal, vacuum and coolant pressure loads for acceptable vacuum liner life. The inside skin is 0.100 in., and the corrugated outside skin, forming the coolant passage is 0.062 in. These gages will accomodate the maximum flexure required for installation.

For the mirror cavity design, the 3/16 in. inside skin is sized to carry all the overall loads. This allows maximum latitude in selection of the coolant channel design. The thick inside skin is needed because of the large number of ports cutting the mirror cavity shell. The thick shell is acceptable on the mirror cavity because it does not have the requirement of being flexible. An outside skin thickness of 0.062 inch minimum will provide adequate structural integrity of the coolant passages at a coolant passage width of up to 1.0 inch.

The elevated temperature of the toroidal vacuum vessel walls during device operation will cause expansion in the toroidal direction. This expansion is accomodated by the flexible vacuum liner side walls. This vacuum liner flexibility is maximized by the poloidal routing of the integral coolant passages. The gages of the inside and outside skins were sized to keep cyclic stresses due to thermal and mechanical loading at a level compatible with the required operating lifetime. The current design calls for a 0.100 in. thick inside skin with a die-formed, 0.062 in. thick outer sheet welded to the inside sheet. A finite element NASTRAN model of the vacuum liner was made to allow more accurate predictions of side wall flexibility. More detailed Title II thermal stress analysis may allow some reduction in inside sheet gage for increased flexibility. The vacuum seal development test plan will also include a test of vacuum liner flexibility which will provide a check on the analytical predictions.

Thermal stresses in both the mirror cavity and the vacuum liner are primarily a function of the maximum distance to coolant of any wall material exposed to plasma heating. This holds true for the range of skin thicknesses of interest in this design. This distance should be held no larger than 0.680 in the vacuum liner areas subjected to 20 W/cm^2 heat flux to assure adequate fatigue life as shown in Figure 5.1-16. The exact spacing of the coolant passages in the mirror cavity will be determined in more detailed Title II analysis. The allowable spacing is significantly larger on the mirror cavity. The wall loading used to analyze these structures is 20 W/cm^2 on the vacuum liner throat, 13.5 W/cm^2 on the vacuum liner side walls and 5 W/cm^2 on the mirror cavity and port side walls.

The mirror cavities are penetrated by several ports for vacuum pumps, diagnostics, limiter feed-thrus, ECRH waveguides and ICRH antenna leads. These penetrations reduce the load carrying capability of the mirror cavity walls. As previously stated, the mirror cavity inside skin will be sized to carry all loads in order to allow maximum latitude in the selection of the coolant passage configuration in the outside skin. It is desirable to minimize the deflections in the area of the port since these deflections tend to cause build up of the toroidal compression loads in areas away from the port penetrations and this load peaking is detrimental to good vacuum sealing of the Wheeler flanges. The predicted running loads in the flanges are 50 lb/in due to evacution and 2.4 lb/in., due to thermal expansion. Peaking of these loads due to ports will be determine during Title II. Preliminary analysis indicates that a 3/16 inch inside skin should keep deflections down to a reasonable level. If more detailed Title II analysis or seal development tests indicate that a thicker inside skin is required, the integral coolant passage concept should allow the inner skin to be somewhat thicker without greatly increasing thermal stresses A modification to the standard Wheeler flanges which allows total flange clamp-up should alleviate some of the seal sensitivity to load peaking. The wheeler flange modifications include 1) Reducing the depth of the alignment lip, 2) Eliminate mating flange gap to ensure full clamp-up and 3) Add a coolant passage for flange cooling. Careful attention to design details at the welded port penetration junctions will be necessary to ensure that bending stresses due to local load path discontinuities do not become excessive.

5.2.1 Toroidal Vessel Support - The adjustable struts that support the vacuum vessel attach to brackets on the upper and lower "horsecollar" diagnostic port extensions on the mirror cavities (see Fig 5.2-1). This deviates from the configuration shown in the proposal

FIGURE 5.2–1 TOROIDAL VESSEL SUPPORT

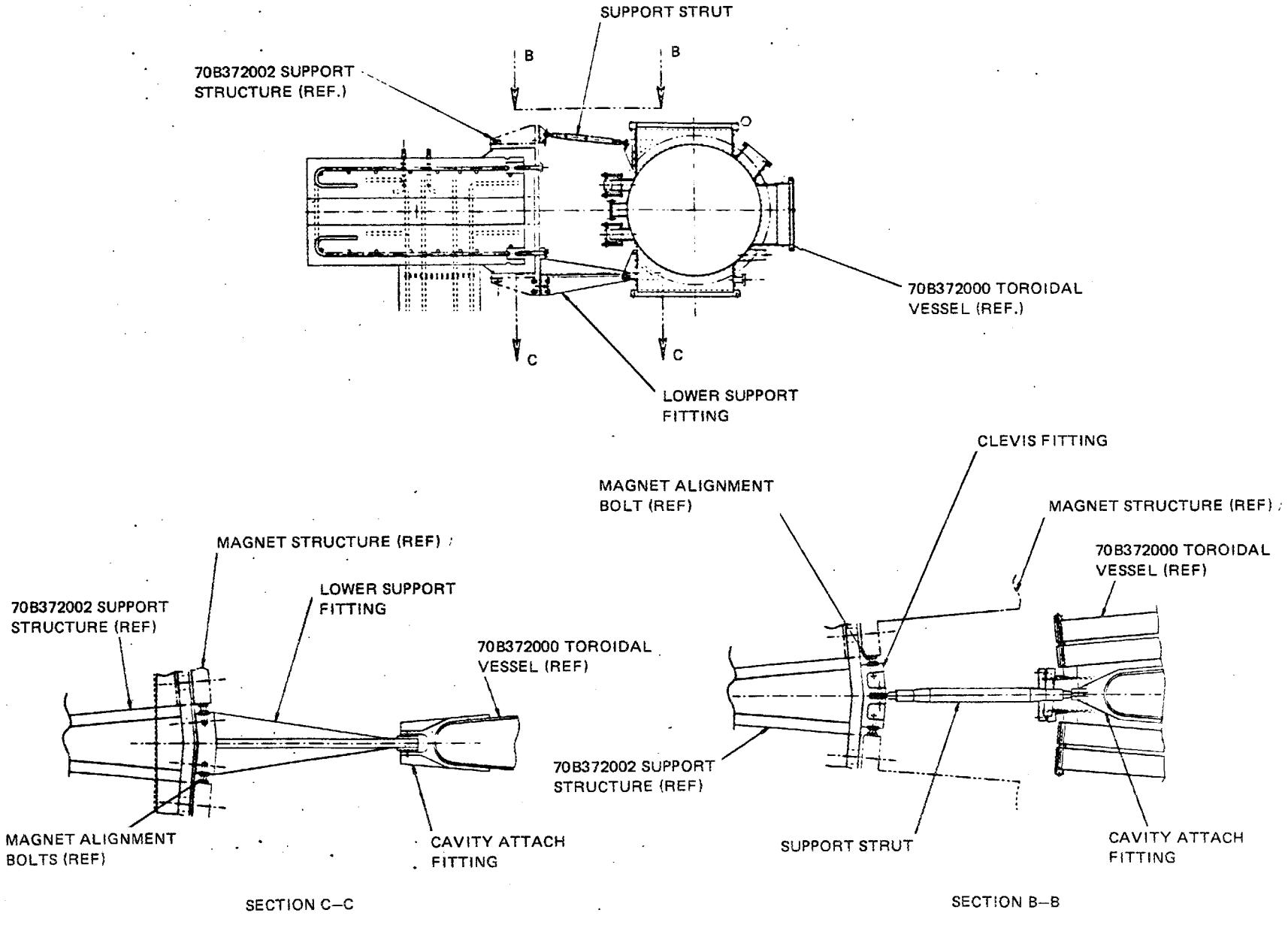

which picked up brackets on the 76 cm. flanges. This relocation was necessary since the large flanges are now covered by the ARE coils. The ARE coils had to be relocated to provide room for the horsecollar ports. To provide for the introduction of load to the port walls, a machined fitting is welded to each horsecollar port extension allows load from the struts to be sheared in to the mirror cavity without bending caused by local eccentricities. The toroidal vessel support must react loads resulting from vessel installation misalignment and preload, dead weight, evacuation pressures, thermal expansion during operation and seismic events. In addition these struts must provide support for the vacuum vessel during possible earthquake occurrences. The determination of these seismic loads will be part of the Title II analytical effort which includes a seismic response analysis of the entire EBT-P device and support structure.

The Title II analytical effort will include a seismic response analysis of the device and the construction of a detailed NASTRAN finite element model of the mirror cavity/vacuum liner assembly. This will allow a more accurate assessment of the internal load distribution and optimization of skin gages and design details. In addition, the tests performed on the seal development article will provide an opportunity to experimentally verify the analytical predictions.

5.3 EBT-P LIMITER DESIGN AND ANALYSIS

The limiters protect the vacuum liner throat from the intense heating and erosion caused by the high energy particles impinging on the liner surface. The limiters are sacrificial elements that eventually wear out and require replacement. Replacement of the limiters is via the horsecollar ports and does not require dismantling of the torus.

Defining the life requirement or frequency of replacement for limiters is very difficult because of the large uncertainty in estimating the heating and sputtering rates. Use of a long limiter life requirement coupled with a conservative estimate of the environment would lead to a very expensive limiter design. Since limiters are sacrificial, the philosophy is to base the limiter design on nominal environment predictions and not require the full 10-year operation of the limiters before replacement. The limiter test program described in section 5.3.5.1 will provide data for scaling to EBT-P criteria for heat flux distributions for use in the Title II limiter design.

The baseline limiter design (Figure 5.3-1) should easily withstand the initial low power operation of EBT-P during Phase III. The environment and performance of the limiters will be determined during this initial phase. Should the environments be significantly worse than currently anticipated, then sufficient time exists, approximately three years, to redesign and build new limiters for the more severe upgrade operation phase.

Alternate limiter materials that could tolerate the higher heating or sputtering rates were evaluated and the important considerations which include sputtering yield, radiation cooling of the plasma, x-ray radiation source strength, and cost factors are presented and compared with aluminum in Table 5.3-1. The comparison shows that aluminum represents the best material choice and should be used to its highest capability. Beryllium has some very attractive features but its high toxicity precludes its use in an experimental facility. Inconel and stainless steel are not viable materials because of their low thermal conductivity. Copper and the refractory metals have a much higher use temperature than aluminum but these metals cause higher radiation cooling of the plasma, have higher x-ray strengths and are more expensive to fabricate than aluminum. Graphite, being a low Z material has low sputtering rates, radiation cooling and x-ray source strengths. Chemical erosion was not included in estimating the erosion rates. A limiter concept of graphite shingles over a metal structure should be further evaluated especially the fabrication technique and associated costs.

To improve the limiter environment definition for Title II design, a substantial effort was spent during Title I to define a limiter and probe heat flux experiment to be conducted in EBT-S. The design of the limiter experimental equipment has been completed and fabrication and purchase of parts is currently underway. Commencement of the EBT-S limiter experiment is planned for in March 1982.

5.3.1 Environment Definition - In this section the heating and sputtering environments are established to support the thermal/hydraulic and thermal stress/life analysis.

5.3.1.1 Limiter Heating - Heating of the aluminum limiters is produced by the impinging plasma particles which have been heated by microwave energy. Microware energy not absorbed by the plasma is absorbed rather uniformly around the interior of the vacuum

FIGURE 5.3–1 LIMITERS

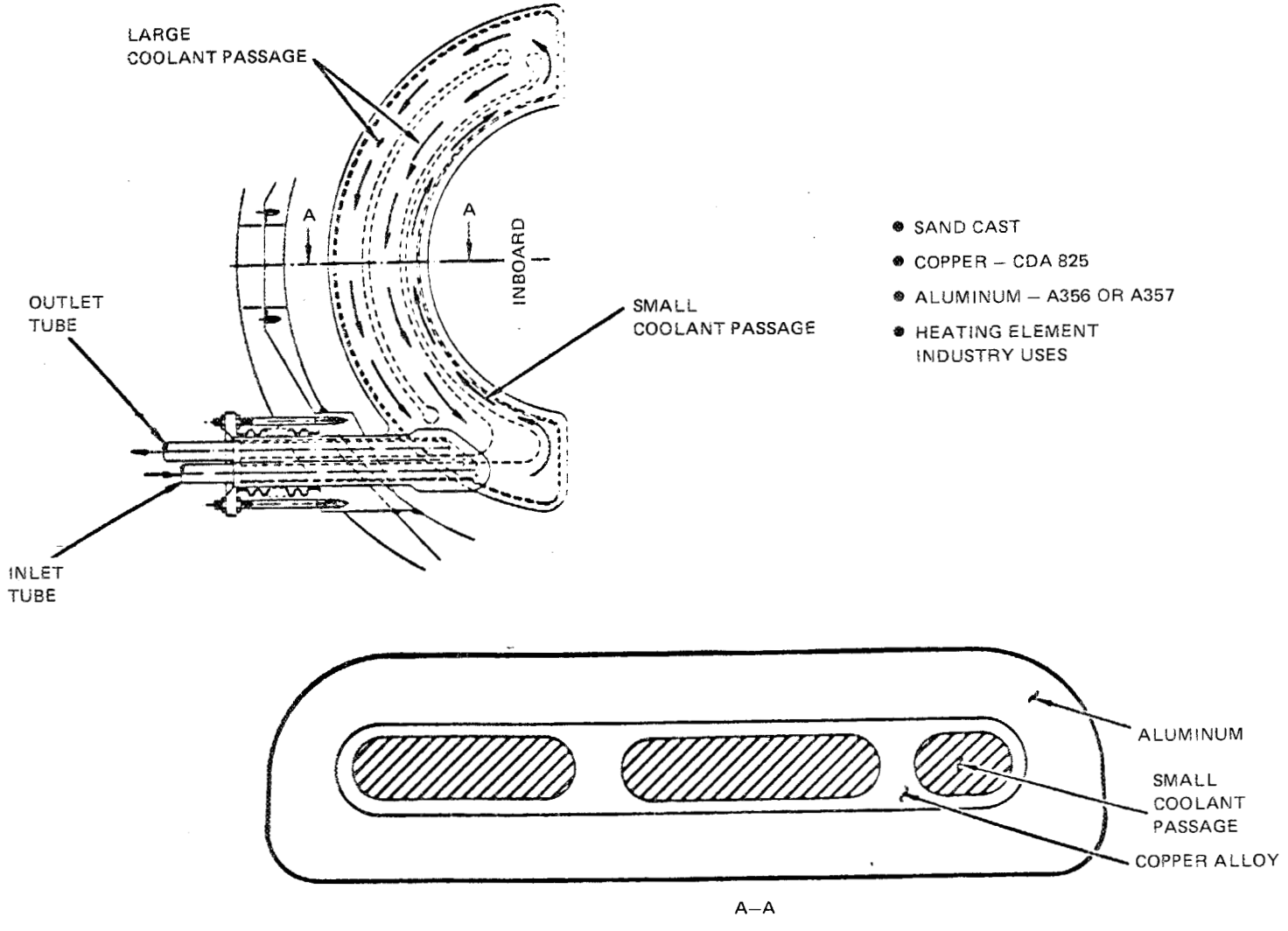

TABLE 5.3-1 ALTERNATE LIMITER MATERIAL COMPARISON

MATERIAL	MELT TEMP °C	THERMAL COND w/cm°C	STRESS PARAM. $\frac{F_{ty}K}{\alpha E}$ ⚠1	ATOMIC NO Z^*_{EFF} / Z^*	RELATIVE TO AL: SPUTTER RATE	RELATIVE TO AL: PLASMA COOLING	RELATIVE TO AL: X-RAY SOURCE SCATTERED/ DIRECT	COST MATERIAL & FAB
ALUMINUM	660	2.1	.359	8/13	1.0	1.0	1.0/1.0	LOW
BERYLLIUM	1277	1.6		4/4	0.1	1.4×10^{-4}	.14/.14	VERY HIGH
COPPER	1083	3.46	.403	10/29				MODERATE
INCONEL	1300	0.22	.006	10/28				MODERATE
STAINLESS STEEL	1300	0.22	.046	10/26	1.5	6.4	3.5/4.9	LOW
MOLYBDENUM	2610	1.47	.232	13/42	1.4	6.0	8.1/12	VERY HIGH
NIOBIUM	2415	.53	.121	13/41	1.2	5.1	7.0/9.4	VERY HIGH
TANTALUM	3000	.55	.109	13/73				EXTREMELY HIGH
TUNGSTEN	3400	1.68	.072	13/74	0.9	3.9	10.1/23	VERY HIGH
GRAPHITE	4000	.24	.097	5/6	0.1	1.4×10^{-3}	0.22/.25	VERY HIGH

⚠1 BASED ON ROOM TEMPERATURE PROPERTIES, HIGHEST BEST

vessel after multiple reflections. This uniform (uncoupled) energy flux does not contribute significantly to limiter heating.

Since establishing the plasma's absorption of microwave energy is extremely difficult, a much simpler, conservative estimate was made. It was assumed that two-thirds of the microwave power that enters the torus is absorbed by the plasma (coupled), and the remaining one-third is removed from the vessel as uniform (uncoupled) power. The coupled power consists of both "passing particle" and "trapped" power, where the former refers to particles moving from cavity to cavity and the latter to particles confined in a cavity's magnetic well. For purposes of this study both coupled forms are treated as a single limiter heating source, and are referred to as coupled power.

An expression was developed to compute the local heat flux to positions on the limiter surface, or a vacuum vessel wall surface in the absence of limiters. This expression, shown below, permits the plasma edge radius and the limiter (or wall) radius to differ and have offset centers, in the general case. For the EBT-P limiter case, coincident plasma and limiter centers are assumed. The local heat flux depends upon the distance from the limiting flux line, x, and the local surface angle, j, between the flux line and the limiter surface. Values of heat fluxes were computed using the expression below:

$$q\ (x) = \frac{P_c}{2\pi r_p N_s \sigma_E e^{-a} I(a)} \sin\theta \exp\left[-x/\delta_E\right] \qquad (1)$$

where nominal input parameters are:

N_s = 72 limiter locations

r_p = 19.0 cm plasma radius

δ_e = 0.64 cm energy fold distance

$a = \epsilon_r/\delta_e; \epsilon_r = r_\ell - r_p = 0$

(coincident centers)

$e^{-a}I(a)$ = modified Bessel function

= 1.0 for a = 0.

coupled power (P_c)

P_c = 2.0 MW*(67%) - Baseline Power

P_c = 5.0 MW*(67%) - Upgrade Power

Because of coincident centers between the plasma and limiter surface, the heating was assumed not to vary in the poloidal direction. This makes the Bessel function unity and no "peaking" is predicted by Equation (1). Uncoupled power was assumed to be uniformly distributed over the interior vacuum vessel area.

Two input power conditions were used to compute heat flux distributions to the limiters. A baseline power input to the torus of 2.0 MW and upgrade power of 5.0 MW were used in Equation 5.3-1 to compute local heat fluxes. Figure 5.3-2 presents results for both baseline and upgrade heating conditions based on nominal input parameters. The results indicate maximum fluxes of about 200 W/cm^2 and 100 W/cm^2 for the upgrade and baseline conditions, respectively.

Uncertainties in the input parameters for Equation 5.3-1 prompted an error analysis to define the uncertainty in the resulting heat flux predictions. A root-sum-square technique was employed where the heat flux uncertainty, $\delta(Q/A)$, was defined as,

$$\delta\left(\frac{Q}{A}\right) = \left[\Sigma\left(\frac{\delta(Q/A)}{\delta f_i} \bullet \delta f_i\right)^2\right]^{1/2} \tag{2}$$

and δf_i is the uncertainty interval of the independent variable f_i.

FIGURE 5.3–2 RESULTING HEAT FLUX DISTRIBUTIONS FOR EBT-P LIMITERS

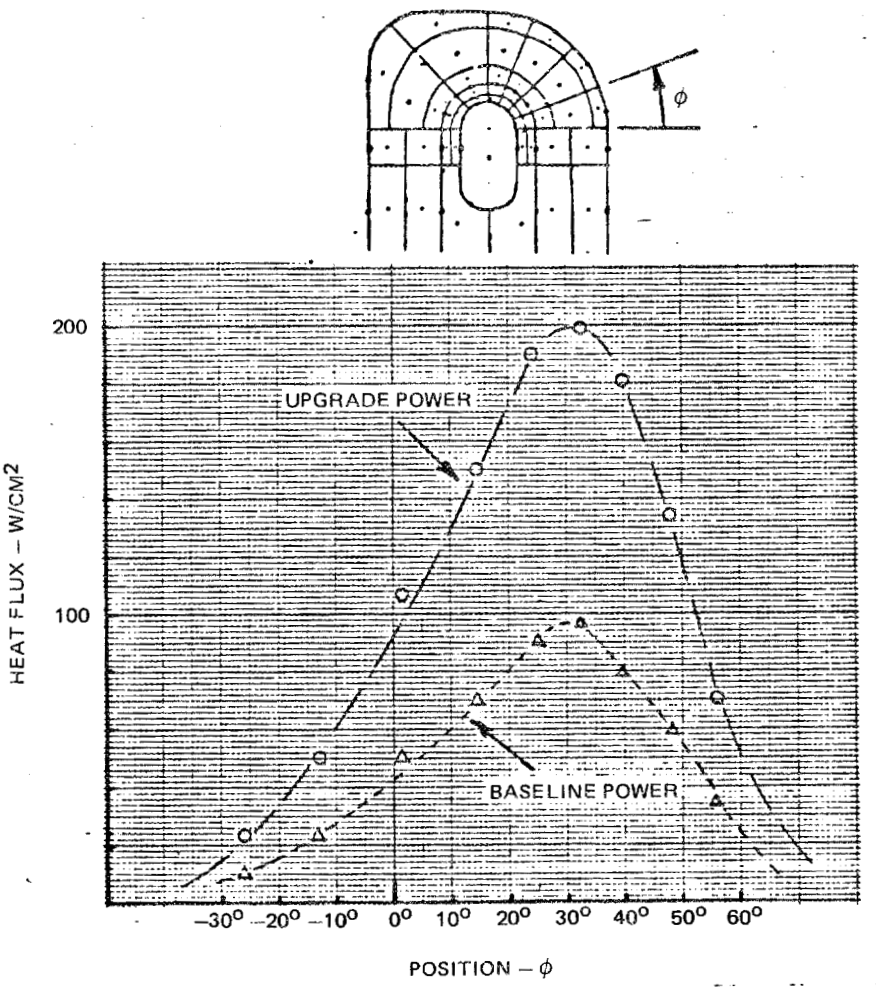

The independent variables which were included in the analysis were P_c, θ, x, δ_e, and r_p. The number of limiter locations, N_s, which were effectively "limiting" was not included since the assumption was made that all limiters were positioned to absorb an equal amount of the plasma power. Results of the uncertainty calculations show $\delta(Q/A) \approx \pm 60\%$, which indicates a rather large degree of uncertainty in the predicted heat fluxes.

5.3.1.2 Sputtering Considerations - In higher power experimental facilities, the interface region between the plasma and the first material boundary, i.e., the limiter scrape-off region, can critically impact the entire design. The material surface exposed to the plasma must remove a significant fraction ($\sim$ 60%) of the power introduced into the plasma in addition to enduring continual bombardment by high energy ions. The energy removal constraint drives the designer towards a strong, yet thin and highly conductive material such as the aluminum proposed for the present design. It must be recognized, however, that this approach carries a high degree of risk from an erosion standpoint due to the potential for runaway sputtering.

As discussed in Reference 18, a sheath potential builds up on the limiter which accelerates the higher Z ion, such as aluminum, to energies many times the average edge temperature before it strikes the limiter surface. The sputtering coefficient for these ions is greater than unity, if the edge temperature is larger than $\sim$ 30 eV. This can result in a runaway situation provided that most of the sputtered atoms enter the plasma. The runaway condition can not exist indefinitely, since the sputtered impurities will eventually cool the plasma edge dropping the self-sputtering yield below unity. An equilibrium is thereby reached where the plasma impurity density is sufficient to cool the edge to the point where the sputtered impurity influx balances the outflux.

This equilibrium has been calculated for EBT-P using a model developed for EBT-R Study[18] under various assumptions for the input power level and for the fraction of the sputtered atoms that enter the plasma. The results of this procedure show that the edge temperature in EBT-P will typically be low (<100 eV) with the plasma outflux being dominated by impurities unless the charge-exchange losses are large. This is a direct consequence of the large heat flow into the plasma edge region, and the relatively low density at the edge. Since the edge temperature cannot rise to disperse this power due to the self-

sputtering limit, the edge impurity density increases in order to dissipate the power via radiation.

If all of the sputtered impurity atoms enter the plasma, this equilibrium occurs at the point where the impurity self-sputtering coefficient is unity, and there is no net erosion of the limiter surface (local areas may erode, but there will be corresponding areas where material builds up). If a fraction of the sputtered atoms do not enter the plasma, however, the limiter surface will erode, and the rate of erosion can be estimated from the impurity flux to the limiter and the impurity self-sputtering coefficient.

The limiters are sacrificial and can be replaced frequently to accomodate erosion. It should also be pointed out that changes in some of the assumptions used in calculating erosion rate can dramatically alter the result. For example, if all of the sputtered atoms enter the plasma, the limiter erosion would theoretically be zero, because one atom would be deposited to replace each one that was sputtered. This, however, is not particularly satisfying since it is a global result and could vary locally as mentioned earlier.

In conclusion, it seems prudent to try to obtain as much information from EBT-S as is possible with regard to migration of aluminum from the corners of the vacuum vessels and the actual plasma edge environment. This information can then be used to attempt to normalize the present model in order to better predict what the actual plasma edge environment will be in EBT-P. Until this procedure can be carried out, definitive conclusions concerning limiter erosion cannot be drawn; however preliminary estimates flag this as a potential problem area.

5.3.2 Thermal/Hydraulic Analysis - The objective of this analysis was to define the limiter temperature gradients for both baseline and upgrade power conditions. The limiter baseline design, Figure 5.3-3, served as the basis of the analysis, and consists of an aluminum alloy cast over the copper alloy water passage insert.

The analysis procedure was to first determine coolant water mass flow rates and associated convective heat transfer coefficients and pressure drops, and then compute limiter temperature distributions using a two-dimensional finite difference computer code. Coolant mass flow rates were chosen to insure turbulent flow within the passages but not excessive

FIGURE 5.3–3 LIMITER TEMPERATURE DISTRIBUTIONS

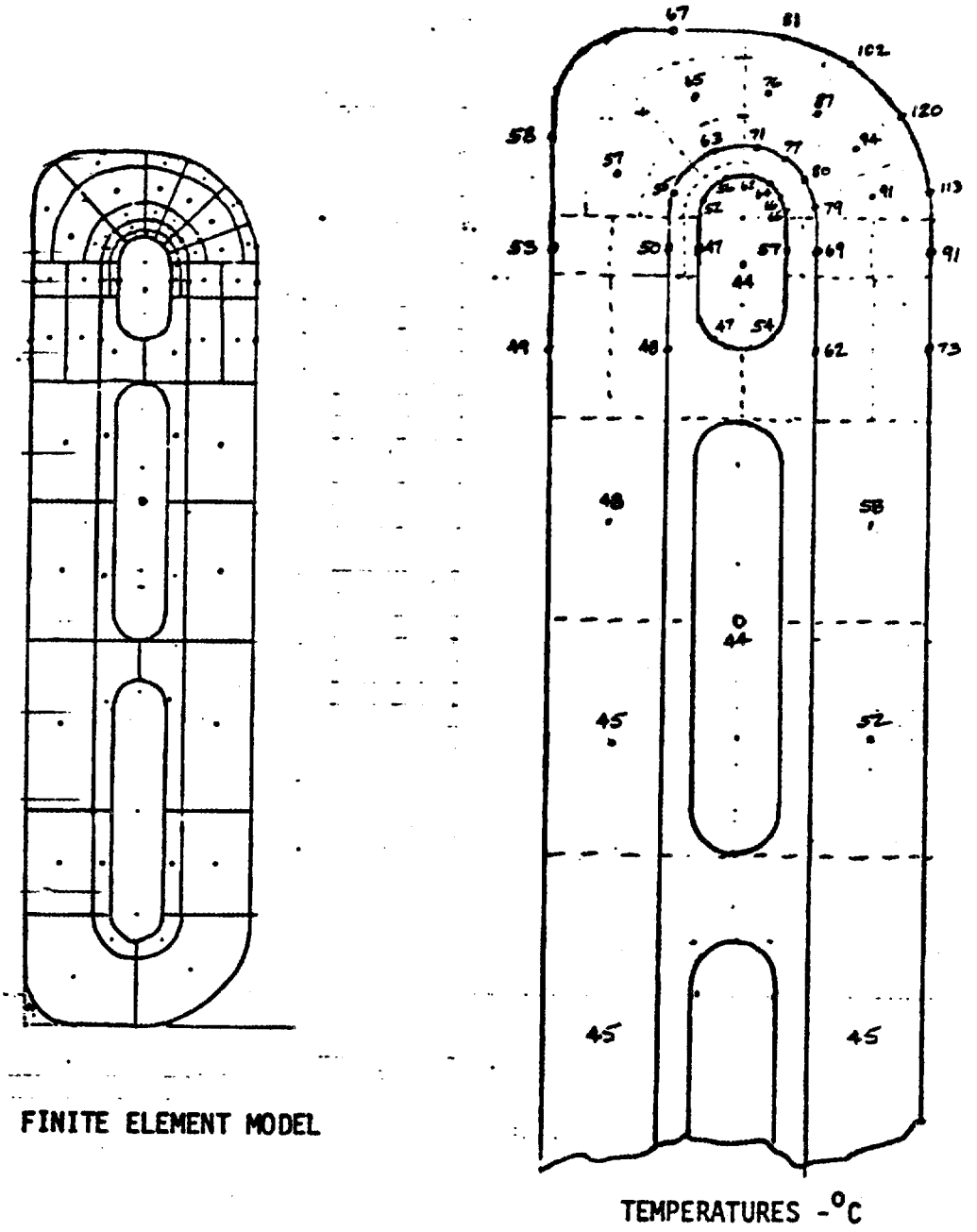

to incur large pressure drops in the coolant system. The 0.95 kg/s (15. GPM) water flow rate was shown to provide adequate cooling with relatively low pressure drops. Table 5.3-2 summarizes these results.

Table 5.3-2. Limiter Hydraulic Parameters

Heat load on 1/2 limiter	23.1 kW
Mass flow	0.95 kg/s (15 GPM)
Flow Velocity in small passage	9.3 m/s
Convective film coefficient in small passage	3.66 W/cm^2°C
Pressure drop thru limiter	~15 psi

Water pressures will be maintained at pressures sufficiently high to prevent boiling within the limiter. That is, coolant pressures in the limiter will be higher than the local saturation pressure of water. This single phase flow condition also provides additional cooling margin, which is desirable in light of the uncertainty on the applied heat flux. A finite difference model of the limiter configuration was constructed using a steady state heat transfer code called STEDROM. Thermal conductivities used for the copper alloy and aluminum castings were 1.31 W/cm°C and 1.51 W/cm°C, respectively. Heat flux distributions from Section 5.3.1 were imposed on the corner of the limiter model for both baseline and upgrade conditions. Figures 5.3-3 and 5.3-4 present the temperature distributions. Maximum aluminum temperatures of 120°C (baseline) and 209°C (upgrade) are shown. For the upgrade condition, the maximum temperature at the coolant/copper interface is 91°C, which implies a pressure requirement of about 15 psia minimum in the limiter to insure single phase flow.

5.3.3 Structural Analysis - The objective of these analyses was to define thermal stress levels in the aluminum/copper limiter composite and predict the fatigue life. Thermal stresses and fatigue life were calculated for both the baseline input power level (2.0 MW) and upgrade input power level (5.0 MW). Thermal stresses result from the temperature gradient through the depth of the limiter and from the temperature gradient across the aluminum and copper at the coolant passage.

FIGURE 5.3–4 TEMPERATURE FOR EBT-P LIMITER
(UPGRADE – 5.0 MW INTO TORUS)

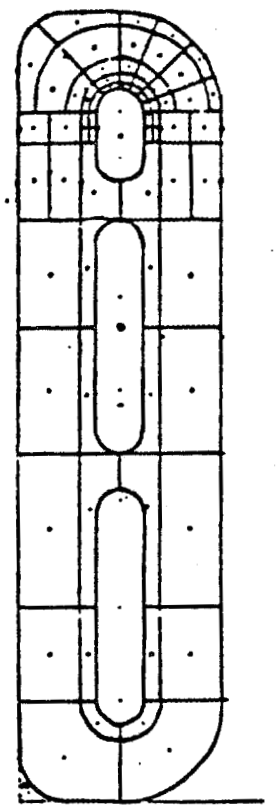

FINITE ELEMENT MODEL

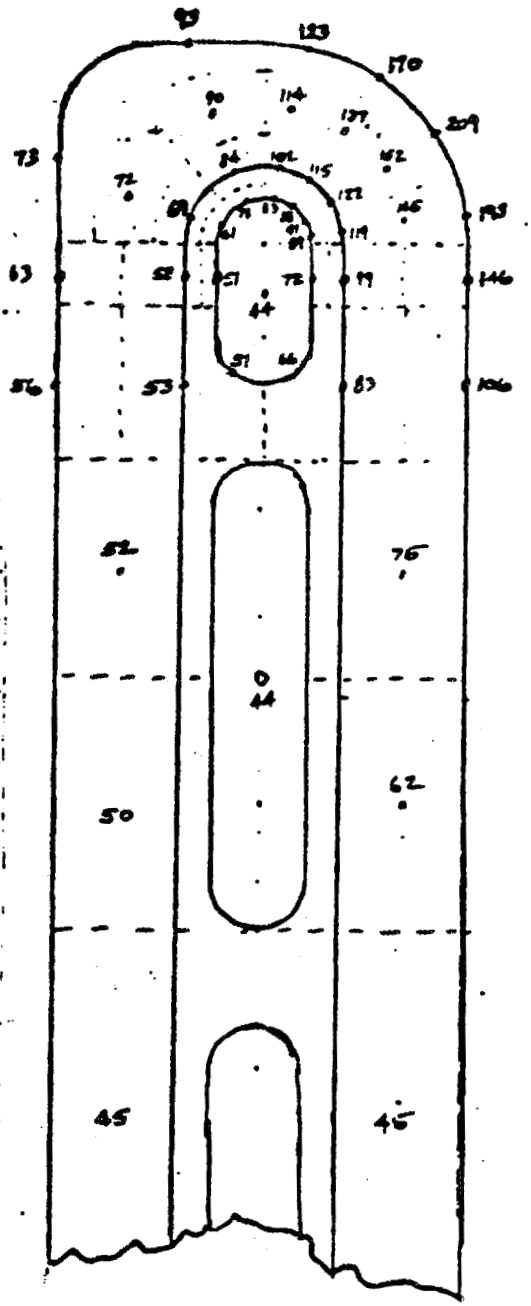

TEMPERATURES - °C

Limiter thermal stresses were calculated with the PLATSA thermal stress code. This is a two-dimensional iterative finite element code, developed at MDAC-St. Louis, that allows the actual nonlinear temperature dependent stress-strain behavior of the material to be included. Temperatures for both the baseline and upgrade conditions were discussed in the previous section. Although the limiter is free to expand, thermal stresses are developed because the local hot region (peak temperature 120°C) is restrained from expansion due to the bulk of the limiter being at approximately 45°C, as shown in Figure 5.3-5. For the baseline condition this internal constraint is 48% of the full constraint condition. Resulting thermal stresses are shown in Figure 5.3-5. The maximum compressive thermal stress is 11,500 psi. This is below the yield strength of A356 aluminum (29,000 psi at 120°C). Increasing the input power to upgrade conditions (5.0 MW) increases the peak temperature from 120°C to 209°C. The resulting thermal stress distribution is shown in Figure 5.3-6. Plastic stress levels are reached in the hot region. Plastic strain levels of 0.10% are reached in the aluminum.

Thermal stresses also result from the temperature gradient across the wall at the hot region. For the baseline condition the temperature gradient is 50°C, as shown in Figure 5.3-3, and results in a compressive stress of 8340 psi. At the upgrade power levels the temperature gradient is 118°C, as shown in Figure 5.3-4, and results in a compressive stress of 20,200 psi. The corresponding thermal strain is 0.00198 in/in.

Thermal stresses resulting from the temperature gradient through the depth of the limiter and from the temperature gradient across the aluminum and copper at the coolant passage is additive. The resulting maximum compressive thermal stress level for the baseline condition is 19,840 psi. This value is less than the yield strength of A356 aluminum at 120°C. At the upgrade condition, stresses are in the plastic region. The resulting plastic strain level is 0.004639 in/in (0.46%). The maximum allowable elongation of A356 aluminum is 3%.

5.3.4 Limiter Fabrication - The approach for fabricating the baseline EBT-P limiters shown in Figure 5.3-1; MDAC's experience with the proposed method is discussed in this section. The baseline limiter concept consists of an internal copper alloy passage with a thick aluminum overcoat. The limiters would be fabricated by first casting a manifold with passages for coolant from a copper base alloy such as alloy 82500. The copper casting would provide the coolant channels and serve as the primary structural member for carry-

Figure 5.3-5 LIMITER THERMAL STRESS DISTRIBUTION—BASELINE POWER

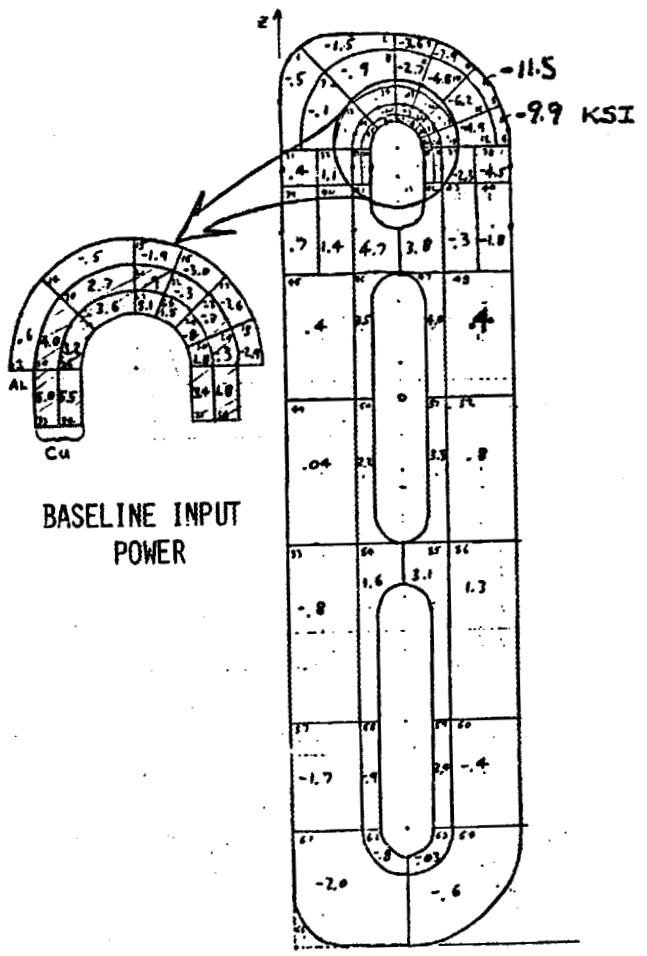

Figure 5.3-6 LIMITER THERMAL STRESS DISTRIBUTION—UPGRADE POWER

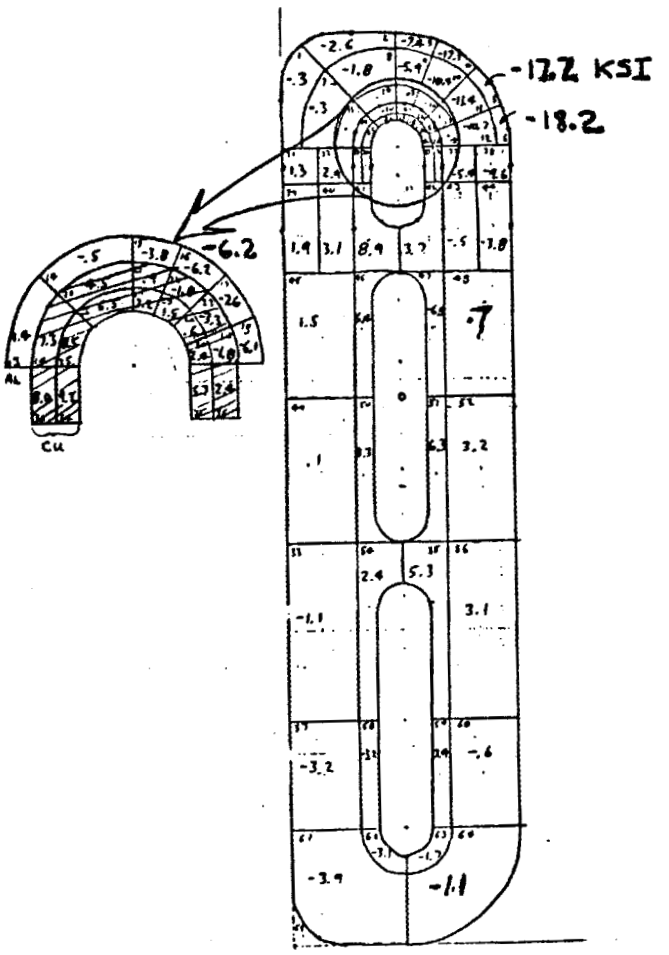

ing the pressure loads. Subsequently, an aluminum alloy, such as A356 or A357, would be cast around the copper manifold to provide a sacrificial material with a low atomic number. Both the copper and aluminum alloys will be sand cast. Sand casting was selected because of its low inherent cost. The concept of casting aluminum around a copper coolant passage is utilized in the heating element industry. The process is not widely known, but is within current state-of-the-art technology and therefore does not require extensive development. As with any casting operation, an iterative process to refine the gating/rising system is needed to develop the procedure for a sound casting. Fortunately, casting is relatively inexpensive and a number of articles can be cast without incurring a large cost penalty.

Casting the copper alloy manifold will require an opening large enough to permit complete removal of the core material. The opening will then be sealed by a brazed-in plug prior to casting the aluminum around the outside of the copper manifold.

Since aluminum and copper form a eutectic at 540°C, the casting process must keep the interface temperature between the copper and aluminum below the eutectic temperature to prevent melting of the copper channels. Melting can be prevented by proper control of the process variables and possibly by plating the copper with a eutectic barrier such as nickel.

MDAC is gaining experience with casting aluminum around copper tubing for the EBT-S limiters. This work has just recently begun and much has been learned towards developing the casting procedure.

5.3.5 Limiter Development Plan - The major limiter development tasks include conducting the limiter and heat flux experiments in EBT-S, using the EBT-S data to establish the heating and sputtering rates for EBT-P, conducting detail design of the EBT-P limiter, fabricating a full size limiter and conducting design verification tests.

5.3.5.1 EBT-S Limiter Experimental Test Program - During Title I the limiter test program was defined and coordinated with ORNL. Detail drawings of the experimental hardware were developed and a plan view of the EBT-S Limiter and Support Structure is shown in Figure 5.3-7. The tests are scheduled to commence in March 1982.

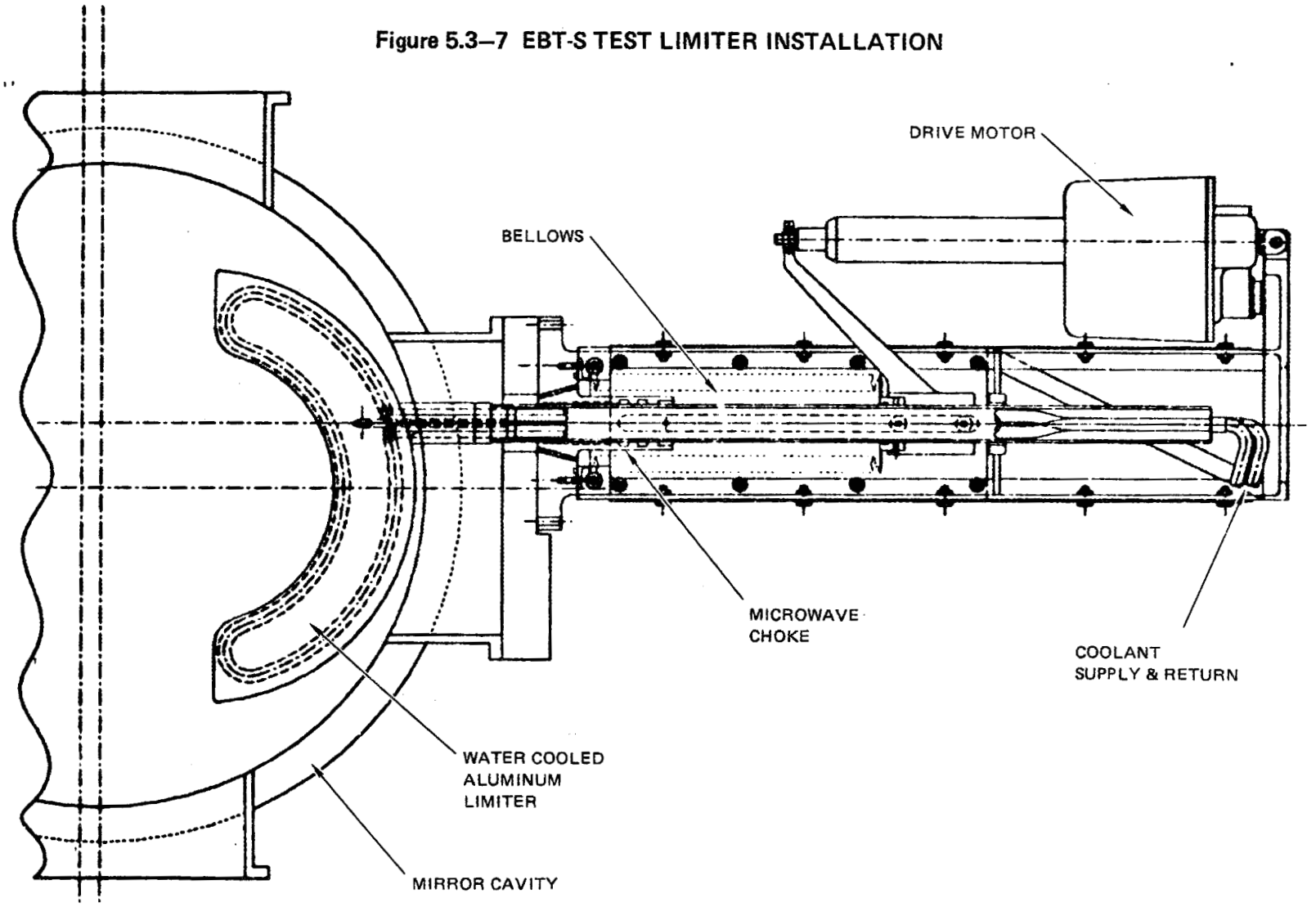

Figure 5.3–7 EBT-S TEST LIMITER INSTALLATION

The objective of the test program is twofold: to determine the effect limiters have on the plasma and second to measure the heating and sputtering rates. Probe calorimeters will be used to measure the heat flux distributions.

The limiter experiments will attempt to determine whether the effects of a limiter in a particular location are localized within the sector or coupled to the toroidal plasma. By locating probes in both the limiter cavity and additional cavity, changes in absorbed power would be measured as the limiter position is varied. A specially modified cavity will be installed to accommodate the limiter.

The experimental program comprises a sequence of steps as follows:

- Measure plasma power near the magnet bobbin wall surface in the equatorial plane as a function of radius with a single probe.
- Measure plasma power near the wall at other poloidal angles (every 45°) as a function of radius using multiple probes.
- Install a special cavity equipped with an adjustable limiter outboard of the torus centerline near the wall of the magnet bobbin. Measure the power near the walls in the same sector and an additional sector as the limiter position is varied radially.
- Install a second limiter covering the cavity wall inboard of the torus centerline and measure changes to the heat flux distribution on the magnet sidewall as the limiters are adjusted radially.

It is anticipated that measurements would be made under various plasma conditions, but primarily in the stable T-mode of operation. One important measurement would be a determination of the particle flux in the plasma boundary region (i.e., between the volume defined by the annulus and the physical limiter) as a function of plasma radius. Since the plasma radius can be varied from −12 to −18 cm (measured in the midplane) the boundary region can be increased up to about 6 cm from the closest point in the magnet aperture. The interpretation of the data obtained in this region would be complicated by the fact that plasma confinement should degrade as the minor radius is decreased. The use of an adjustable limiter in conjunction with the point probe measurements would be useful in distinguishing the boundary effects from plasma changes due to the variation in minor radius.

The EBT-P limiter development plan involves the following activities. The heating and sputtering data measured in EBT-S will be used to calibrate the analytical models for predicting heating and erosion rates for EBT-P. Detailed thermal, hydraulic and strength analysis will be conducted to refine the current limiter concept. In addition, the limiter support structure and positioning mechanism design will be reviewed and improvements made as necessary. A preliminary fabrication processes specification will be written and refined during the fabrication of the prototype limiter. Thermal/hydraulic/mechanical tests will be conducted to verify the limiter design.

6.0 SCHEDULE

The major Toroidal Vessel milestones for Title II Design, sustaining engineering, fabrication and installation is presented in Figure 6-1.

FIGURE 6–1 TOROIDAL VESSEL SCHEDULE

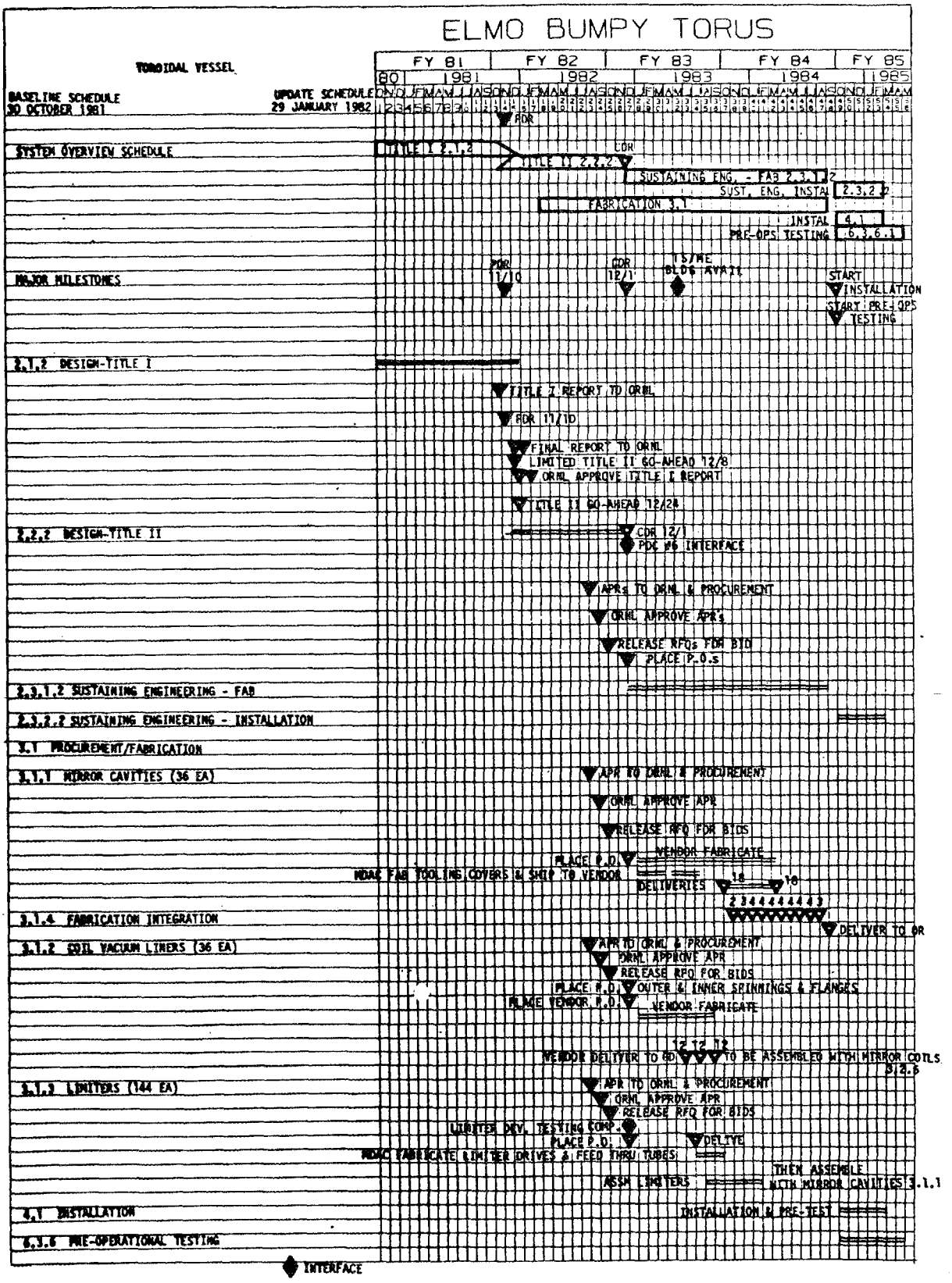

7.0 REFERENCES

1. Mezines, S. A., et. al., *"Vacuum Vessel Seals and Wall Material Trade Study"*, EBT-P-TN-001, 1 June 1981.
2. Dillow, C. F., *"Supplement No. 1 to Vacuum Vessel Seals and Wall Material Trade Study"*, EBT-P-TN-001 Supplement No. 1, 30 July 1981.
3. Mezines, S. A., *"Vacuum Vessel Material and Seals Recommendation for EBT-P"*, EBT-P-TN-002 Supplement No. 2, 17 August 1981.
4. Lang, G. P., *Use of Non-Metallic Vacuum Seals on EBT-P,* EBT-237, 14 Nov 80.
5. Peacock, R. N., *Practical Selection of Elastomer Materials for Vacuum Seals,* J. Vac. Sci. Tech, Jan/Feb 1980.
6. Mullaney, D. H., *PPPL,* Personal Communication, 20 Jul 81.
7. Fleming, R. B., *PPPL,* Personal Communication, 21 Jul 81.
8. Polk, D., *United Technologies,* Personal Communication, 20 Jul 81.
9. Doggett, J., *LLL,* Personal Communication, 24 Jul 81.
10. Miller, J., *General Atomic,* Personal Communication, 22 Jul 81.
11. Ishimaru, H., *Aluminum Alloy Vacuum Chamber with Conflat Type Seal to an Aluminum Alloy Flange for Ultrahigh Vacuum,* 3rd Symposium on Accel. Sci. and Tech., Aug 1980.
12. Sakai, I., et. al., *Sealing Characteristics of All Aluminum Vacuum System Using Elastic Metal Gasket,* 3rd Symposium on Accel. Sci. and Tech., Aug, 1980.
13. Wheeler, W. R., *The Design of Large Vacuum Seals for Nuclear Fusion Machines,* Proc. 7th Intern Vac. Congr. Vienna, 1977.
14. Miyahara, A., et. al., *Development of Large Diameter Metal Gaskets for Sealing Ultra-High Vacuum Flange Connections,* Copyright 1979 IEEE.
15. Fleming, R. B., et. al., *Development of Bakeable Seals for Large Noncircular Ports on the Tokamak Fusion Test Reactor,* J. Vac. Sci. Tech., Jan/Feb 1980.
16. Hager, R., *General Atomic,* Personal Communication, 20 Jul 81.
17. Johnson, R., *ORNL,* Personal Communication, 27 Jul 81.
18. Driemeyer, D. E., McDonnell Douglas Astronautics Co., *Studies of Fusion Product Confinement and Heating in EBT Reactors,* 9th Symposium on Engineering Problems of Fusion Research, Chicago, Ill., October 26-29.

APPENDIX A - X-RAY ANALYSIS

A.1 METHODOLOGY OVERVIEW

There are two primary sources of x-rays in the EBT-P device. The first is due to direct Bremsstrahlung emission by the high-energy ring electrons, and the second is due to Bremsstrahlung radiation emitted by electrons which are scattered out of the ring, as they slow down in the wall or limiter. Generally the two components are approximately equal in power level; however the direct source can exceed that from scattered electrons by a factor of three or more for ring temperatures in excess of 2 MeV and higher plasma purity levels. In any event, the x-ray losses amount to less than 0.5% of the total power required to sustain the ring against all losses for all of the cases discussed herein.

In order to develop estimates of the x-ray radiation level in the EBT-P device over a range of ring/plasma and wall/limiter conditions, the present analysis began by considering the Bremsstrahlung emission on a per electron basis. The direct x-ray power emitted by an electron of energy, γ, per unit of emitted x-ray energy, E, is then given by [1].

$$P_D(\gamma, E) = c\sigma_0 \Sigma n_i Z_i^2 \, B(\gamma, E) \, (\gamma^2-1)^{1/2}/(\gamma-1), \tag{A-1}$$

where

$$\gamma = \frac{E_e}{m_0 c^2} = \left(1 - \frac{v^2}{c^2}\right)^{-1/2}$$

$$\sigma_0 = \frac{1}{137}\left(\frac{e^2}{m_0 c^2}\right)^2 = 5.80\ (10)^{-2\sigma}\ \text{cm}^2/\text{nucleus}$$

N_i = i-th background ion density at the ring location

Z_i = i-th background ion charge

c = speed of light

m_0 = electron rest mass

a 2:1 mirror is given approximately by $n_R(\gamma_o)\ \nu_{\epsilon O}/2$, where ν_{90} is the 90° collison frequency; hence the "scattered" x-ray power per unit x-ray energy per unit ring volume is

$$p_s(E) = \frac{16\ e^4 n_R \ln\text{-}\ \Sigma n_i Z_{ef}^2}{\pi\ m_o^2 C^3}\ \alpha \int_{E+1}^{\infty} \Delta E\ (\gamma_o, E) \quad \left(\frac{\gamma_o^2}{\gamma_o^2-1}\right)\ e^{-\gamma_o/T}\ d\gamma_o. \tag{A-6}$$

Here the term Z_{ef} has been introduced to account for the fact that in scattering events the ring electrons see only the effective charge of the nucleus, not the total nuclear charge Z_i.

It is convenient to write both these losses in terms of the magnetic field strength at the ring, B_R. This is done by expressing the background ion density in terms of the ratio, f_c, of the background electron density to the microwave cutoff density.

$$n_i = 1(10)^{13} \left[\frac{f_c B_R^2}{1 + f_z\ (Z_{ef}-1)}\right], \tag{A-7}$$

and by writing the ring density in terms of the ring beta, β_R,

$$n_R = 5(10)^{12} \left[\frac{\beta_R\ B_R^2}{T}\right]. \tag{A-8}$$

For a ring volume V_R, the direct and scattered x-ray powers (in watts) per unit of emitted x-ray energy are then

$$P_D\ (E) = 7.12\ (10)^{-5}\ V_R f_c \beta_R\ B_R^4 \left[\frac{1 + f_z\ (Z_i^2-1)}{1 + f_z\ (Z_{ef}-1)}\right] F_D(E) \tag{A-9a}$$

$$P_S\ (E) = 7.12\ (10)^{-5}\ V_R \left(\frac{\ln\Lambda}{25}\right) f_c \beta_R\ B_R^4 \left[\frac{1 + f_z\ (Z_{ef}^2-1)}{1 + f_z\ (Z_{ef}-1)}\right] F_S(E) \tag{A-9b}$$

where,

$$F_D(E) = \left(\frac{\alpha}{T}\right) \int_{E+1}^{\infty} (\gamma, E)\ \gamma\ (\gamma+1)\ e^{-\gamma/T}\ d\gamma \tag{A-10a}$$

FIGURE A–1 X–RAY SPECTRA FOR AN ALUMINUM WALL

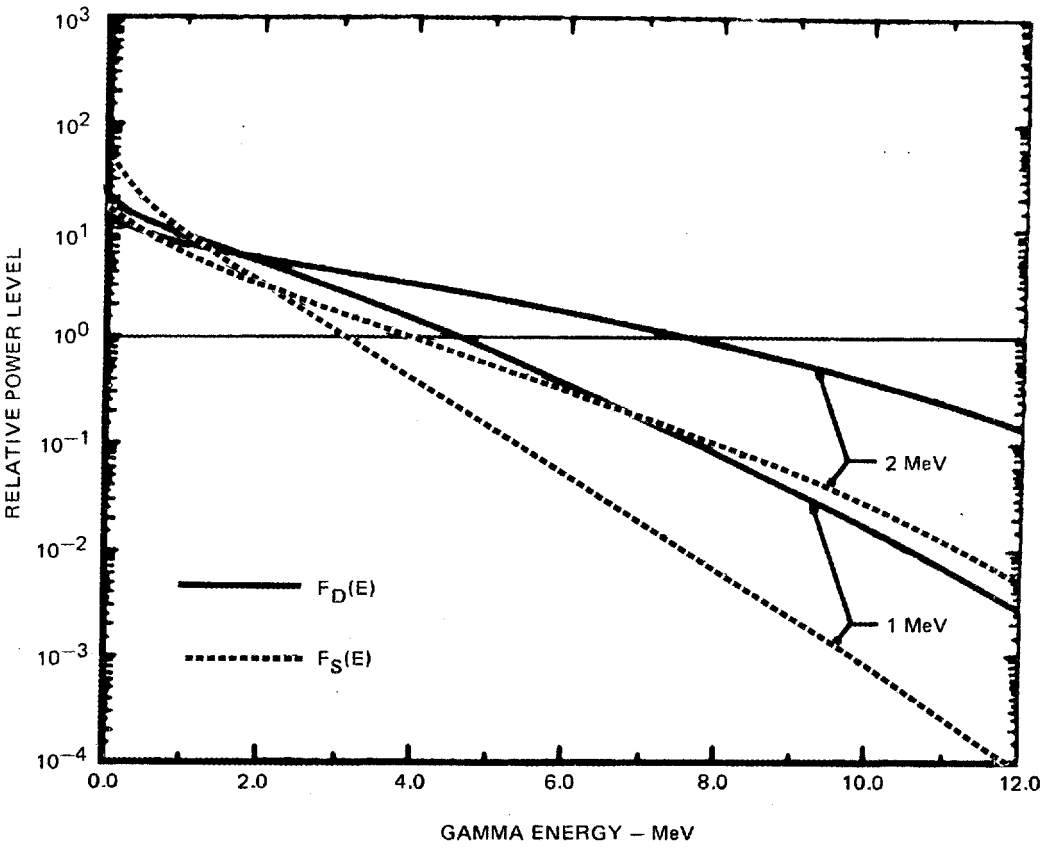

Table A-1

Parameter Values Utilized in the X-ray Analysis

Parameter	Baseline	Upgrade
V_R (cm^3 per cavity)	8333	8333
β_R	0.3	0.3
B_R (T)	1.07	1.6
$\bar{T}_R$ (MeV)	1 - 2	1 - 2
f_C	0.5	0.5
f_Z	0 - 0.02	0 - 0.02
Z_i, Z_{ef} (Al ions at 100 eV)	13, 8	13,8

Several assumptions have been made in arriving at the parameters given in Table A-1. The first is that the ring occupies ~ 10% of the total plasma volume of 3 m^3. This is based on observations from EBT-I and S, and is thought to represent an upper bound on the actual ring volume. The second assumption is that the ring beta will be ~ 30%. This is somewhat optimistic from the standpoint of x-ray generation, since operation at higher ring beta values is desirable, but is thought to be realistic when coupled with the pessimistic upper limit of 2% Al impurity in the plasma to provide a "worst case" x-ray power level. In addition, for the 2% impurity "worst case" analysis, an edge temperature of ~ 100 eV was assumed which gives an effective Al charge, Z_{ef}, equal to 8. Finally, the local electron density at the ring was assumed to be 1/2 of the microwave cutoff density for all cases. This is a pessimistic assumption from the standpoint of x-ray generation and is thought to be an upper physics bound on this parameter based on EBT-S measurements.

The x-ray power level in each mirror cavity is calculated from the information given in Table A-1 and Figure A-1, and the results of two such calculations are summarized in Table A-2. This table compares the emitted x-ray power distribution for the baseline configuration with no impurities, to that for the same case with 2% Al impurity in the plasma. As is expected, the power level with impurities increases by a factor of ~ 3 with the bulk of the increase occuring in the direct component. Table A-2 also gives the powers corresponding to the other ring loss mechanisms for comprison. These values indicate that electron drag and synchrotron radiation comprise the majority of the ring loss. Scattering losses

amount to only 3% of the total with no impurities and increase to ~ 6% of the total of the 2% impurity level. In both cases ~ 2% of the scattered electron power is converted to x-rays as the electrons are stopped in the limiters.

The data summarized in Table A-2 is subsequently used to evaluate the radiation dose rate at the vacuum seals. Since the direct and scattered sources are roughly distributed over the surface of a sphere centered at the midpoint of each cavity, they can be approximated by a single point source located at the cavity mid-point. Assuming a vacuum seal radius of 38 cma nd no shielding, the x-ray source distribution given in Table A-2 can be scaled to various power levels and combined with the energy dependent mass attenuation coefficients of Table A-3 to yield the dose rate at the vacuum seal location. As is indicated in Table 3.2-3, this results in a dose rate of 8.4 rad/sec for the baseline configuration with 2% Al impurity. A similar series of dose rate calculations has been used to generate the vacuum seal dose accumulation curves shown in Figure A-2 where continuous operation under the indicated conditions has been assumed. These curves illustrate that even under the most optimistic of assumptions, e.e., the baseline case with no impurities, the dose to the seals reaches its maximum allowable level of ~ 10^8 rads in less than 1 year of operating time. The ramifications of this result are discussed in detail in Section 4, while a summary of the present analysis along with a calculation of the actual does accumulation for the proposed operating parameters is presented in Section 3.2.

References

1. R.D. Evans, The Atomic Nucleus (McGraw-Hill Book Co., New York, 1965) pp. 600-631.
2. W. Heitler, The Quantum Theory of Radiation (Oxford at the Clarendon Press, 1954) pp. 248-253.

Figure A–2 DOSE ACCUMULATION IN VACUUM SEALS AS A FUNCTION OF OPERATING TIME FOR THREE DIFFERENT SETS OF MACHINE OPERATING CONDITIONS

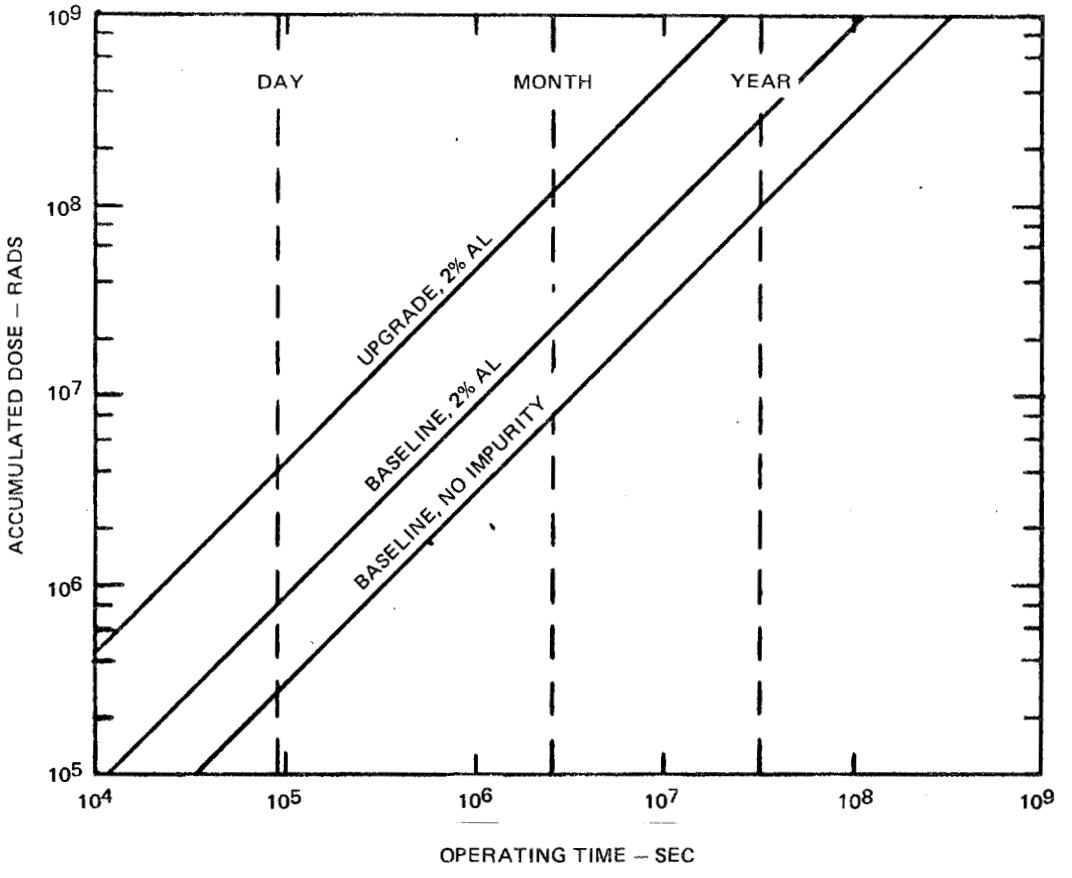

Table A-2

X-Ray Source Levels as a Function of Energy for the EBT-P Baseline Configuration at two Different Plasma Impurity Concentrations.

	No Impurities		2% Al Impurity	
Group Energy (MeV)	**Direct Power (Watts)**	**Scattered Power (Watts)**	**Direct Power (Watts)**	**Scattered Power (Watts)**
5.000E-02	1.944E-01	5.246E-01	7.435E-01	1.040E+00
1.500E-01	1.912E-01	4.033E-01	7.312E-01	7.995E-01
3.000E-01	3.295E-01	5.777E-01	1.260E+00	1.145E+00
7.000E-01	7.353E-01	9.714E-01	2.813E+00	1.926E+00
1.250E+00	4.357E-01	4.127E-01	1.666E+00	8.182E-01
1.750E+00	3.288E-01	2.388E-01	1.257E+00	4.734E-01
2.250E+00	2.480E-01	1.407E-01	9.486E-01	2.789E-01
2.750E+00	1.855E-01	8.359E-02	7.095E-01	1.657E-01
3.250E+00	1.372E-01	4.988E-02	5.246E-01	9.889E-02
3.750E+00	1.002E-01	2.984E-02	3.833E-01	5.916E-02
4.250E+00	7.237E-01	1.788E-02	2.768E-01	3.544E-02
4.750E+00	5.169E-02	1.072E-02	1.977E-01	2.125E-02
5.250E+00	3.656E-02	6.429E-03	1.398E-01	1.275E-02
5.750E+00	2.562E-02	3.857E-03	9.798E-02	7.647E-03
6.250E+00	1.781E-02	2.314E-03	6.810E-02	4.587E-03
6.750E+00	1.228E-02	1.378E-03	4.697E-02	2.751E-03
7.250E+00	8.410E-03	8.314E-04	3.217E-02	1.648E-03
7.750E+00	5.722E-03	4.976E-04	2.188E-02	9.865E-04
9.000E+00	9.354E-03	6.417E-04	3.577E-02	1.272E-03
1.100E+01	1.772E-03	7.537E-05	6.775E-03	1.494E-04
1.300E+01	2.589E-04	5.825E-06	9.902E-04	1.155E-05
TOTALS	3.128E+00	3.477E+00	1.196E+01	6.893E+00

Ring Totals	**No Impurity**	**2% AL Impurity**
Scattering Loss (Watts)	200	390
Drag Loss (Watts)	2600	2600
Synchrotron Loss (Watts)	4180	4180
Bremsstrahlung Loss (Watts)	3	12

Table A-3

Dose Calculation for Baseline Configuration
with 2% AL Impurity in the Plasma.

Group Energy (MeV)	Unshielded Energy Flux (W/cm^2)	Attenuation Coefficient ($cm^2/9$)	Dose Rate (Rad/s)
0.05	9.78E-5	0.196	1.92
0.15	8.39E-5	0.134	1.12
0.30	1.32E-4	0.106	1.40
0.70	2.60E-4	0.075	1.95
1.25	1.36E-4	0.058	0.79
1.75	9.49E-5	0.048	0.46
2.25	6.73E-5	0.042	0.28
2.75	4.80E-5	0.038	0.18
3.25	3.42E-5	0.034	0.12
3.75	2.43E-5	0.033	0.08
4.25	1.71E-5	0.030	0.05
4.75	1.20E-5	0.028	0.03
5.25	8.37E-6	0.027	0.02
5.75	5.79E-6	0.026	0.02
6.25	3.98E-6	0.025	0.01
6.75	2.73E-6	0.024	0.01
7.25	1.85E-6	0.023	–
7.75	1.25E-6	0.022	–
9.00	2.03E-6	0.021	–
11.00	3.80E-7	0.020	–
13.00	5.48E-8	0.019	–
TOTAL	1.03E-3	0.082	8.44

TORODAL VESSEL ASSEMBLY

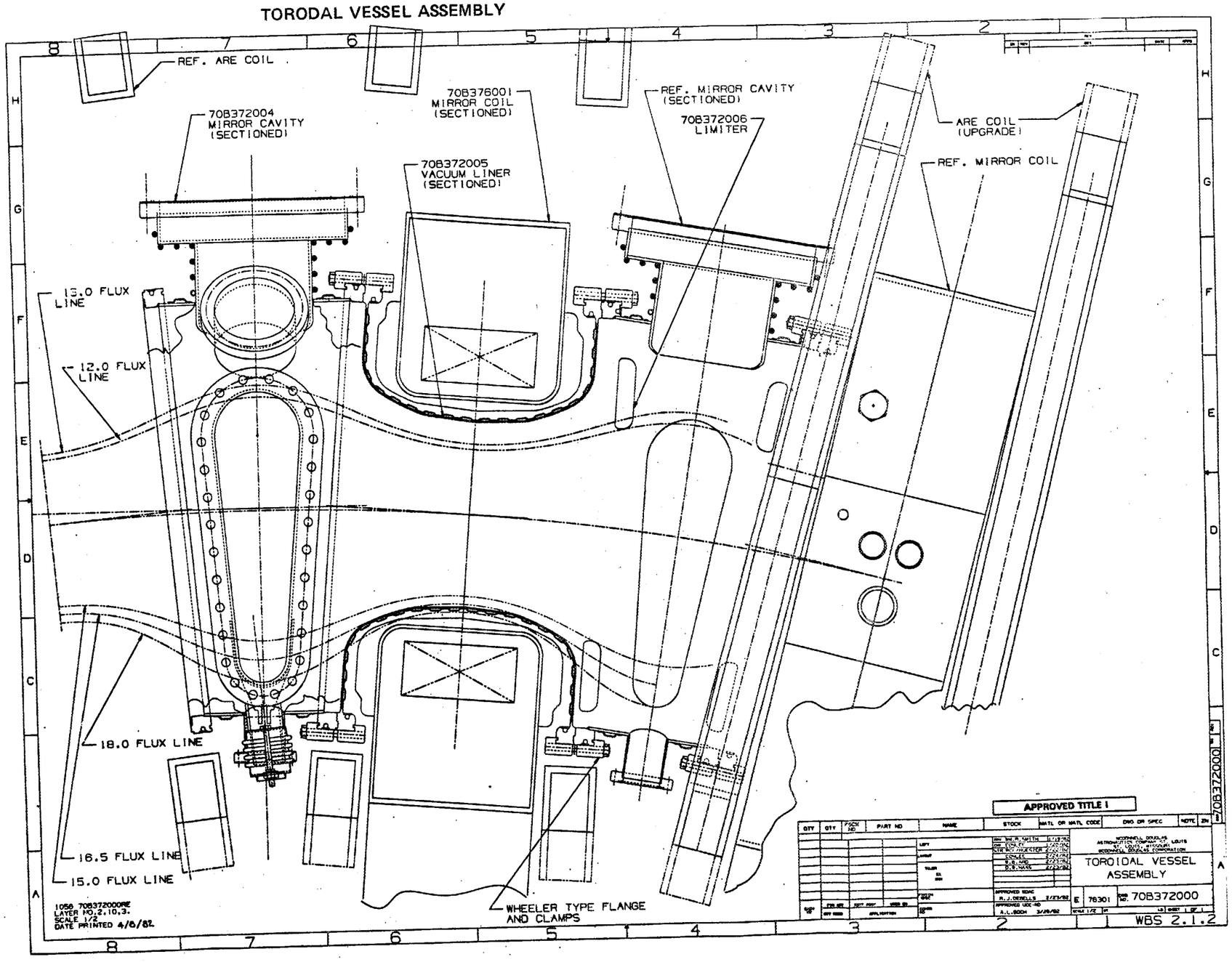

MIRROR CAVITY PORT ARRANGEMENT

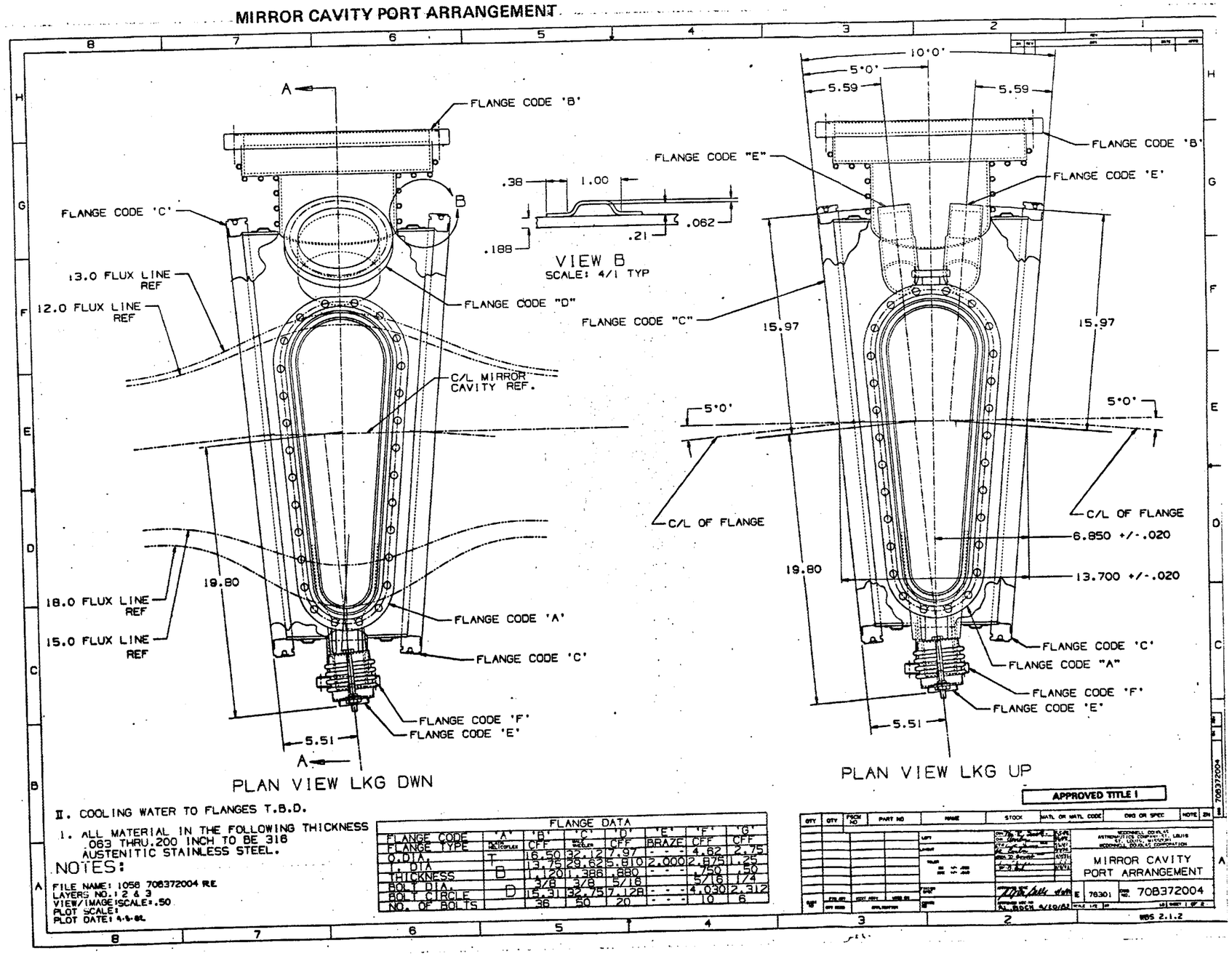

II. COOLING WATER TO FLANGES T.B.D.

1. ALL MATERIAL IN THE FOLLOWING THICKNESS .063 THRU.200 INCH TO BE 316 AUSTENITIC STAINLESS STEEL.

NOTES:

FILE NAME: 1058 708372004 R.E.
LAYERS NO.: 2 & 3
VIEW/IMAGE:SCALE=.50
PLOT SCALE:
PLOT DATE: 4-5-82

FLANGE DATA

FLANGE CODE	'A'	'B'	'C'	'D'	'E'	'F'	'G'
FLANGE TYPE	NOTE 1	CFF	NOTE 1	CFF	BRAZE	CFF	CFF
O.DIA.	T	16.50	32.12	7.97	- - -	4.62	2.75
I. DIA		13.75	29.625	5.810	2.000	2.875	1.25
THICKNESS	D	1.120	1.386	.880	- - -	.750	.50
BOLT DIA.		3/8	3/8	5/16	- - -	5/16	1/4
BOLT CIRCLE	D	15.31	32.75	7.128	- - -	4.030	2.312
NO. OF BOLTS		36	50	20	- - -	10	6

MIRROR CAVITY PORT ARRANGEMENT

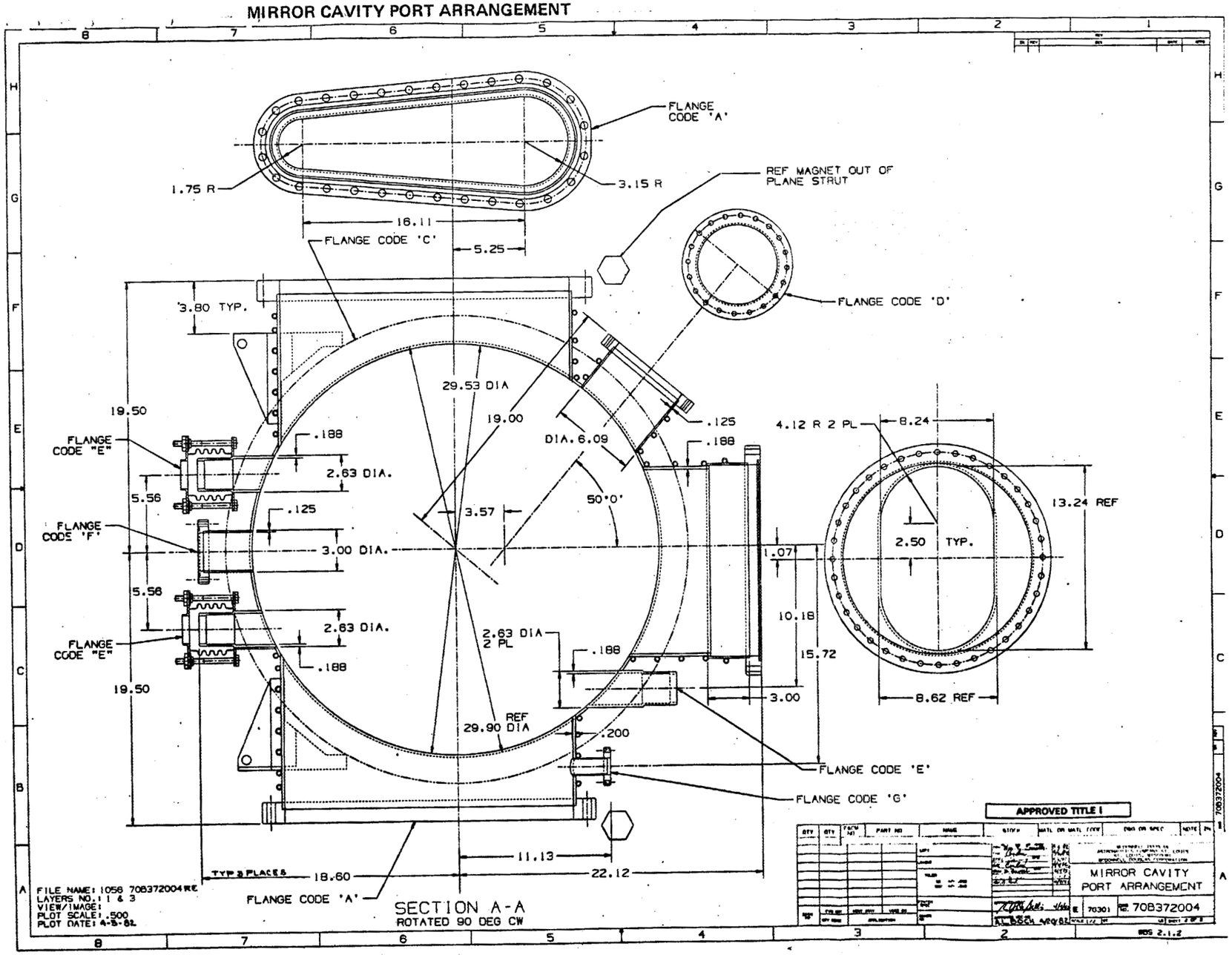

VACUUM LINER

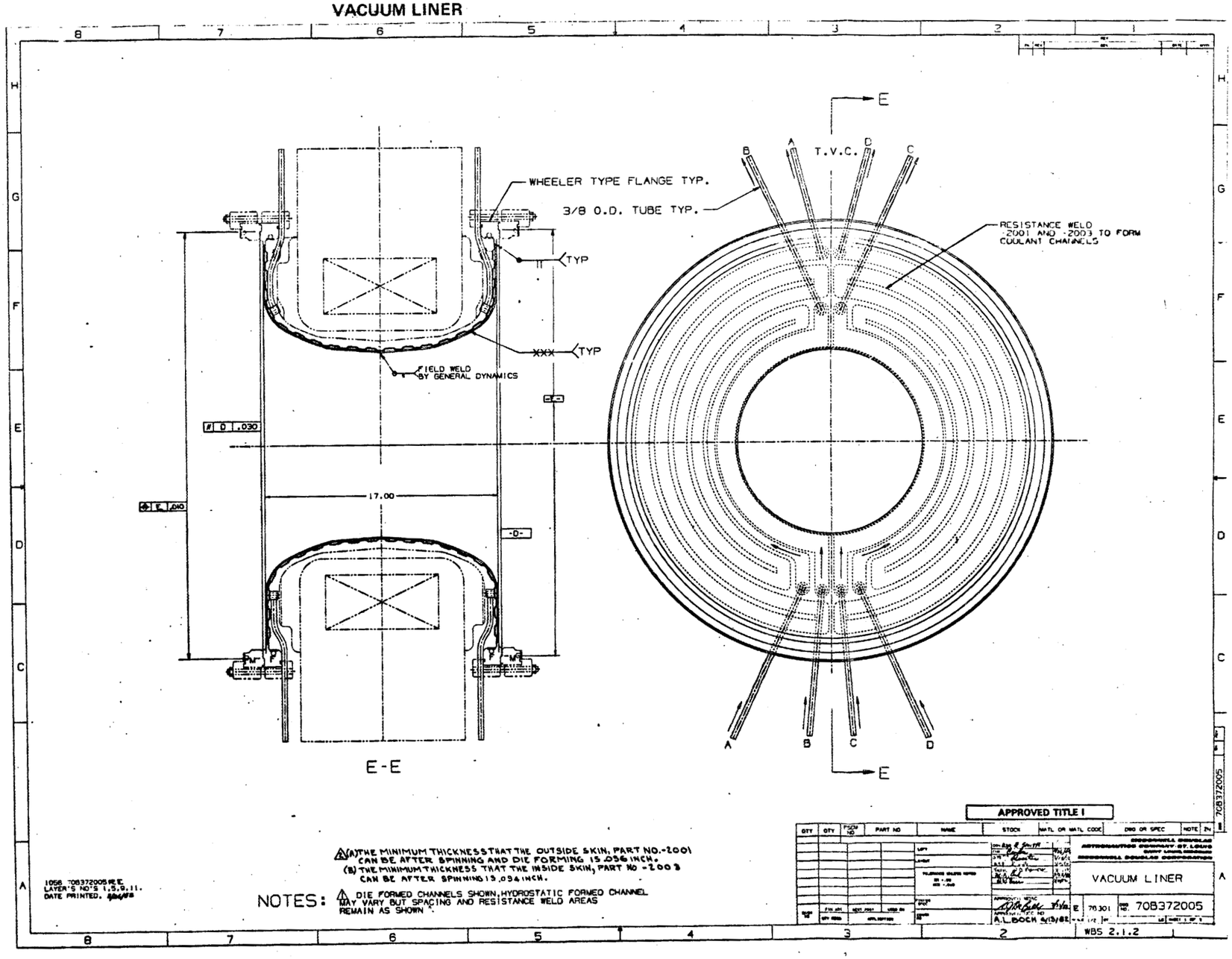

VACUUM LINER

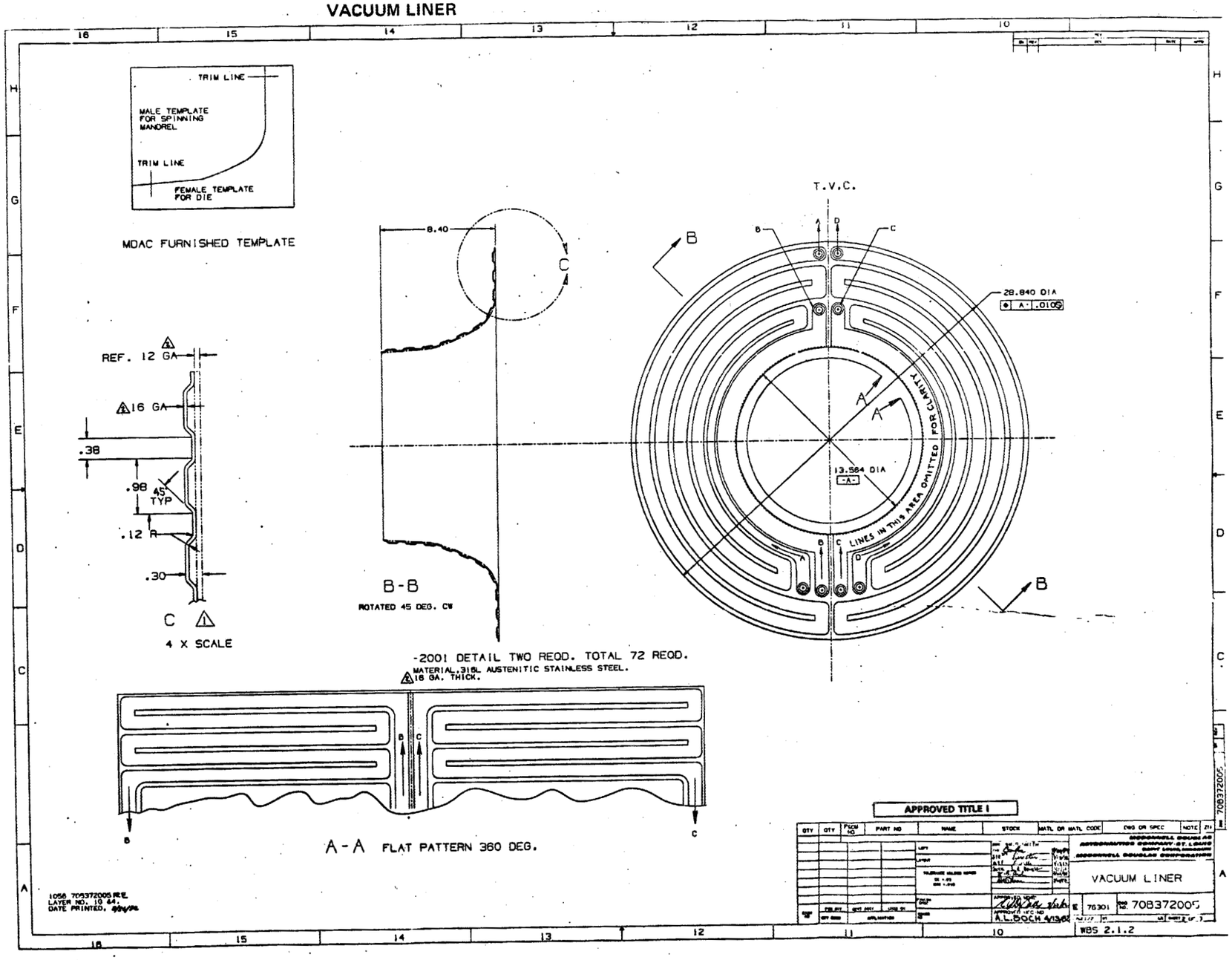

VACUUM LINER

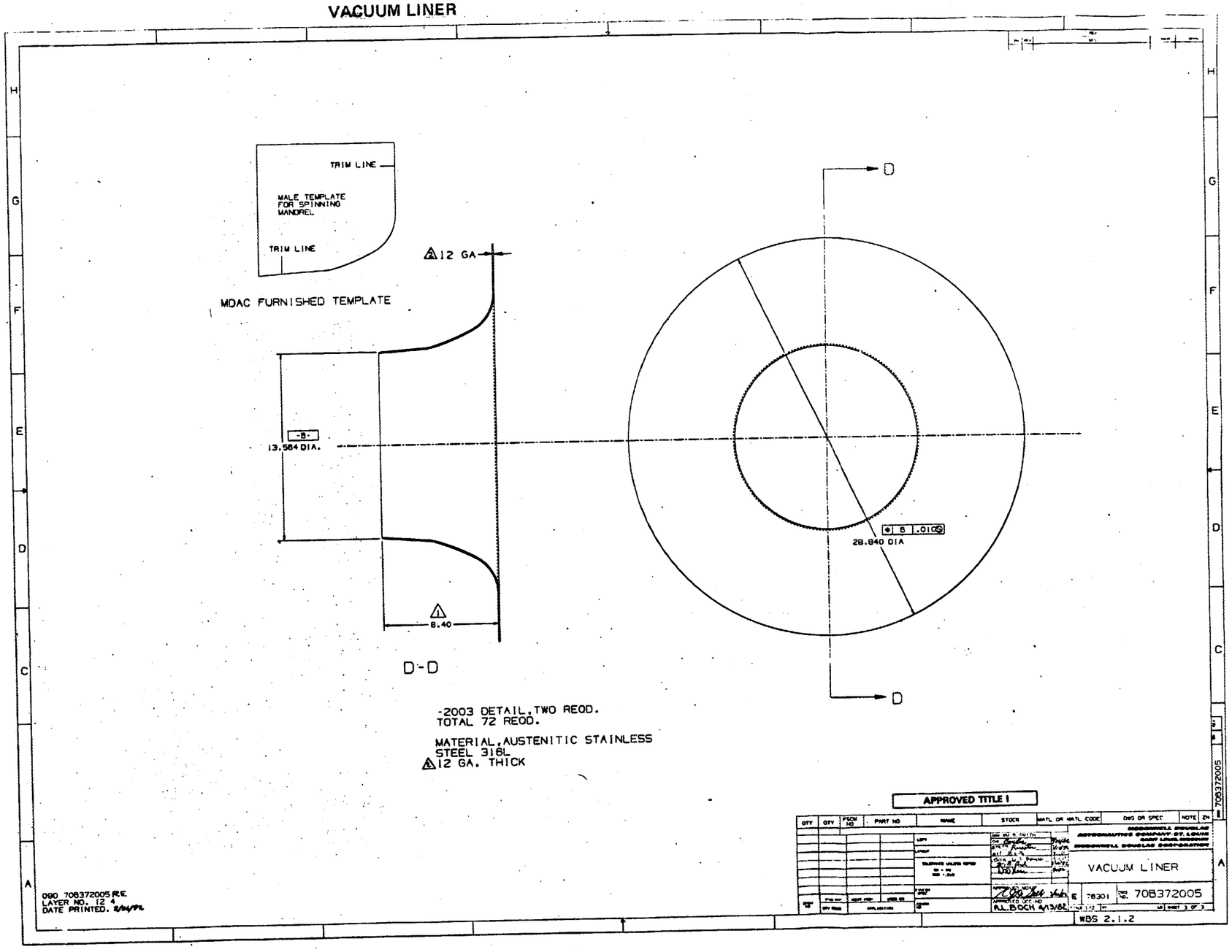

EBT-P TOROIDAL VESSEL SUPPORT

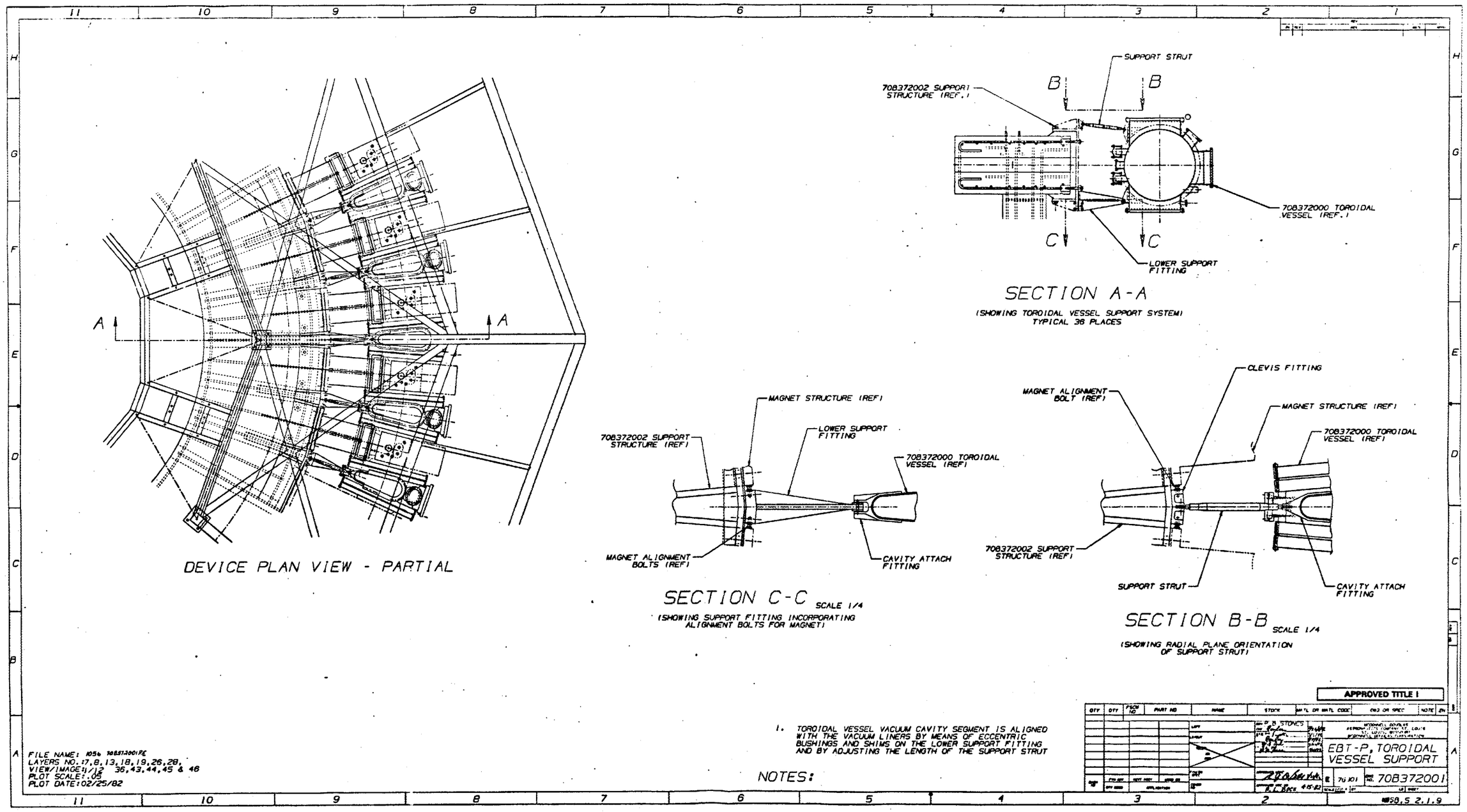

EBT–DI WATER MANIFOLDS/INTERFACE

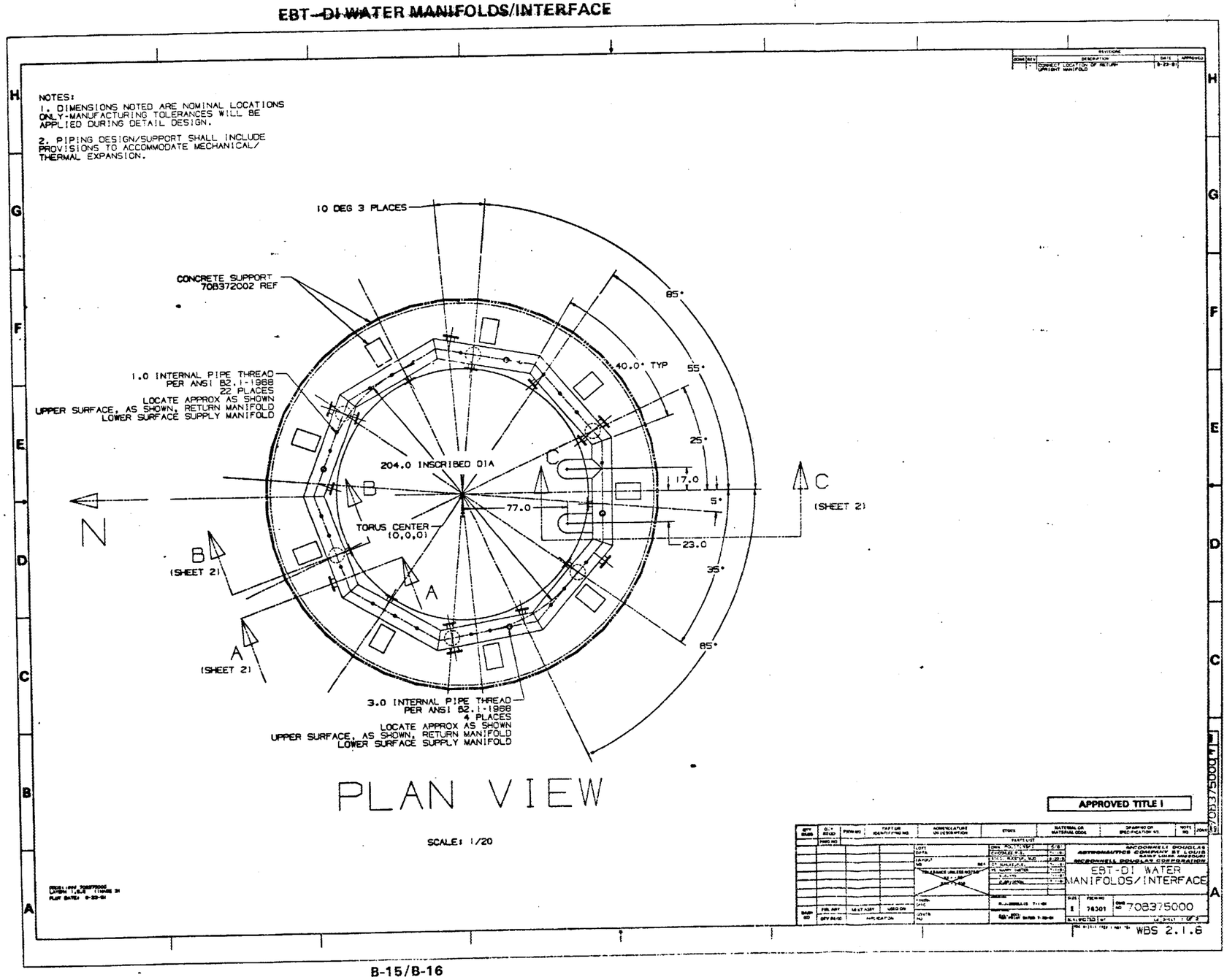

EBT–DI WATER MANIFOLDS/INTERFACE

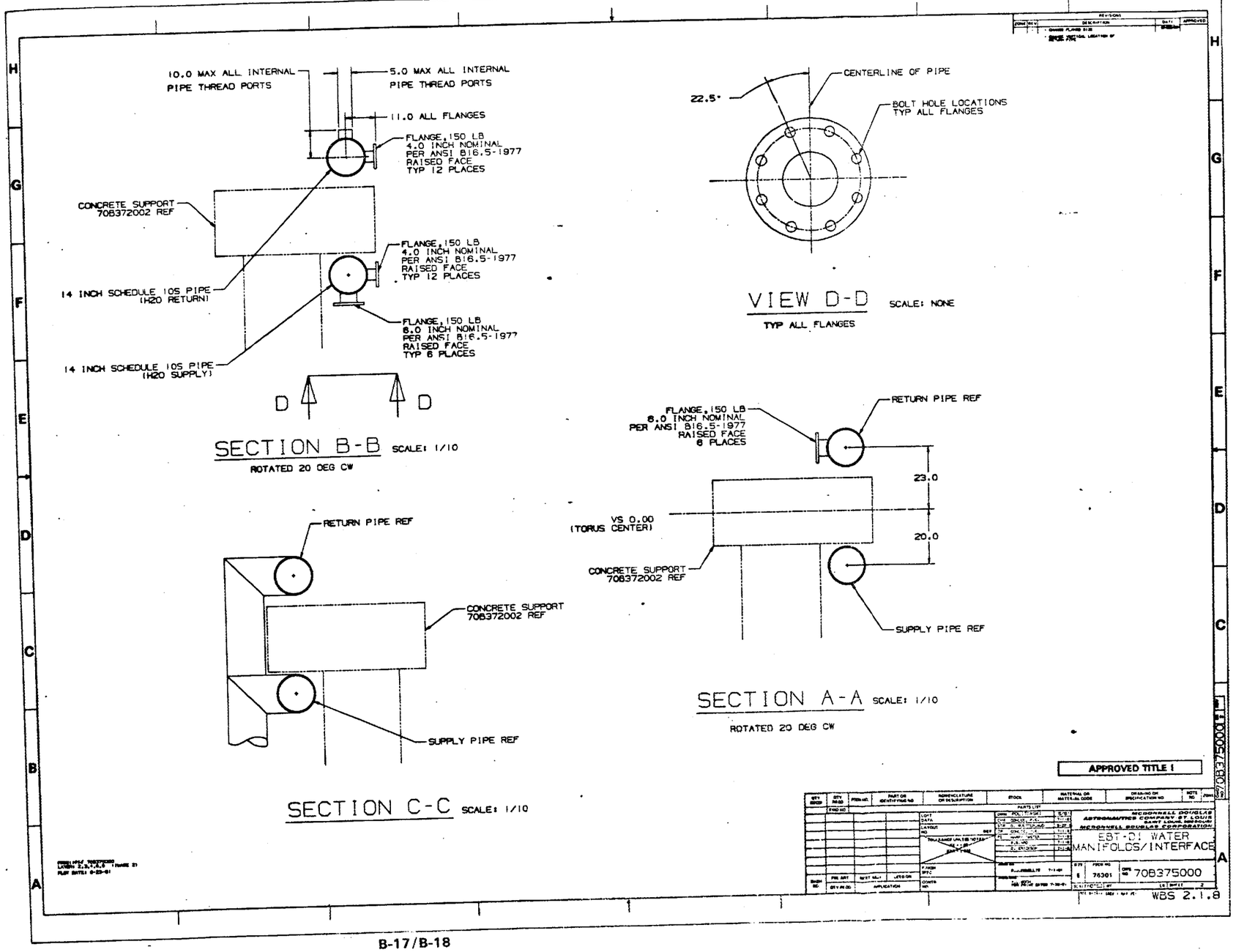

EBT-P CONTROL PANEL – DEVICE COOLANT, FULL SECTOR

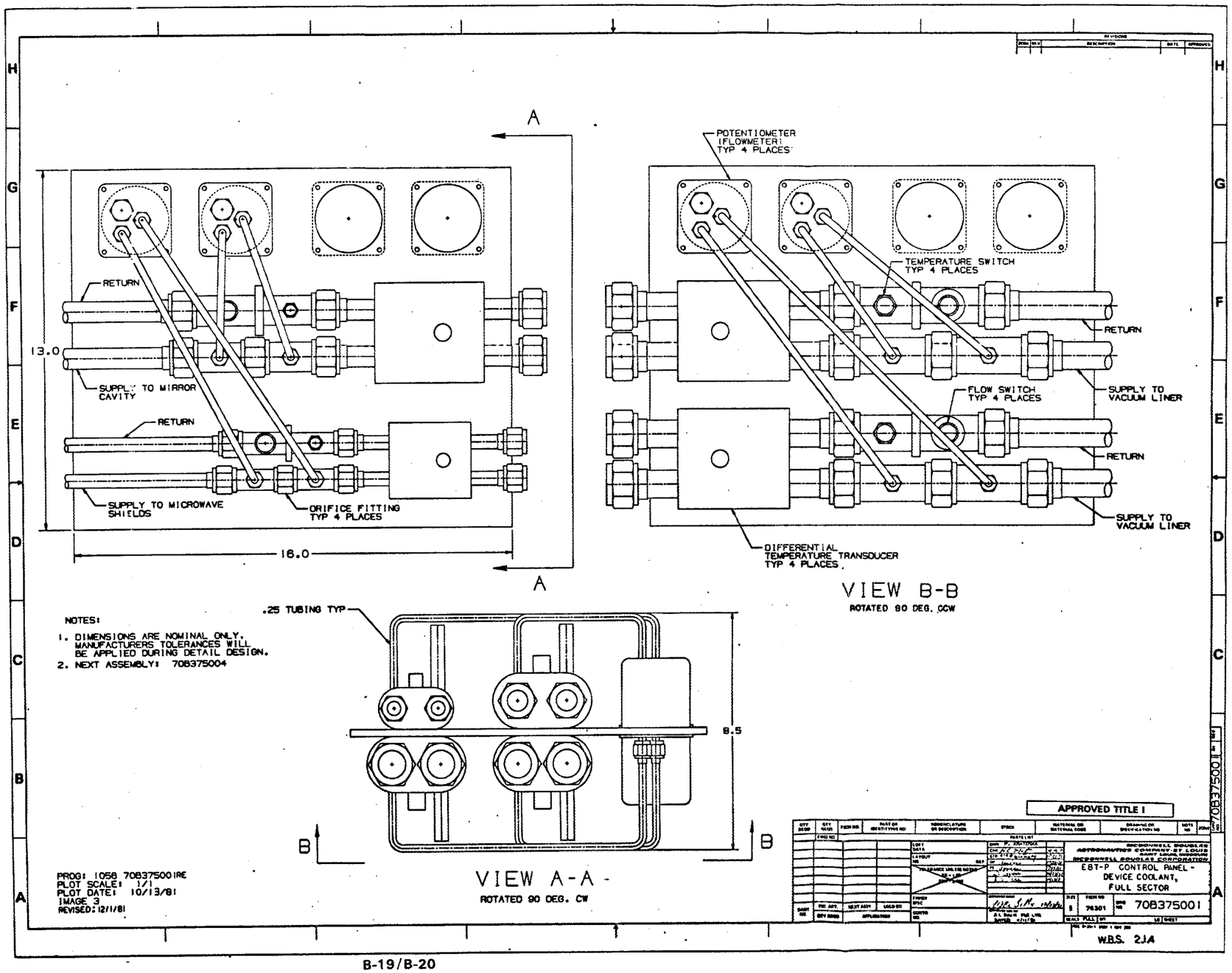

EBT–P INSTALLATION–DEVICE COOLANT, TORUS

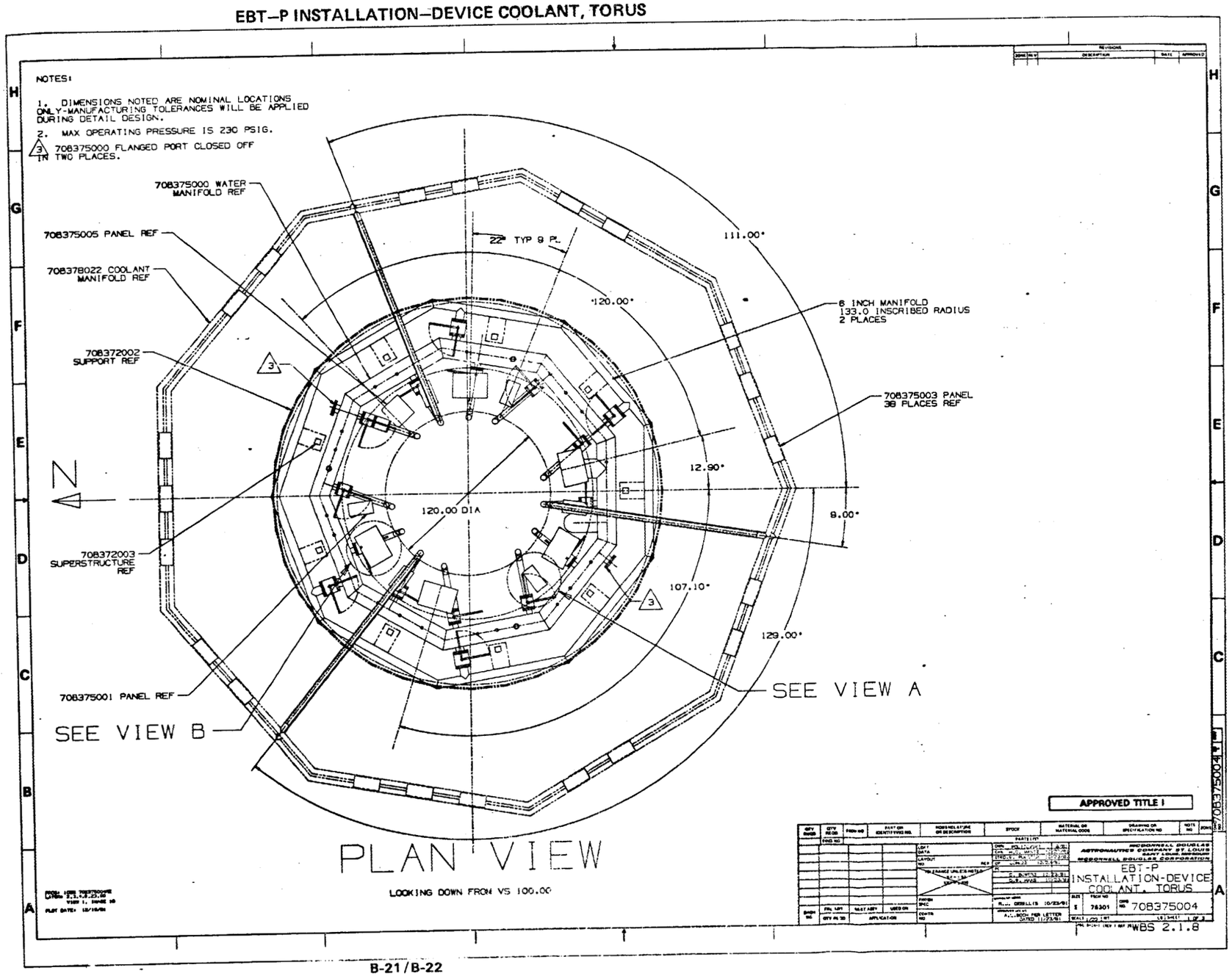

EBT–P INSTALLATION–DEVICE COOLANT, TORUS

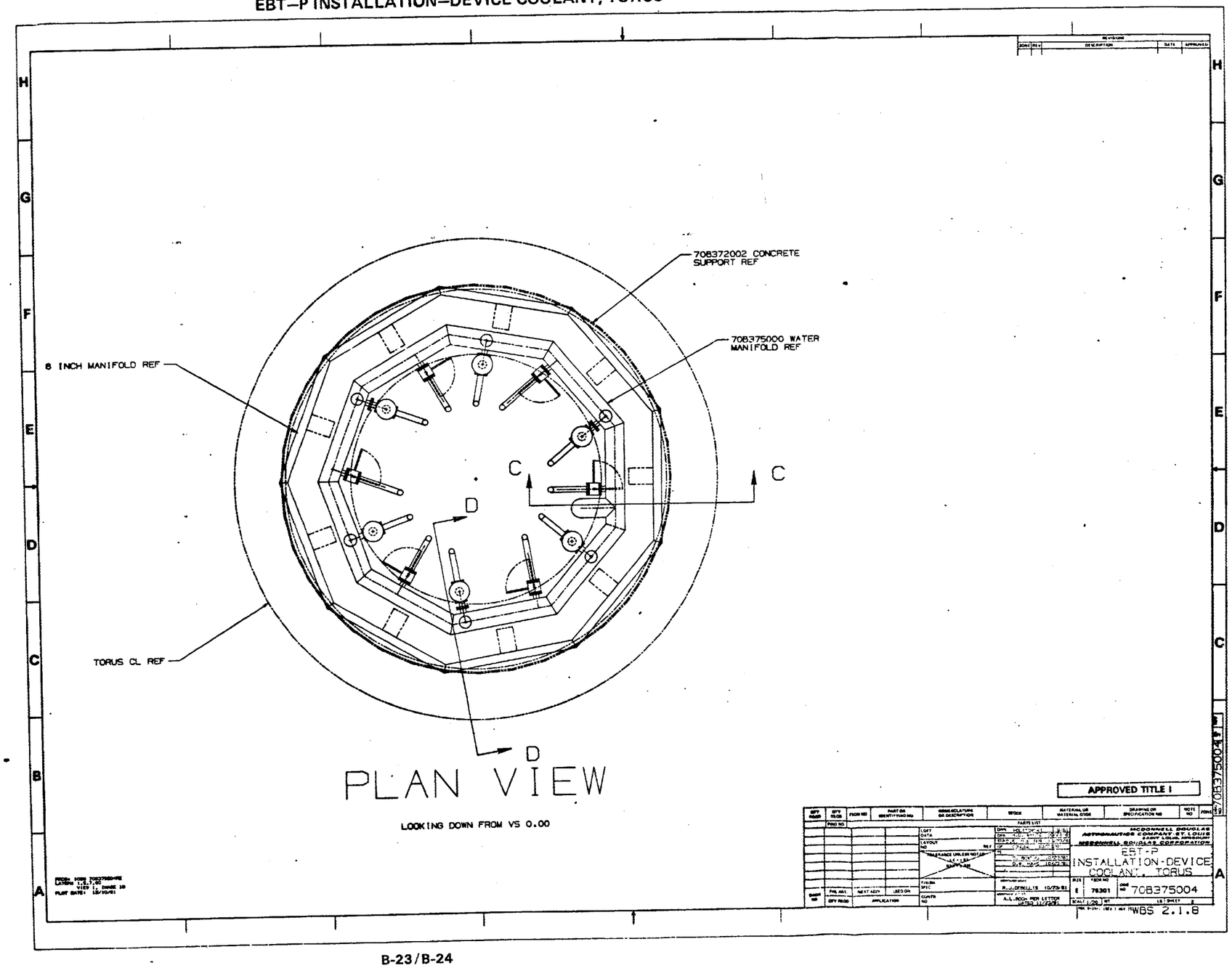

EBT–P INSTALLATION–DEVICE COOLANT, TORUS

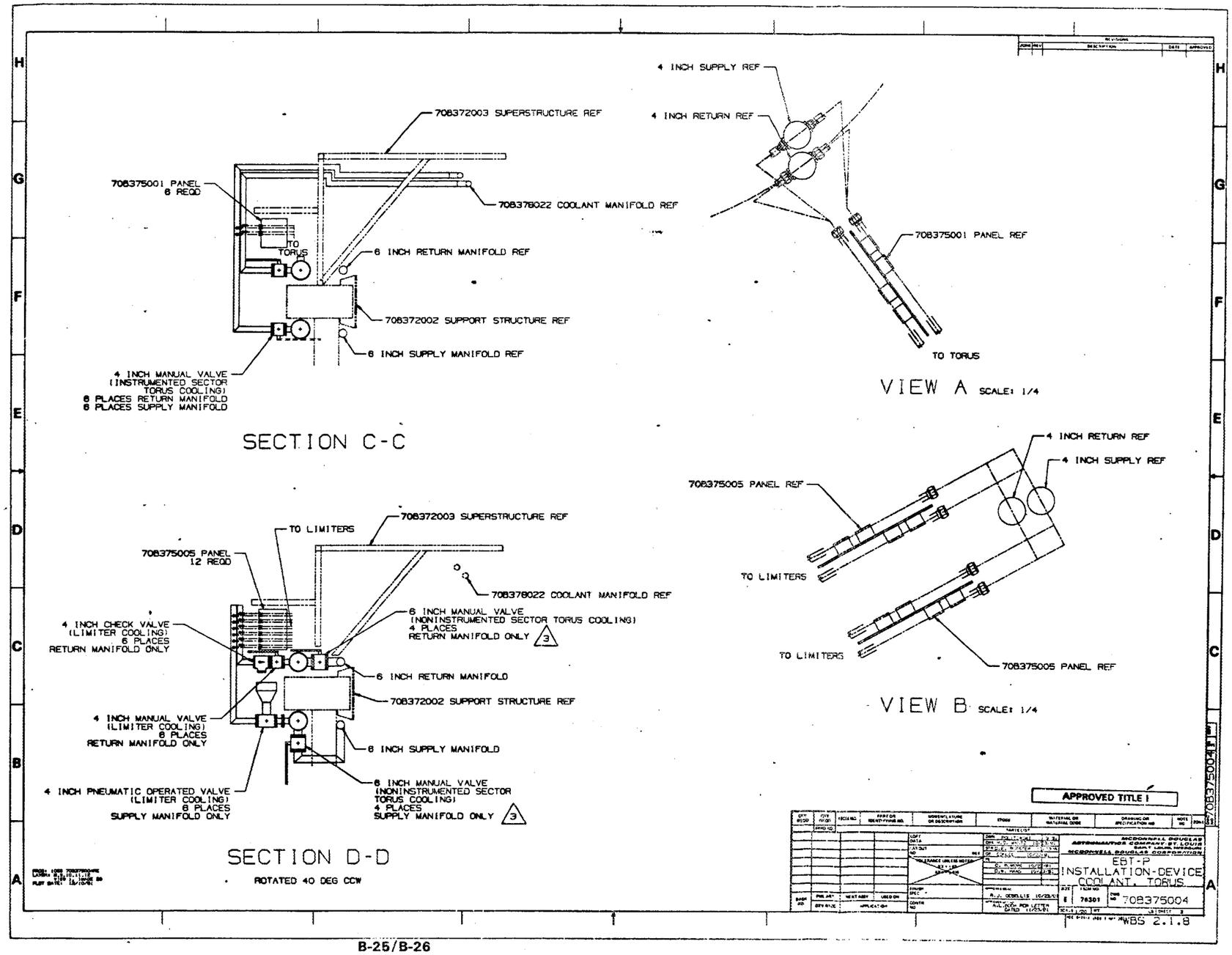
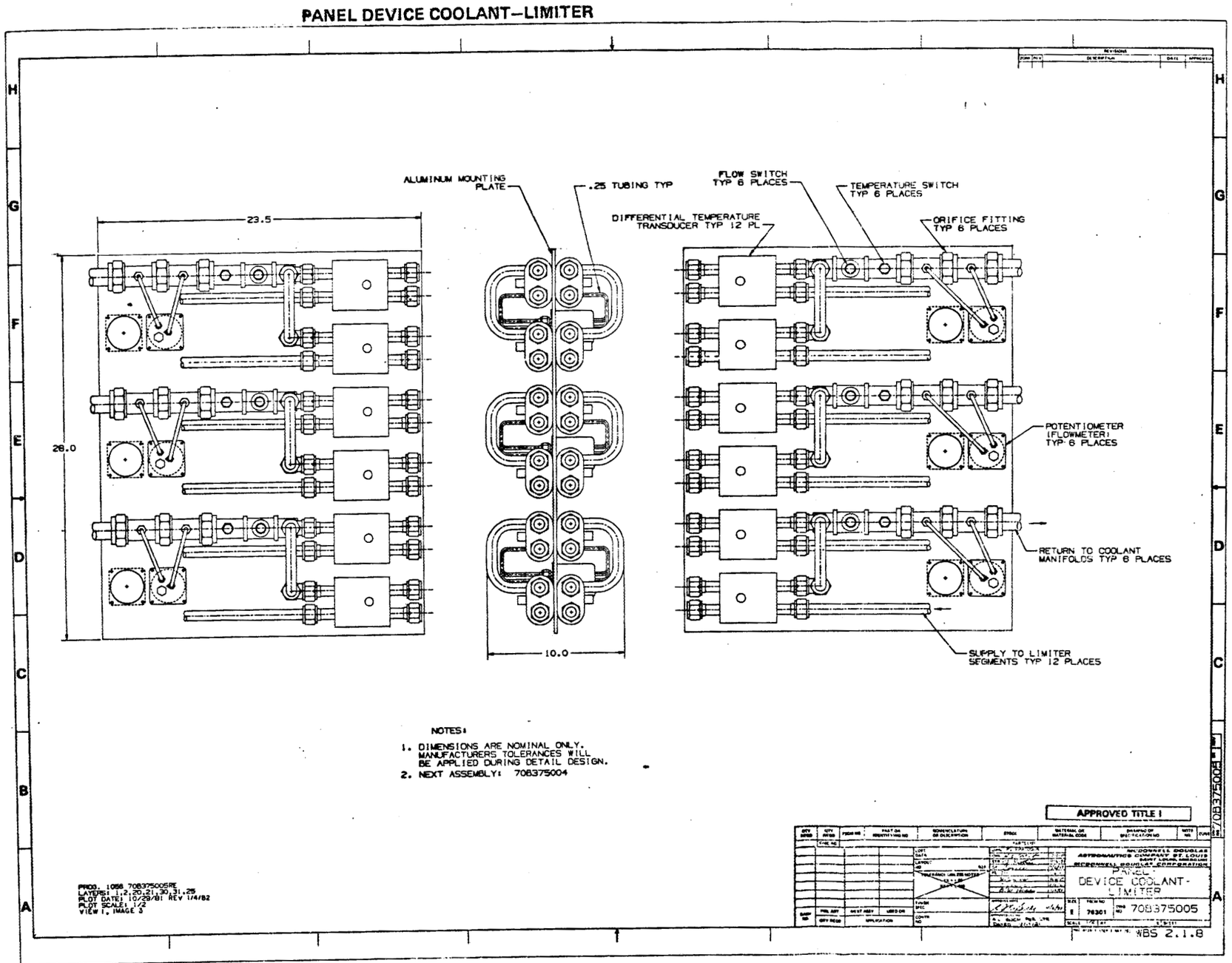
PANEL DEVICE COOLANT–LIMITER